UNIVERSIDADE FEDERAL DE SANTA CATARINA
CENTRO TECNOLÓGICO
PROGRAMA DE PÓS-GRADUAÇÃO EM ENGENHARIA DE AUTOMAÇÃO E SISTEMAS

Michael Feliphe da Silva Barbosa

Optimal control strategies for grid-assisted green hydrogen generation systems based on PEM technology: Production and energy storage applications

Florianópolis
2024

Michael Feliphe da Silva Barbosa

Optimal control strategies for grid-assisted green hydrogen generation systems based on PEM technology: Production and energy storage applications

Dissertação submetida ao Programa de Pós-Graduação em Engenharia de Automação e Sistemas da Universidade Federal de Santa Catarina para a obtenção do título de Mestre em Engenharia de Automação e Sistemas.
Orientador: Prof. Gustavo Artur de Andrade, Dr.

Florianópolis
2024

Ficha catalográfica gerada por meio de sistema automatizado gerenciado pela BU/UFSC.
Dados inseridos pelo próprio autor.

Barbosa, Michael Feliphe da Silva
Optimal control strategies for grid-assisted green hydrogen generation systems based on PEM technology : Production and energy storage applications / Michael Feliphe da Silva Barbosa ; orientador, Gustavo Artur de Andrade, 2024.
99 p.

Dissertação (mestrado) - Universidade Federal de Santa Catarina, Centro Tecnológico, Programa de Pós-Graduação em Engenharia de Automação e Sistemas, Florianópolis, 2024.

Inclui referências.

1. Engenharia de Automação e Sistemas. 2. Controle ótimo. 3. Hidrogênio . 4. Energia renovável . I. de Andrade, Gustavo Artur. II. Universidade Federal de Santa Catarina. Programa de Pós-Graduação em Engenharia de Automação e Sistemas. III. Título.

Michael Feliphe da Silva Barbosa

Optimal control strategies for grid-assisted green hydrogen generation systems based on PEM technology: Production and energy storage applications

O presente trabalho em nível de mestrado foi avaliado e aprovado por banca examinadora composta pelos seguintes membros:

Prof. Dachamir Hotza, Dr.
Universidade Federal de Santa Catarina

Prof. Rodolfo César Costa Flesch, Dr.
Universidade Federal de Santa Catarina

Certificamos que esta é a **versão original e final** do trabalho de conclusão que foi julgado adequado para obtenção do título de Mestre em Engenharia de Automação e Sistemas.

Documento assinado digitalmente
JULIO ELIAS NORMEY RICO
Data: 06/06/2024 17:00:05-0300
CPF: ***.840.859-**
Verifique as assinaturas em https://v.ufsc.br

Coordenação do Programa de
Pós-Graduação

Documento assinado digitalmente
Gustavo Artur de Andrade
Data: 06/06/2024 17:19:33-0300
CPF: ***.316.109-**
Verifique as assinaturas em https://v.ufsc.br

Prof. Gustavo Artur de Andrade, Dr.
Orientador

Florianópolis, 2024.

Dedico esse trabalho para minha mãe e minha esposa,
pelo apoio e amor incondicionais, por acreditarem e
investirem em mim. Por me trazerem paz e me
impulsionarem na direção do meu objetivo.

ACKNOWLEDGEMENTS

Agradeço a meus pais e minha irmã, que me deram total apoio para a realização deste trabalho. Mesmo precisando me ausentar em diversos momentos, sempre me motivaram a nunca desistir dos meus sonhos.

Agradeço ao professor Gustavo, por me aceitar como aluno e topar o desafio de me orientar, apesar do meu trabalho em tempo integral e pouco tempo para a realização da pesquisa.

Agradeço ao PosAutomação, ao INCT-CAPE e ao coordenador, Professor Júlio, por estar inserido em um projeto de importância nacional no ramo da energias renováveis.

Agradeço a minha esposa Rafaela, pela compreensão e encorajamento durante o trabalho. Sua presença foi uma parte crucial desta etapa. Obrigado por tolerar meus momentos de estresse, cansaço e cuidar da nossa família para que eu pudesse dedicar tempo à pesquisa.

Agradeço ao professor José Gabriel, da Universidad Nacional de La Plata, pela colaboração na escrita do artigo, pelas sugestões e revisões. Com certeza foi de grande valia para a conclusão deste trabalho.

Agradeço aos membros da banca por dedicarem o seu tempo e conhecimento para contribuir com o meu trabalho de pesquisa.

Agradeço a todos os meus colegas de trabalho e a empresa DTI Sistemas Ltda, por me proporcionarem flexibilidade de horários para poder conciliar todas as atividades. O apoio de vocês foi essencial durante toda essa caminhada.

Agradeço aos meus amigos Victor e Tiago, pois sempre me incentivaram a crescer na profissão e nunca desistir dos meus sonhos.

Agradeço a todos os professores da UFSC pela oportunidade de conhecê-los. Vocês são minha inspiração para seguir multiplicando o conhecimento que recebi.

Eu gostaria de agradecer a mim mesmo por ter concluído essa etapa na minha carreira. Vivenciar a realidade de trabalhar em tempo integral e fazer um projeto de mestrado foi um processo bem desafiador. É uma conquista muito grande, que exigiu abdicação em diversos aspectos e trouxe um imenso crescimento profissional e pessoal.

“A ciência é uma iniciativa de cooperação, que cobre gerações.
É a passagem da tocha do professor para o aluno e de volta ao professor.
Uma comunidade de mentes, voltando no tempo e alcançando as estrelas.”
(Neil Degrasse Tyson, 2014)

ABSTRACT

In the context of escalating energy demands and environmental concerns, hydrogen emerges as a promising avenue for sustainable energy production, especially when integrated with renewable energy sources (green hydrogen). However, the current global hydrogen production landscape predominantly relies on non-renewable sources, highlighting a significant gap in achieving a sustainable energy future. Developing optimal control systems in green hydrogen production is essential to bridge this gap. This research employed phenomenological mathematical modeling to simulate the behavior of green hydrogen production systems powered by grid and photovoltaic panels. Furthermore, it formulates single-phase, multi-phase, and hybrid optimal control strategies. The methodology also included developing a MATLAB toolbox based on CasADi for solving multi-phase optimal control problems by direct transcription. The study's key results show that the multi-phase control strategies reduced grid energy consumption under different solar energy conditions. In a year-long simulation using real-world data, the study found a reduction of up to four times compared to a single-phase strategy.

Keywords: Optimal control. Hydrogen. Renewable energy.

RESUMO

No contexto de demandas energéticas crescentes e preocupações ambientais, o hidrogênio surge como uma via promissora para a produção de energia sustentável, especialmente quando integrado a fontes de energia renováveis (hidrogênio verde). Contudo, o cenário atual da produção global de hidrogênio depende predominantemente de fontes não renováveis, destacando uma lacuna significativa para alcançar um futuro energético sustentável. Desenvolver sistemas de controle ótimos na produção de hidrogênio verde é essencial para preencher essa lacuna. Esta pesquisa empregou modelagem matemática fenomenológica para simular o comportamento dos sistemas de produção de hidrogênio verde alimentados por rede elétrica e painéis fotovoltaicos. Ademais, formula estratégias de controle ótimo de fase única, multifase e híbridas. A metodologia também incluiu o desenvolvimento de uma biblioteca MATLAB baseada em CasADi para resolver problemas de controle ótimo multifase por transcrição direta. Os principais resultados do estudo mostram que as estratégias de controle de multifase reduziram o consumo de energia da rede sob diferentes condições de energia solar. Em uma simulação ao longo de um ano utilizando dados reais, o estudo encontrou uma redução de até quatro vezes em comparação com uma estratégia de fase única.

Palavras-chave:Controle ótimo. Energia renovável. Hidrogênio.

RESUMO EXPANDIDO

Introdução

As emissões antropogênicas de carbono são amplamente reconhecidas como a principal causa do aquecimento global. A utilização de recursos energéticos limpos e renováveis para substituir os combustíveis fósseis e neutralizar a emissão de carbono tem sido uma tendência inevitável, dado que a geração de energia renovável está tornando-se cada vez mais competitiva com os combustíveis fósseis. No entanto, a gestão de tal mudança no sistema energético requer transições substanciais da estrutura energética existente baseada em combustíveis fósseis para uma estrutura de elevada penetração renovável.

O hidrogênio apresenta uma oportunidade para a geração de energia sustentável, especialmente em conjunto com fontes de energia renováveis, como a energia solar. Vários autores afirmam que a economia do hidrogênio, na qual o fornecimento de energia dependeria do hidrogênio, será iminente no futuro devido às capacidades de armazenamento e transporte do hidrogênio num mundo com emissões líquidas zero.

Neste trabalho, são propostas estratégias de controle ótimas para minimizar o consumo de energia da rede elétrica em sistemas fotovoltaicos-hidrogênio. Para atender às especificações de operação variável da planta, são propostas estratégias monofásicas, multifásicas e híbridas, nas quais os subintervalos de tempo para a troca das dinâmicas são predefinidos, e as variáveis de otimização são restritas para diferentes condições. Para resolver esses problemas numericamente, é aplicado o método de transcrição direta Hermit-Simpson, que converte o problema de controle ótimo em um programa não linear (NLP), o qual é resolvido com o otimizador IPOPT (Interior Point OPTimizer). Um estudo quantitativo sobre o desempenho das metodologias propostas é apresentado considerando diferentes cenários numéricos juntamente com índices de desempenho.

Esta dissertação foi desenvolvida no contexto do projeto de pesquisa *Controle e Otimização Avançados para Sistemas de Energia Renovável com Armazenamento de Energia em Hidrogênio*, projeto CNPq 403949/2021-1, e do *Instituto Nacional de Ciência e Tecnologia de Controle e Automação de Sistemas de Produção de Energia*, projeto CNPq 406477/2022-1, onde o orientador desta dissertação era membro da equipe de pesquisa. Além disso, parte dos resultados deste trabalho foram motivados pelo *Desafio de Sustentabilidade e Energia Renovável* organizado pela *MathWorks* (MATHWORKS, 2023c). Este desafio recebe a participação de estudantes, pesquisadores e engenheiros interessados em desenvolver soluções inovadoras para questões ambientais relacionadas à energia renovável e sustentabilidade.

Objetivos

Objetivo Geral

O objetivo geral desta dissertação é contribuir para o desenvolvimento de estratégias de controle ótimo para a minimização do consumo de energia da rede elétrica em sistemas fotovoltaico-hidrogênio. O estudo tem foco no problema de controle ótimo em um eletrolisador PEM para produção de hidrogênio, e de uma célula de combustível

reversível PEM para armazenamento hidrogênio como reserva de energia em uma micro rede.

Objetivos Específicos
Os objetivos específicos para a execução do estudo, definidos no objetivo geral, são descritos abaixo:

- Desenvolver modelos matemáticos fenomenológicos de sistemas de produção de hidrogênio fotovoltaico usando um eletrolisador PEM e uma micro rede usando uma célula de combustível reversível PEM para armazenamento de energia de hidrogênio.
- Formular estratégias de controle ótimo que minimizem a energia consumida da rede elétrica.
- Projetar uma biblioteca MATLAB, baseada em CasADi, para resolver problema de controle ótimo multifásicos.
- Analisar e comparar as soluções das estratégias de controle ótimo formuladas em cenários da realidade.

Metodologia
A metodologia consiste no desenvolvimento de modelos matemáticos para sistemas fotovoltaicos-hidrogênio, com foco na dinâmica de eletrolisadores PEM e de célula de combustível reversível PEM. Inclui a formulação de estratégias de controle ótimo monofásicas, multifásicas e híbridas. A pesquisa emprega métodos de transcrição direta, especificamente colocação Hermite-Simpson, para a solução numérica problemas de control ótimo, e desenvolve uma bilbioteca MATLAB, baseada na biblioteca CasADi, para solução problemas de controle ótimo mutifásicos.

Resultados e Conclusão
Os resultados da simulação permitiram avaliar o potencial da proposta para reduzir a energia elétrica da rede utilizada nas plantas. Para o sistema de produção de hidrogênio estudado, em um ano de avaliação da proposta com o cenário brasileiro, a redução foi de até quatro vezes ao comparar a estratégia multifásica com uma estratégia de fase única.

É importante destacar que a análise foi conduzida sob um cenário ideal para o problema de controle. Isso incorpora a suposição de dados futuros precisos sobre radiação solar, demanda de hidrogênio e demanda de energia, juntamente com uma correspondência exata entre o modelo e as dinâmicas da planta. Consequentemente, o desempenho alcançado serve como um ponto de referência teórico para a operação do sistema, que, em condições reais, enfrentará desafios como imprecisões de modelagem, distúrbios não considerados no modelo e incertezas nas previsões meteorológicas.

Palavras-chave Controle ótimo. Hidrogênio. Energia renovável.

LIST OF FIGURES

LIST OF TABLES

LIST OF ABBREVIATIONS AND ACRONYMS

AC/DC	Alternating Current to Direct Current
AD	Algorithmic Differentiation
AEM	Anion Exchange Membrane
BB	Branch-and-bound
CCS	Carbon Capture and Storage
CPU	Central Processing Unit
DC	Direct current
DC/DC	Direct Current to Direct Current
EL	Electrolyzer
EU	European Union
eVTOL	Electric Vertical Takeoff and Landing
FC	Fuel Cell
FW	Fixed window
GHG	Greenhouse Gases
GPER/UFSC	Research Group on Renewable Energies of UFSC
GPU	Graphics Processing Unit
HBVP	Hamiltonian Boundary-Value Problem
HMPC	Hybrid Model Predictive Control
HS	Hermite-Simpson
HSC	Hermite-Simpson collocation
HyCi	Hydrogen Civilization
HyS	Hybrid strategy
HyS-BB	Hybrid strategy with BB algorithm
HyS-OA	Hybrid strategy with OA decomposition algorithm
IAHE	International Association for Hydrogen Energy
MILP	Mixed-integer Linear Programming
MINLP	Mixed-integer Nonlinear Programming
MPC	Model Predictive Control
MPP	Maximum Power Point
MPPT	Maximum Power Point Turacking
MPS	Multi-phase Strategy
MPS-FW	Multi-phase strategy with fixed window algorithm
MPS-VW	Multi-phase strategy with variable window algorithm
NLP	Nonlinear Programming
NP	Non-deterministic Polynomial
OA	Outer approximation
OCP	Optimal Control Problem

ODE	Ordinary Differential Equation
PEM	Proton Exchange Membrane
PID	Proportional-Integral-Derivative
PV	Photovoltaic
RAM	Random Access Memory
RES	Renewable Energy Source
RFC	Reversbile fuel cell
RHGS	Renewable Hydrogen Generation System
RHGUS	Renewable Hydrogen Generation and Utilization System
SO	Solid Oxide
SPS	Single Phase Strategy
SQP	Sequential Quadratic Programming
URFC	Unitized Reversbile fuel cell
USD	United States Dollar
VW	Variable window

LIST OF SYMBOLS

A_S	Cell deviation factor
A_E	Electrolyzer area
A_F	Fuel cell area
δ_B	Membrane thickness
ε	Constant in approximation of Lambert function
D_{off}	Days with electrolyzer off and without hydrogen consume
D_{off}^{dm}	Days with electrolyzer off and with hydrogen consume
D_{off}^{Total}	Total days with electrolyzer off
E_g	Semiconductor band gap
E_E	Energy consumed by electrolyzer
E_G^-	Energy delivered by the electric grid
E_G^+	Energy absorbed by the electric grid
F	Faraday constant
f_{H_2}	Hydrogen flow rate
$f_{H_2}^{dm}$	Rate of hydrogen leaving the tank
f_p	Right side of the ODE system for phase p
i_E	Electrolyzer current
i_S	Solar panel current
I_a	Anode current density
I_c	Cathode current density
I_E	Electrolyzer current density
I_E^m	Current in standby or maintenance mode
$I_E^{\max}$	Rated power designed by the manufacturer
$I_E^{\min}$	Minimum operating limit for safe operation
I_{or}	I_{rs} at T_{sr}
I_{ph}	Photo-generated current
I_{rs}	Corrente reversa de saturação
I_{sc}	Short circuit current at T_{sr}
K	Boltzmann constant
K_L	Short circuit current by temperature
L_p	Stage cost of phase p
λ_S	Solar radiation intensity
λ_E	Membrane water content
m_{H_2}	Mass of hydrogen in the tank
$\dot{m}_{H_2}$	Rate of change of hydrogen mass in the tank
$m_{H_2}^{max}$	Maximum mass of hydrogen in the tank
$m_{H_2}^{min}$	Minimal mass of hydrogen in the tank

M_{H_2}	Total of hydrogen produced
N_p	Number of phases
N_{PS}	Number of solar panels in parallel
N_{SE}	Number of electrolytic cells in series
N_{SS}	Number of solar panels in series
P_D	Power demand of the consumer
P_E	Power consumed by the electrolyzer
P_F	Power in fuel cell
p_{H_2}	Hydrogen partial pressure
p_{O_2}	Oxygen partial pressure
$p_{\mathrm{H}_2\mathrm{O}}$	Water partial
P_S	Power generated by the solar panel
Q	Elementary charge
R	Gas constant
R_{PS}	Resistance in parallel
R_{SS}	Resistance in series
$\lambda_S^{\min}$	Minimum solar radiation intensity for the EL operation
s	Solar radiation
s_E	Electrolyzer operating mode
s_F	Fuel cell operating mode
σ_B	Membrane conductivity
t_{i_p}	Initial time of phase p
t_{f_p}	Final time of phase p
t_N	End of the first night period
t_D	End of the day interval
T_E	Electrolyzer temperature
T_F	Fuel cell temperature
T_{SR}	Reference temperature
T_S	Solar panel temperature
u	Control input function
u_p	Control input of phase p
v_0	Reversible potential
v_E	Electrolyzer voltage
v_{etd}	Electrode overpotential
v_{ion}	Ionic overpotential
v_{ohm}	Ohmic overvoltage
v_S	Solar panel voltage
W	Lambert function
x_p	State of phase p

z	Lambert function parameter
i_{loss}	Lost internal current density
$i_{0_{anode}}$	Anode exchange current density
$i_{0_{cathode}}$	Cathode exchange current density
$i_{l_{anode}}$	Anode limiting current density
$i_{l_{cathode}}$	Cathode limiting current density
n	Number of electrons
N_S	Number of cells in of URFC
R_{elec}	Area specific resistance
R_{ion}	Area specific ion resistance
R_{cr}	Area specific contact resistance
v_{rev}	Reversible potential of URFC

CONTENTS

1 INTRODUCTION

1.1 MOTIVATION

Energy and the environment have been two major concerns of this century. Anthropogenic carbon emissions are widely acknowledged to be the primary cause of global warming and other detrimental climate changes (FAWZY et al., 2020; CRUTZEN, 2002), which leads to frequent and intense weather events, such as droughts and storms. This has led to the Paris Climate Agreement's ambition to keep the global temperature increase below 1.5 °C (UNFCCC, 2020). The use of clean and renewable energy resources to replace fossil fuels has been an inevitable trend (YAN et al., 2020) given that renewable energy generation is becoming increasingly competitive with fossil fuels on an economic scale. However, managing such a change in the energy system requires substantial transitions from the existing fossil fuel-based energy structure to a high renewable penetration structure (ZHAO; YOU, 2021). Many challenges still need to be faced for a smooth and safe transition of the global energy scenario (YAN, 2020).

Hydrogen (H_2) presents an opportunity for sustainable energy generation, particularly in conjunction with renewable energy sources such as solar energy and feedstocks, mainly water or biomass. Several authors claim that the hydrogen economy, in which energy supply would depend on H_2, will be imminent in the future due to the storage and transportation capabilities of H_2 in a world with net-zero emissions (IEA, 2022). The trend of the constantly growing H_2 demand is evident from the estimated values presented by Hydrogen Council (2021), as shown in Figure 1.

Figure 1 – Global hydrogen demand by segment until 2050.

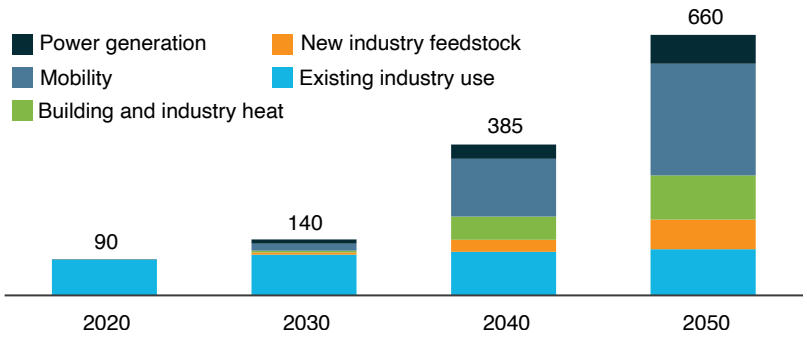

Source: Adapted from Hydrogen Council (2021).

Hydrogen can be produced from various sources, both renewable and non-renewable, each with different costs and carbon dioxide emissions (YU; WANG; VREDENBURG, 2021). Currently, most hydrogen is produced through the reforming of natural gas, which results in significant carbon dioxide emissions (IEA, 2022). However, by utilizing electrolyzers, low-carbon hydrogen can be generated through the electrolysis of

water using electricity from renewable sources, known as green hydrogen. Research by Newborough and Cooley (2020) suggests that green hydrogen is expected to become the most cost-effective production method in the future.

On the supply side, H_2 can be used to generate electrical power and heat production with low carbon emissions through the utilization of fuel cell (FC) systems. An FC is a device that converts the energy from a chemical reaction into electricity. According to Genovese et al. (2023), the proton exchange membrane fuel cell was the most extensively installed type of fuel cell worldwide in 2021.

Brazil, due to its geographical location and orographic conditions, has grand potential for using wind and solar energy. The country ranks as the sixth wind energy producer in the word, with an installed capacity of 25.75 MW at the end of 2022, with an increase of 5.57 MW for that year as a sample (BRASIL, 2023c). Regarding solar energy, Brazil is the 8th country in the world in terms of total installed solar power, which was estimated at 34.2 GW in 2023 (BRASIL, 2023c).

The need to develop renewable energy storage systems has led numerous countries to promote projects and research focused on different technologies such as compressed air, water pumping, H_2. However, there are still technical and economic barriers that must be overcome to achieve complete implementation (AMIR et al., 2023). In Brazil, companies have highlighted their interest in these technologies for the development of renewable energies in the country, and to this end, they are actively promoting national projects (HOTZA; DINIZ DA COSTA, 2008). By 2023, Brazil has already recorded US$ 30 billion in announced low-carbon hydrogen projects at different stages of implementation (BRASIL, 2023b). At an international level, there are various examples of projects financed by the European Union (WULF; ZAPP; SCHREIBER, 2020) or by the United States Department of Energy (USA, 2023).

This interest has led to the development of numerous demonstration projects in the last decade. The operating results compiled by Valverde et al. (2013a) demonstrate that numerous technical problems can be avoided with advanced control strategies that take into account more parameters during operation. This work highlights the importance of control strategies in hydrogen production, safe plant operation, and component durability. In this way, more complex control strategies are called for that can include parameters such as the economic benefit of its operation to increase reliability and performance, and reduce operating costs.

In this work, optimal control strategies are proposed to optimize the electric grid energy consumption in photovoltaic-hydrogen systems. To meet the variable operation specifications of the plant, single-phase, multi-phase, and hybrid strategies are proposed, in which time subintervals for switching the dynamics are predefined, and the optimization variables are restricted for different conditions. To solve these problems numerically, the Hermit-Simpson direct transcription method is applied, which converts

the optimal control problem into a nonlinear program (NLP), which is in turn solved with the IPOPT (Interior Point OPTimizer) optimizer. A quantitative study on the performance of the proposed methodologies is presented considering different numerical scenarios together with performance indexes.

This dissertation was developed in the context of the research project *Advanced Control and Optimization for Renewable Energy Systems with Hydrogen Energy Storage* (in Portuguese), project CNPq 403949/2021-1, and the *National Institute of Science and Technology of Control and Automation of Energy Production Systems* (in Portuguese), project CNPq 406477/2022-1, where the supervisor of this dissertation was a research team member. Additionally, part of the results of this work were motivated by the *Sustainability and Renewable Energy Challenge* organized by *MathWorks* (MATHWORKS, 2023c). This challenge welcomes participation from students, researchers, and engineers who are interested in developing innovative solutions to environmental issues related to renewable energy and sustainability

Regarding the technological contributions, this research is justified by a gap in research regarding the application of multi-phase optimal control in the domain of RHGUS. Despite its widespread use in areas such as aerospace (YANG et al., 2021), aeronautics (PRADEEP; WEI, 2018), automotive (XIAOFENG, 2022), and robotics (LIU et al., 2021), the application of multi-phase optimal control in hydrogen systems has not been extensively studied. Therefore, this study seeks to bridge this gap by proposing a multi-phase optimal control strategy and comparing it with commonly employed single and hybrid approaches.

1.2 OBJECTIVES

1.2.1 General Objective

The general objective of this dissertation is to contribute to the development of optimal control strategies for the minimization of electric grid energy consumption in photovoltaic-hydrogen systems. The study is concerned with such optimization problems in a PEM electrolyzer for hydrogen production, and a PEM fuel cell for hydrogen energy storage in a microgrid, however, the results are presented, whenever possible, in a general framework to reach a relevant portion of the scientific community.

1.2.2 Specific Objectives

The specific objectives for the execution of the study, defined in the general objective, are described below:

- To develop phenomenological mathematical models of photovoltaic-hydrogen production systems using a PEM electrolyzer, and a microgrid using PEM fuel cell for hydrogen energy storage.

- To formulate optimal control strategies that minimize the electric grid energy consumed.
- To design a MATLAB toolbox CasADi to solve optimal control problems using CasADi.
- To analyze and compare the solutions of formulated optimal control strategies in real-life scenarios.

1.3 ORGANIZATION

The remainder of this dissertation is organized into four chapters to deliver a cohesive and comprehensive examination of the research on optimal control within photovoltaic-hydrogen systems. In Chapter 2 reviews hydrogen production with energy solar energy, optimal control problems and how to solve them using Hermite-Simpson collocation. Chapter 3 includes description of a photovoltaic-PEM electrolyzer system for hydrogen production, formulation of optimal control, and data collection and comparison procedures. This chapter also incorporates a comparative analysis of multi-phase and hybrid approaches, evaluating their performance and discussing their benefits and limitations. Chapter 4 focuses on applying a multi-phase optimal control strategy in a photovoltaic-PEM unitized regenerative fuel cell system for hydrogen energy storage. Finally, Chapter 5 concludes the study by summarizing the key findings, emphasizing the contributions to the field, acknowledging the study's limitations, and proposing potential avenues for future research.

2 THEORETICAL BACKGROUND

In this chapter, a literature review is presented, covering the key topics of this work. The review is structured into four sections. Firstly, section 2.1 delves into the concepts of the hydrogen economy and hydrogen civilization, along with hydrogen production methods and mathematical models of a PEM electrolyzer and a PEM reversible fuel cell. Following this, section 2.2 offers an overview of solar energy and a model of a photovoltaic panel.

In section 2.3, a basic material on optimal control theory is presented. First, a primer on the classical optimal control methodology, called *single-phase optimal control*, is discussed focusing on direct resolution approaches, also known as *first-discretize-then-optimize* approaches. Next, the extensions of this control theory to the cases where the problem involves discontinuous and integer control variables are discussed. It will be referred to as *multi-phase optimal control* in the case where the optimization process has continuous and discontinuous control variables and state dynamics, and as *hybrid optimal control* in the case where the optimization process has mixed-integer control variables. This material was extracted from the references (BETTS, 2010; TOPPUTO; ZHANG, C., 2014; KELLY, 2017a, 2017b). The practical implementation of the controller through a closed-loop framework is also discussed in this section.

Finally, section 2.4 presents some research on multi-phase optimal control and optimal control in hydrogen production systems.

2.1 HYDROGEN

2.1.1 The Hydrogen Economy

H_2 is the most prevalent element in the universe, and it is primarily found on Earth in water and organic compounds. It is the lightest and simplest element, consisting of one electron and one proton, and is a colorless, odorless, and flammable gas (ISHAQ; DINCER; CRAWFORD, 2022). Hydrogen is a material that has been known for more than 200 years, some milestones in history of hydrogen discovery and usage are presented in Table 1.

Table 1 – Historical milestones in hydrogen discovery and usage.

Year	Event
16th Century	Paracelsus from Switzerland discovers the formation of gas during the reaction between sulfuric acid and iron.
17th Century	Myelin, also from Switzerland, reports that this gas can burn.

Continued on next page

Continued from previous page

Year	Event
1761	Robert Boyle produces hydrogen by reacting iron filings and dilute acids.
1776	Henry Cavendish identifies hydrogen as a unique substance and is credited as the discoverer of hydrogen.
1783	Antoine Lavoisier produces hydrogen and names it "hydrogen" (Hydrogenous) from the Greek roots "hydro" (water).
1800	English scientists Nicholson and Carlisle use electrolysis of water to produce hydrogen for the first time.
1898	James Dewar liquefies hydrogen.
1839	British scientist Sir William Robert Grove develops the first hydrogen-powered fuel cell.
1900	Count Ferdinand von Zeppelin of Germany invents the first balloon using hydrogen to maintain the buoyancy of an airframe.
1920s and 1930s	Airships powered by hydrogen are used for transatlantic travel.
1954	Detonation of the first hydrogen bomb.
1961	NASA becomes the world's largest user of liquid hydrogen as a fuel.
1988	The Soviet Union completes a flight with the TU-155, the world's first jet engine aircraft using liquid hydrogen as fuel.

Source: Compiled from (DAWOOD; ANDA; SHAFIULLAH, 2020; ISHAQ; DINCER; CRAWFORD, 2022).

One of the ways to obtain H_2 is from the separation of water, which is found in abundance on Earth. This process is synthesized with the H_2 production block of Figure 2, where the provided water can be separated into its basic components of H_2 and oxygen (O_2) delivering the amount of energy E_i needed. This is the chemical reaction that takes place carried out, for example, in an electrolyzer. The H_2 utilization block synthesizes the reverse process that occurs in fuel cells, which releases the amount of energy *Eo*. The cycle is closed with oxygen and water vapor, which are the only byproducts released into the atmosphere, so it is a 100 % environmentally benign cycle.

The other advantages offered by this energy vector are:

- Can be produced from renewable energy sources, such as solar and wind energy sources.
- Can be stored, transported, and distributed in several ways.

- Its use for electricity generation or transportation consumption can replace the use of fossil fuels.

Figure 2 – The hydrogen cycle.

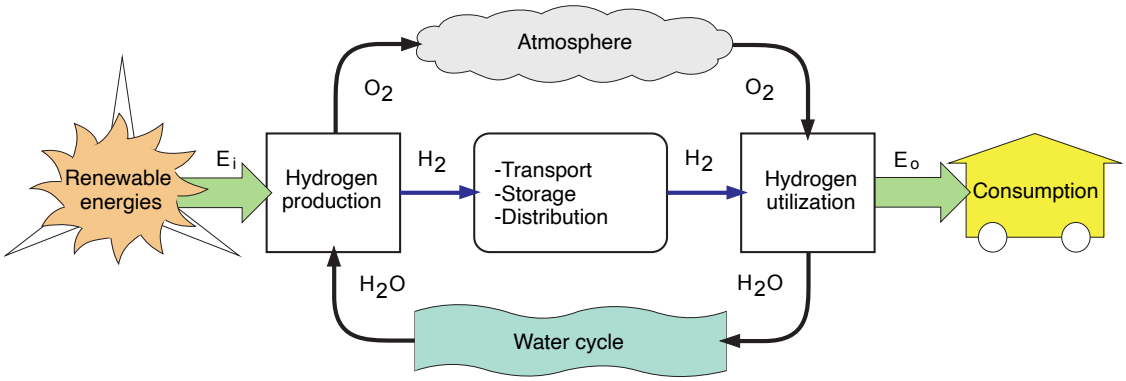

Source: Adapted from García-Clúa (2013).

The idea of a society capable of using H_2 as an energy vector has been systematically attracting the attention of scientists and engineers for decades. Even in 1874, at the level of science fiction, the French novelist Jules Verne (1828-1905) expressed in his book *The Mysterious Island*:

> Yes, my friends, I believe that water will one day be employed as fuel, that hydrogen and oxygen which constitute it, used singly or together, will furnish an inexhaustible source of heat and light, of an intensity of which coal is not capable (VERNE, 1965, chap. 11).

By the first half of the 20th century, warnings were beginning to emerge about the environmental dangers of indiscriminate exploitation of non-renewable resources implicit in human activity and the unpredictable nature of its consequences. In this context, between the 1920s and 1970s, enthusiastic representatives of the world scientific community wanted to revive Jules Verne's fantasy, taking it to a high scientific and engineering level (GARCÍA-CLÚA, 2013). They proposed multiple ways to produce and use H_2 in numerous applications, but the relatively low price of fossil fuels made these opportunities uneconomical.

During the energy crisis of 1973, the United States and Europe were forced to reconsider alternatives to fossil fuel-based energy. This is how the International Association for Hydrogen Energy (IAHE) was created in 1974, based in Miami. Through the publication of journals and the holding of conferences biennials, this society began to form a scientific community under the term *hydrogen energy* (VEZIROGLU, T. N., 2000). This concept holds that hydrogen-based energy systems offer the optimal solution to the world's interrelated problems and encompasses the production of H_2 (using renewable and non-renewable energy sources); its delivery, transportation, and storage; its use in industry, transportation, and homes; and issues related to materials and safety.

In the last decade of the 20th century, the commercialization of hydrogen-based technologies began (hydrogen-powered automobiles, fuel cells, advanced electrolyzers,

hydrogen-nickel batteries, etc.) and the term *hydrogen economy* began to be used to describe an alternative to the fossil fuel-based economy (BOCKRIS, 1975). This concept also emerged as an extension of the all-electric economy proposed in those years with the advent of low-cost nuclear electricity. The main weak point of this economy was the complex and expensive storage of electricity. Consequently, the electrical distribution companies began to evaluate the potential benefits of combining the H_2 and all-electric economies, and the term *hydrogen–electricity economy* was introduced to describe the possibilities of combining the production, transmission, and sale of both energy vectors (LOTKER, 1974). The stable scientific community that had been formed then was already dedicated to studying how to produce H_2 economically to power internal combustion machines or fuel cells that were capable of delivering electrical power in distributed applications. Different solutions were proposed to increase the efficiency of these systems, such as combining heat and electrical power flows so that the loads take advantage of the heat produced by the distributed generators. The study of the prospects for the development of different aspects of the hydrogen economy was projected up to the year 2050 and even further.

All of these advances provided the practical framework necessary for a better understanding of a long-term sustainable future. Indeed, at the end of the 20th century, it was warned that human activity based on the use of fossil fuels was reaching irrational scales and that the threat of a climate catastrophe was certain. A sustained movement began to be promoted towards the hydrogen era that will lead to global transformations in all aspects of human existence: mentality, society, international politics, and development related to the environment. The hydrogen civilization (HyCi) (GOLTSOV, V.; VEZIROGLU, T.; GOLTSOVA, 2006) then emerges as a doctrine whose general principle is the following: *humanity can prevent the global ecological catastrophe and preserve the capacity of the biosphere to preserve life by the movement along the vector:*

$$\textit{Hydrogen Energy} \rightarrow \textit{Hydrogen Economy} \rightarrow \textit{Hydrogen Civilization}.$$

The following statement from the HyCi doctrine offers a new vision of hydrogen energy and economy:

> Hydrogen energy and the hydrogen economy are the technical, economic and ecological foundations of the conversion towards a sustainable human future: the hydrogen civilization. It means that every advance in hydrogen energy and economics, every new investigation of its partial problems is a step forward on the path towards hydrogen civilization (GOLTSOV, V. A., 2010, p. 12).

2.1.2 Hydrogen Production and Energy Storage Application

Hydrogen can be produced from several feedstocks, such as water, coal, natural gas, biomass, hydrogen sulfide, and others, through thermal, electrolytic, or photolytic

processes. F. Zhang et al. (2016), Kumar and Lim (2022) and Van, Chi, and Duc (2023) describes the main hydrogen production technologies, along with their components, materials, and required energy supply.

The hydrogen produced on a global scale is estimated to be 87 million tons per year (KUMAR; LIM, 2022). However, as of 2020, 95% of the hydrogen was produced from non-renewable fossil fuels especially steam reforming of natural gas, emitting 840 million tons per year of CO_2, and the rest of the hydrogen was produced from renewable resources including water electrolysis (IEA, 2022).

The state-of-the-art technologies for hydrogen production are very diverse. While some technologies are still in the research stage, others are already being tested on a laboratory scale or have been commercialized for years. Depending on the production process and kind of energy used, hydrogen costs and related emissions could be very different. This is the reason that hydrogen generation technologies are often classified based on different colors (AJANOVIC; SAYER; HAAS, 2022), such as grey, blue, turquoise, green, purple, yellow, white, and orange as shown in Table 2. Some of the production technologies are well-developed and mature, but some methods are still under fundamental research.

Conventional production methods use natural gas, coal, or oil as feedstock and convert them by steam reforming or gasification to obtain hydrogen, which emits CO_2 unless it is captured and stored, or used. A large amount of this hydrogen is used for industrial applications, such as metal refining, chemical production as well as fats and oil production.

The method mostly referred to when talking about renewable hydrogen is electrolysis, with renewable electricity as input. This kind of hydrogen, also called *green hydrogen*, is of special interest toward a more sustainable energy and transport system. Importantly, all electricity needed for this production process has to be solely from renewable energy sources to be regarded as green hydrogen.

Overall only 0.03 % of global hydrogen production is done via electrolysis, also including yellow and pink hydrogen (IEA, 2022). This means that green hydrogen to date is still very much a niche product. However, the research developed by Newborough and Cooley (2020) found that green hydrogen will be the production method of the future as it will become cheaper than alternatives like blue hydrogen caused by cheaper renewable electricity and electrolyzers.

2.1.3 Green Hydrogen Generation Systems

The renewable electrical conversion stage integrates different natural sources. The short-term energy storage stage consists of battery banks or supercapacitors to contribute to the power balance, which can be destabilized with sudden changes in renewable sources and loads.

Table 2 – Hydrogen classification.

Color	Description
Gray	Hydrogen produced by fossil fuels, mostly natural gas and coal, causing CO_2 emissions in the process.
Blue	Hydrogen produced from fossil fuels with carbon capture and storage (CCS) reduces greenhouse gas emissions.
Turquoise	Hydrogen produced via pyrolysis of fossil fuels, where the by-product is solid carbon.
Green	Hydrogen produced by electrolysis using electricity generated from renewable energy source (RES).
Purple	Hydrogen produced by electrolysis using electricity from nuclear power plants.
Yellow	Hydrogen produced by electrolysis using electricity from the grid.
White	Hydrogen naturally produced deep within the Earth becomes trapped by impermeable barriers, similar to petroleum.
Orange	Hydrogen produced from the anthropogenic stimulation of the same geochemical processes that produce white hydrogen.

Source: Adapted from Ajanovic, Sayer, and Haas (2022) and Blay-Roger et al. (2024).

The hydrogen generation stage is where the water dissociation takes place. The hydrogen storage stage is necessary to have variability in the generation and/or demand. This is done through the incorporation of devices that accumulate hydrogen in its gaseous or liquid phase, or absorbing it in metals or some forms of carbon.

The hydrogen utilization block represents its final destination, such as electricity generation through a fuel cell, combustion engines, or heating processes. According to Deshmukh and Boehm (2008), a renewable hydrogen generation system (RHGS) is limited to producing and storing H_2, while a renewable hydrogen generation and utilization system (RHGUS) includes a load of thermal or electrical nature that makes use of H_2. If the electrical energy generated by the hydrogen is reinjected into the RHGUS, the electrolyzer, the gas tank, and the fuel cell assembly will serve as long-term energy storage. The basic configuration of a renewable hydrogen generation system is shown in Figure 3.

Figure 3 – Schematic diagram of a green hydrogen generation system.

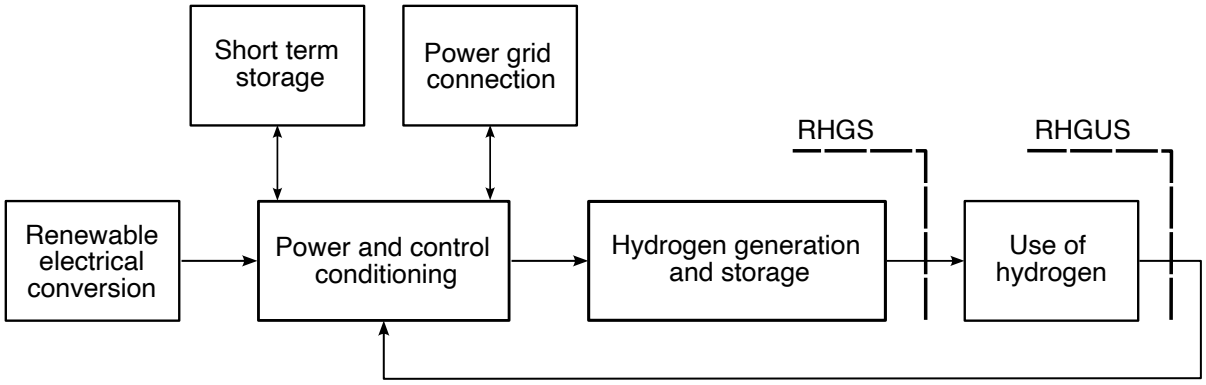

Source: Adapted from García-Clúa (2013).

Regardless the application, the RHGUS frameworks proposed in the literature can be classified as (*i*) grid-dependent generation of H_2; (*ii*) grid-assisted renewable H_2 generation; (*iii*) renewable generation of H_2 and electricity; (*iv*) integrated H_2 renewable electricity system; and (*v*) grid-independent integrated renewable electricity system based on H_2. All of these frameworks have the electrolyzer as the common component and differ in the fuel cell existence and/or grid connection.

On-grid systems has a stable power supply, high electrolyzer load factors, and revenue-stacking opportunities in power markets. However, they cannot ensure the renewable origin of the electricity used and hydrogen produced. Furthermore, on-grid configuration is less feasible for remote regions that encounter difficulties in connecting to the grid. On the other hand, off-grid systems that rely on renewable power for electrolysis ensure renewable hydrogen but necessitate electrolyzers to respond quickly to fluctuating power inputs, potentially reducing load factors. Therefore, effective operational optimization is crucial for both configurations.

2.1.4 Electrolyzer

Water electrolysis is one such electrochemical water-splitting technique for green hydrogen production with the help of electricity, which is emission-free. The basic reaction of water electrolysis is given by

$$H_2O + \text{Electricity} + \text{Heat} \longrightarrow H_2 + (1/2)\,O_2.$$

This reaction requires 1.23 V theoretical thermodynamic cell voltage to split the water into hydrogen and oxygen at room temperature. However, experimentally the required cell voltage must be bigger due to the kinetics and ohmic resistance of the electrolyte and cell components of the electrolyzer. An ideal electrolyzer requires 39 kWh and 8.9 liters of water to produce 1 kg of H_2 under normal conditions of temperature and pressure (WITKOWSKI et al., 2017). Usually, commercial electrolyzers require a higher electrical energy to produce the same amount of H_2 (KROPOSKI et al., 2006).

There are four main water electrolysis technologies based on their electrolyte, operating conditions, and their ionic agents (OH^-, H^+, O^{2-}): (*i*) alkaline water electrolysis; (*ii*) Anion exchange membrane (AEM) water electrolysis; Proton exchange membrane water electrolysis; and (*iv*) Solid oxide SO water electrolysis ().

Table 3 – Electrolyzer technologies.

Type	**Efficiency [%]**	**Operating Temp. [K]**	**Operating Pressure [bar]**	**Hydrogen Purity [%]**	**Technology Level**
PEM	50–75	323–353	<80	99.9–99.9999	Commercialized
SO	>80	973–1123	1	99.9	Lab scale and small applications
Alkaline	50–70	343–363	<35	99.5–99.9998	Mature
AEM	55–60	313–333	<35	99.9–99.9999	Research and development

Source: Adapted from Genovese et al. (2023).

In recent years, PEM electrolysis has become increasingly popular due to its high performance. (FALCÃO; PINTO, 2020). Figure 4 illustrates the basic working principle of the PEM electrolyzer. A PEM electrolyzer cell consists of two half-cells separated by a thin PEM. The reaction of the half cell of each electrode (anode and cathode) and the overall reaction are as follows:

$$\textbf{Anode:} \quad 2\,H_2O(l) \longrightarrow 4\,H^+(aq) + O_2(g) + 4\,e^-$$
$$\textbf{Cathode:} \quad 4\,H^+(aq) + 4\,e^- \longrightarrow H_2(g)$$
$$\textbf{Overall:} \quad 2\,H_2O(l) \longrightarrow H_2(g) + O_2(g)$$

at the anode (positive electrode), water is oxidized to produce oxygen gas, positively charged hydrogen ions, and electrons. At the cathode (negative electrode), water is reduced to form hydrogen gas and hydroxide ions in the presence of electrons. The combination of anode and cathode reactions results in the overall electrolysis of water in a PEM electrolyzer, resulting in the production of hydrogen gas and oxygen gas (SOOD et al., 2020).

Figure 4 – Schematics of PEM electrolyzer.

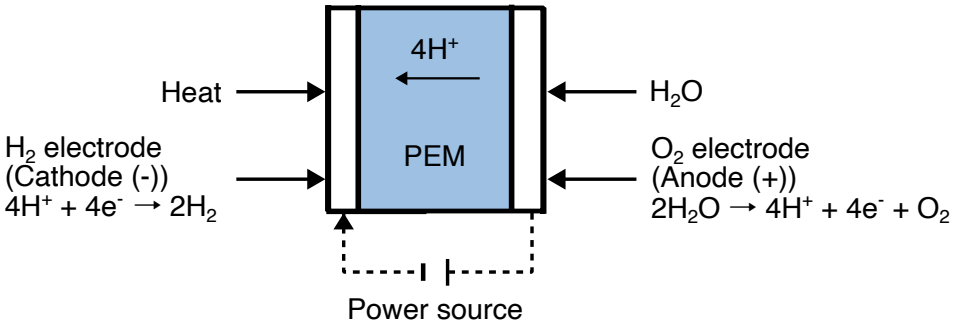

Adapted from Ogbonnaya et al. (2021).

According by Valverde et al. (2013b), the operation of an electrolyzer consists of applying a current to the stack, which leads to the resulting differential potential v_E, given by

$$v_E(i_E) = N_{SE}(v_0 + v_{etd} + v_{ohm} + v_{ion}), \tag{1}$$

where N_{SE} is the number of cells connected in series in the stack; v_0 is the reversible potential; v_{etd} is the electrode overpotential; v_{ohm} is the ohmic overvoltage; and v_{ion} is the ionic overpotential. Therefore, the voltage decrease is a total of four components, which can be represented by the following equations:

$$v_0 = 1.23 - 0.9 \times 10^{-3}\,(T_E - 298) + 2.3\frac{RT_E}{4F}\ln\left(p_{\mathrm{H_2}}^2 \cdot p_{\mathrm{O_2}}\right), \tag{2}$$

$$v_{etd} = \frac{RT_E}{F}\left[\sinh^{-1}\left(\frac{I_E}{2I_a}\right) + \sinh^{-1}\left(\frac{I_E}{2I_c}\right)\right] + \frac{\delta_B}{\sigma_B}I_E, \tag{3}$$

$$v_{ohm} + v_{ion} = \frac{\delta_B i_E}{\sigma_B A_E}, \tag{4}$$

where I_E is the electrolyzer current density in A/cm^2 given by $I_E = \frac{i_E}{A_E}$, and σ_B is the membrane conductivity. The electrolyzer temperature T_E was considered constant at 25 °C. The membrane conductivity, given by:

$$\sigma_B = (0.005139\lambda_E - 0.00326)e^{1268\left(\frac{1}{303} - \frac{1}{T_E}\right)}. \tag{5}$$

The production rate f_{H_2} in mol/s is given by:

$$f_{H_2}(i_E) = \begin{cases} \eta_F(i_E)N_{SE}\dfrac{i_E}{F}, & \text{if } s_E = 1, \quad (6a) \\ 0, & \text{if } s_E = 0, \quad (6b) \end{cases}$$

$s_E \in \{0,1\}$ is a binary variable that describes the operating mode (more details will be given in the next section), and $f_{H_2}^{dm}$ is the flow rate demand of hydrogen leaving the tank.

The Faraday efficiency is given by (HERNÁNDEZ-GÓMEZ; RAMIREZ; GUILDBERT, 2020)

$$\eta_F(i_E) = B_1 + B_2 \mathrm{e}^{\left(\frac{B_3 + B_4 T_E + B_5 T_E^2}{i_E}\right)}, \tag{7}$$

where B_i, for $i \in \{1, \ldots, 5\}$, are empirical constants that can be estimated with real data.

2.1.5 Fuel cell

Hydrogen FC harness the chemical energy of hydrogen to produce electricity and heat through an electrochemical reaction without combustion, making it a clean and efficient energy conversion technology. The following equation represents the core reaction within a hydrogen fuel cell:

$$\mathrm{H_2} + (1/2)\,\mathrm{O_2} \longrightarrow \mathrm{H_2O} + \text{Electricity} + \text{Heat}.$$

This reaction is remarkable because it directly converts the chemical energy stored in hydrogen gas into electrical energy, with water vapor as the only emission. Unlike traditional combustion-based power generation methods, hydrogen fuel cells emit no pollutants or greenhouse gases, positioning them as a cornerstone technology for sustainable energy systems.

The unitized reversible fuel cell (URFC) is a compact version of a fuel cell comprising only one electrochemical system. It can produce hydrogen through the electrolyzer (EL) mode, and electricity in the fuel cell (FC) mode. These reactions can proceed continuously if water and electrical energy are supplied in EL mode, while hydrogen and oxygen are supplied in FC mode.The model couples the electrochemical and thermodynamic characteristics of the process.

According to Ogbonnaya et al. (2021), the reversible potential of the EL mode can be calculated by:

$$v_{F,EL} = v_{rev} + \frac{RT_F}{nF} + \log\left(\frac{p_{H_2}}{p_{H_2}\sqrt{p_{O_2}}}\right) + v_{act} + v_{Ohm} + v_{con}, \tag{8}$$

whereas the reversible potential in the FC mode is:

$$v_{F,FC} = v_{rev} + \frac{RT_F}{nF} + \log\left(\frac{p_{H_2}\sqrt{p_{O_2}}}{p_{H_2}}\right) - v_{act} - v_{Ohm} - v_{con}. \tag{9}$$

The total activation overpotential of a URFC system is given by the sum of the activation overpotential at the positive and negative electrodes:

$$v_{act} = \frac{RT_F}{n\alpha F}\left[\log\left(\frac{i_{loss} + I_F}{i_{o_{anode}}}\right) + \log\left(\frac{i_{loss} + I_F}{i_{o_{cathode}}}\right)\right], \tag{10}$$

where I_F is the density current i_F/A_F.

Figure 5 – Schematics of proton exchange membrane reversible fuel cell.

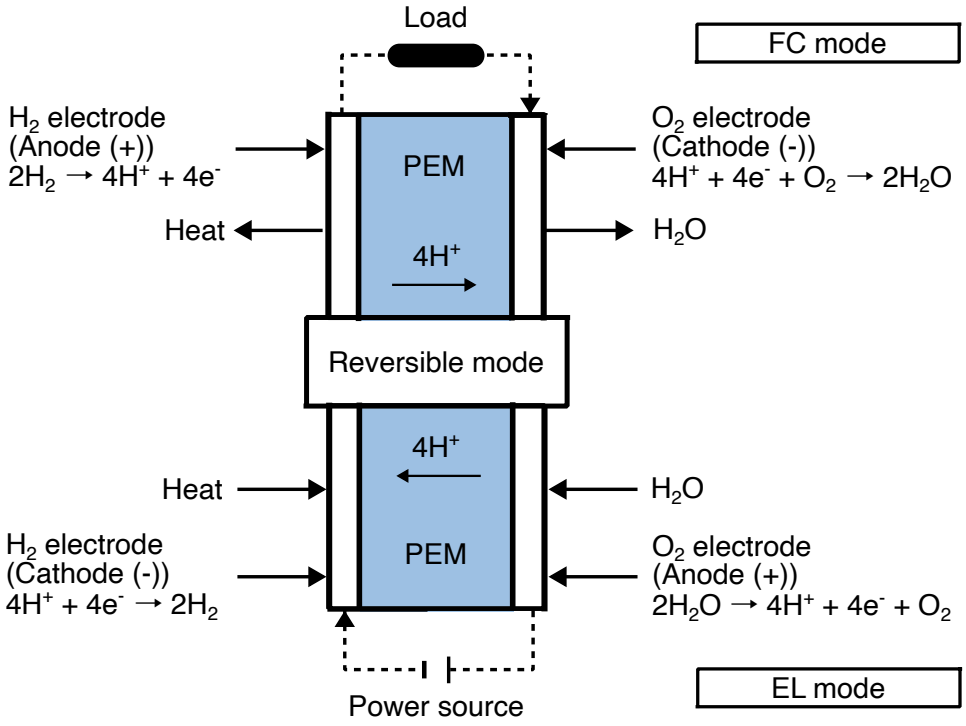

Source: Adapted from Ogbonnaya et al. (2021).

The ohmic overpotential results from the resistance to electricity passing through the conducting plates and connections, protons flowing through the polymeric membrane, and the resistance due to specific contacts. The sum of these components provides the total ohmic overpotential:

$$v_{Ohm} = I_F \left(R_{elect} + R_{ion} + R_{cr}\right). \tag{11}$$

Concentration overpotentials arise from incomplete removal of reactants, products, and ions in the system. The concentration of protons across the polymeric membrane changed according to the operating conditions of the URFC. Furthermore, water formation during the FC mode requires the efficient transport of protons from the positive electrode to the negative electrode passing through the membrane. The total concentration overpotential in the URFC system is given by the sum of the overpotentials at the positive and negative electrodes:

$$v_{conc} = \frac{RT_F}{nF}\left[\log\left(1 - \frac{I_E}{i_{l_{anode}}}\right) + \log\left(1 - \frac{I_E}{i_{l_{cathode}}}\right)\right]. \tag{12}$$

Finally, the voltage in the URFC is given by:

$$v_F(i_F) = \begin{cases} N_{SF} v_{F,FC} & \text{for } s_F = 0 \quad (13a) \\ N_{SF} v_{F,EL} & \text{for } s_F = 1\,, \quad (13b) \end{cases}$$

where N_{SF} is the number of cell in the stack, and s_F is a binary variable the describe the operating mode, $s_F = 0$ in FC mode and $s_F = 1$ in EL mode. The power in the

URFC is expressed by

$$P_F(i_F) = \begin{cases} i_F v_F & \text{if } s_F = 0 \quad (14a) \\ -i_F v_F & \text{if } s_F = 1\ . \quad (14b) \end{cases}$$

Hydrogen generation varies with power consumption in the EL mode, and power generation varies with hydrogen consumption in the FC mode. The following equation expresses the net balance of hydrogen in the URFC system:

$$f_{H_2}(i_F) = \begin{cases} -N_S i_F / F & \text{if } s_F = 0 \quad (15a) \\ N_S i_F / F & \text{if } s_F = 1 \quad (15b) \end{cases}$$

where F is the Faraday constant.

2.2 SOLAR ENERGY

2.2.1 Renewable Energy Overview

In the last four decades, the world energy demand and carbon dioxide (CO_2) production have more than doubled and, according to the projections of IEA (2020a), which incorporates existing energy policies as well as an assessment of the results likely to stem from the implementation of announced political intentions, an increase of 6.19% in the world production of CO_2 is expected until 2040. In a scenario of sustainable development with public policies that outlines an integrated approach to achieving internationally agreed objectives on climate change, air quality and universal access to energy, it is expected that CO_2 emissions would reduce 52.86%. The CO_2 emissions data by region and perspective for global emissions in the 2040 scenario are shown in Figure 6.

In 2018, only 9.8 % of the total energy generated in the world came from renewable sources, considering hydro, this value reaches up to 25.6 % (IEA, 2020b). In the same period, Brazil was the third country in the world in the production of renewable energies with 495 TW h, behind only China and the United States. However, despite the good results, in the last ten years, Brazil has been experiencing a significant increase in the use of non-renewable energy sources, as can be seen in Figure 7.

Figure 7 – Primary Energy Production in Brazil from 1970 to 2022.

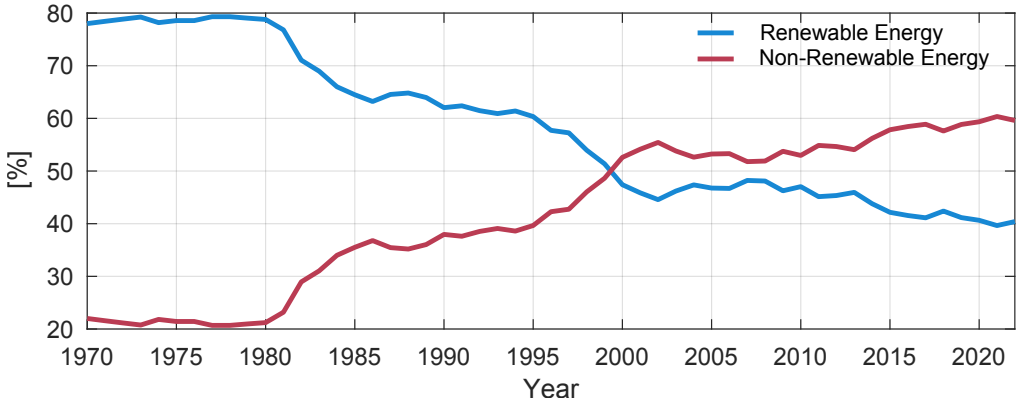

Source: Adapted from Balanço Energético Nacional Interativo (2023d).

According to the 2023 National Energy Balance Report with the base year 2022 (BRASIL, 2023c), of the total electricity generated in the country in that year, 61.9% came from hydraulic energy, while 10% came from oil products, coal, and natural gas. Nuclear energy accounted for 2.1% of the total electricity produced and biomass 8%. Other renewable and non-renewable sources produced 18% of the country's total electricity that year.

In Brazil, investments in solar and wind energy have increased a lot in recent years and several regions of the country have favorable conditions to exploit these en-

Figure 6 – CO_2 emissions data by region and perspectives for global CO_2 emissions by region in the 2040 scenario.

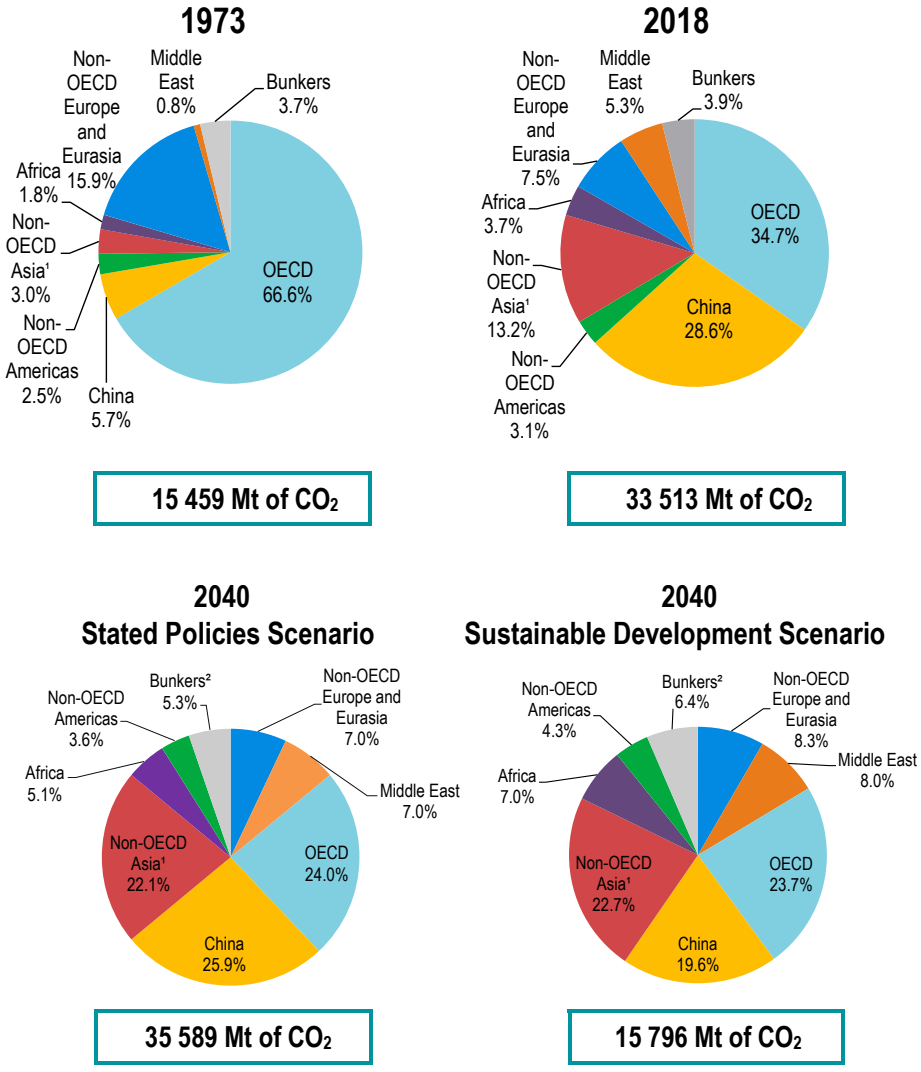

1. Non-OECD Asia excludes China. 2. Includes international aviation and international marine bunkers. 3. CO_2 emissions are from fossil fuel combustion only.

Source: Adapted from IEA (2020a).

ergy sources (TIBA, 2000). According to the Ten-Year Energy Expansion Plan (BRASIL, 2020), the share of renewable energy in total electricity produced in 2030 will be more than 31% without considering hydraulic energy. In addition, the perspective for the coming years is that renewable energy sources will increase their total contribution, representing 86% of the installed electricity generation capacity.

2.2.2 Photovoltaic panel

The PV solar panels consist of a photovoltaic cell array exposed to solar radiation that generates a direct current (DC). It flows from n-type to a p-type semiconductor at each cell junction and is based on a physical principle known as photoelectric effect (ZWEIBEL, 2013). The bandgap of the semiconductor material and its ability to absorb

photon energy over a wide range determine the photovoltaic conversion efficiency. In the case of gallium arsenide (GaAs), theoretical maximum values of the order of 30% are reached (GREEN, 1982).

A commonly used model in the literature to predict the power output of photovoltaic solar panels is the standard model, also known as the single-diode model. A representation of this model is shown in Figure 8, where i_{CS} and v_{CS} are the electric current and voltage in one cell of the panel, respectively.

Figure 8 – Equivalent circuit of cell of a photovoltaic solar panel.

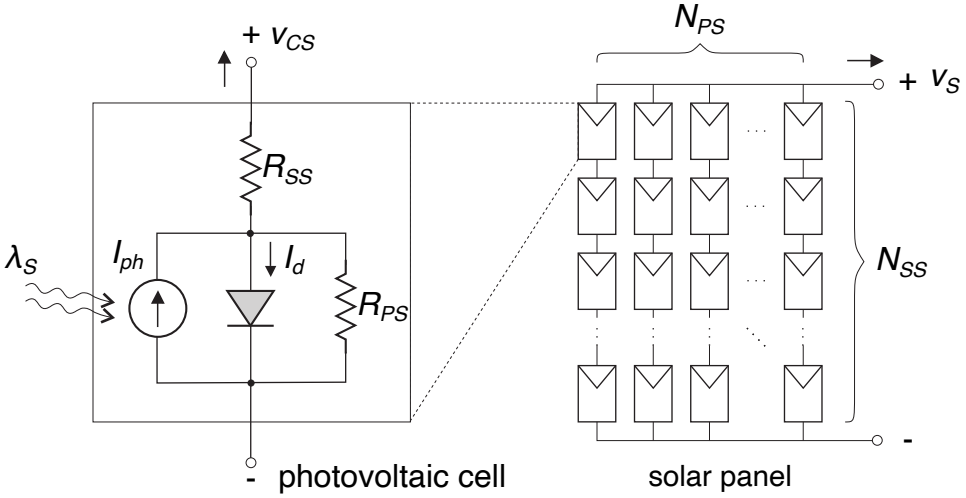

Source: Adapted from García-Clúa (2013).

This model incorporates an electric current source dependent on solar irradiation I_{ph}, a diode, and two resistors. Assuming a solar panel with N_{PS} modules in parallel and N_{SS} cells in series, and disregarding the resistances R_{SS} and R_{PS} the relationship between the current i_S and the voltage v_S at the terminals depends on the normalized solar radiation λ_S and is given by (DE ANDRADE et al., 2020):

$$i_S(v_S) = N_{PS}\left[I_{ph}(\lambda_S) - I_d\right], \tag{16}$$

with

$$\begin{aligned}
V_T &= \frac{KT_s}{q}, \\
I_{ph} &= \lambda_S[I_{sc} + K_L(T_S - T_{SR})], \\
I_d &= I_{rs}\left(e^{\frac{v_S}{N_{SS}V_T}} - 1\right), \\
I_{rs} &= I_{or}\left(\frac{T_S}{T_{SR}}\right)^3 e^{\left[qE_g\left(\frac{T_r^{-1} - T_S^{-1}}{KA_S}\right)\right]},
\end{aligned}$$

were T_S is the temperature of the panel and λ_S is the solar radiation.

A DC/DC converter will be considered at the output of the solar panel for connection to a DC microgrid. This converter acts as an interface between the solar panel and

the common bus, reducing the voltage v_S to the value V_{DC}. Therefore a boost elevator converter was selected, whose duty cycle δ_S imposes the following voltage inequality:

$$0 < \delta_S = 1 - \frac{V_{DC}}{v_S} < 1. \tag{17}$$

The converter controller commands the electronic switch to set the desired duty cycle $\delta_S^{\max}$ The maximum power point (MPP) represents the operating point at which the power output of the photovoltaic panel is higher. The MPP can be influenced by changes in natural conditions, such as temperature and irradiation. A maximum power point tracking (MPPT) algorithm is generally used to maintain the MPP (BOLLIPO; MIKKILI; BONTHAGORLA, 2020). Assuming that the system is equipped with an MPPT algorithm, the panel voltage can be calculated as follows (DE ANDRADE et al., 2019):

$$v_S(t) = N_{SS} V_T \left[W\left(e^{\frac{I_{ph}(\lambda_S)}{I_{rs}} + e} \right) - 1 \right], \tag{18}$$

where, W is the Lambert function. The Lambert function must be solved using numerical methods, as it cannot be expressed in terms of elementary functions. In this study, the following approximation was used:

$$W(z) = (1+\varepsilon)\ln\left[\frac{1.2z}{\ln\left[\frac{2.4z}{\ln(2.4z+1)}\right]}\right] - \varepsilon \ln\left[\frac{2z}{\ln(2z+1)}\right],$$

with $\varepsilon = 0.4586887$. This approximation guarantees a numerical error of less than 0.2% for $z \geq 3 \times 10^{-5}$ (BATZELIS et al., 2020).

2.2.3 Solar Radiation

In order to compute the values of I_{ph} in (16) more precisely, the changing pattern of λ_S is now specified. Note that the time interval [0, 24] of one day is divided into three subintervals: $[0,\ t_N)$, $[t_N,\ t_D)$, and $[t_D,\ 24]$ where t_N represents sunrise and t_D represents sunset, with the condition that $0 < t_N < t_D < 24$. The values of t_N and t_D depend on the day of the year. Then, the solar radiation is described as follows:

$$\lambda_S(t) = \begin{cases} s(t), & \text{if } t \in [t_N,\ t_D), \\ 0, & \text{if } t \in [0,\ t_N) \text{ or } t \in [t_D,\ 24], \end{cases} \tag{19}$$

where $s : [t_N,\ t_D) \to \mathbb{R}_+$ is a function that describes the variation in solar radiation during the day such that $0 < s(t) \leq 1$, $\forall\, t \in [t_N,\ t_D)$.

2.3 OPTIMAL CONTROL

2.3.1 Single-phase Optimal Control

Optimal control is an extension of the calculus of variations and aims to determine control signals that will cause a process to satisfy some constraints while minimizing (or maximizing) a specific cost function (KIRK, 2004; WILLEMS, 1996). The history of optimal control theory and its roots in other fields, such as classic control and calculus of variations, was presented by Bryson (1996). Nowadays optimal control has several applications in engineering problems including train control (HOWLETT; PUDNEY P. J.AND VU, 2009), sensor scheduling (WU et al., 2020), hybrid electric vehicle (SCIARRETTA; BACK; GUZZELLA, 2004), and hybrid power systems (LIN; ZHENG, 2011).

The advantages of a control system based on the optimal control theory stand out when it comes to multiple-input multiple-output systems, where traditional performance measures such as settling time, static gain, and phase margin may be inadequate for describing the desired behavior. There are several ways to formulate an optimal control problem (OCP), which may depend on the performance index, the type of time domain (continuous, discrete), the presence of different types of constraints, and what variables are free to be chosen. The interested reader is referred to Kirk (2004) for more details. In what follows, the basic concepts of the optimal control theory in continuous time and its solution using numerical methods will be discussed.

The following equation is the most common framework to describe an OCP in continuous time:

$$\underset{t_i,t_f,\boldsymbol{u}(t)}{\text{minimize}} \quad \int_{t_i}^{t_f} L(t,\boldsymbol{x}(t),\boldsymbol{u}(t))\,dt, \tag{20a}$$

$$\text{subject to} \quad \dot{\boldsymbol{x}} = \boldsymbol{f}(t,\boldsymbol{x}(t),\boldsymbol{u}(t)), \tag{20b}$$

$$\boldsymbol{x}(t_i) = \boldsymbol{x}_0, \tag{20c}$$

$$\boldsymbol{g}(t,\boldsymbol{x}(t),\boldsymbol{u}(t)) \leq \boldsymbol{0}, \tag{20d}$$

where $\boldsymbol{x} \in X \subset \mathbb{R}^{n_x}$ is the states vector, being X the set of allowable state values, $\boldsymbol{u} \in U \subset \mathbb{R}^{n_u}$ is the vector of control variables, being U the set of allowable control values, $f : [t_i,t_f] \times \mathbb{R}^{n_x} \times \mathbb{R}^{n_u} \to \mathbb{R}^{n_x}$ is a given vector valued function, and t_i and t_f, with $0 < t_i < t_f$, are the initial and the final time, respectively. The initial condition of the system is given by $\boldsymbol{x}_0 \in \mathbb{R}^{n_x}$, and $g : [t_i,t_f] \times \mathbb{R}^{n_x} \times \mathbb{R}^{n_u} \to \mathbb{R}^{n_g}$ is the path inequality constraint. Finally, the running cost, also called Lagrange term, is given by $L : [t_i,t_f] \times \mathbb{R}^{n_x} \times \mathbb{R}^{n_u} \to \mathbb{R}$.

2.3.2 Open-loop vs Closed-loop solutions of OCPs

There are two primary types of solutions for an OCP: open-loop and closed-loop. An open-loop solution entails a succession of controls presented as a function of time $u(t)$, which guides the system from an initial state A to a final state B. This succession of controls is known as an optimal trajectory. Conversely, a closed-loop solution involves a control law $u(x)$ or policy that directs the system from any state in state space A to state B (KELLY, 2017a). An illustration of both solutions is shown in Figure 9.

Figure 9 – Illustration of an open-loop solution and a closed-loop solution.

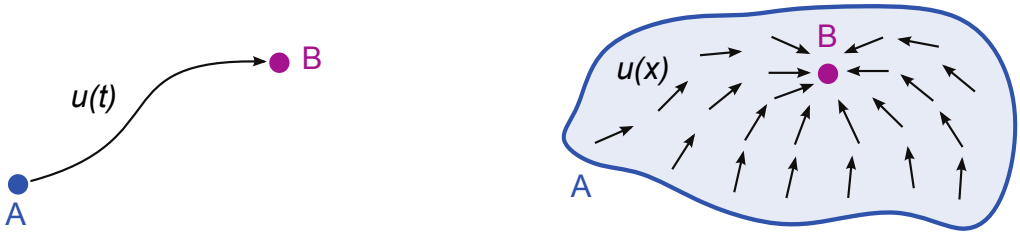

(a) Open-Loop Solution (optimal trajectory) (b) Closed-Loop Solution (optimal policy)

Source: Adapted from Kelly (2017a).

2.3.3 Transcription Methods

There are three basic approaches to the computational solution of an OCP: (*i*) dynamic programming, (*ii*) indirect methods, and (*iii*) direct methods (KELLY, 2017b).

Dynamic programming involves solving the Hamilton-Jacobi-Bellman equation. One advantage of this approach is the potential to obtain an explicit optimal control law. For example, for linear dynamical systems, the Hamilton-Jacobi-Bellman equation degenerates into a Riccati equation, which is very easy to solve. However, for nonlinear cases, the Hamilton-Jacobi-Bellman equation may be hard to solve analytically. When discretizing the Hamilton-Jacobi-Bellman equation, the problem can become impossible due to its sheer size, which can occur even for a relatively small number of states. This phenomenon is known in the literature as the Bellman's curse of dimensionality (LEEK, 2016).

Indirect methods adhere to the *first-optimize-then-discretize* approach, where the Pontryagin's maximum principle is employed to transform the OCP (20a)-(20d) into a Hamilton Boundary Value Problem (HBVP). The optimal trajectories are subsequently derived by solving this HBVP. The strengths of these methods lie in their well-established theoretical foundation and often commendable computational efficiency. For a comprehensive overview of indirect methods applied in chemical engineering problems, one may refer to (ANDRÉS-MARTÍNEZ; PALMA-FLORES; RICARDEZ-SANDOVAL, 2022). However, indirect methods can exhibit numerical instability and may pose challenges in implementation and initialization (KELLY, 2017b).

Direct methods are based on *first-discretize-then-optimize*. First, the OCP is discretized, and in the subsequent stage, an optimization algorithm is applied to solve the resulting nonlinear programming problem (NLP). Well-established nonlinear optimization algorithms are often employed for solving this NLP. An advantage of direct methods lies in their effective handling of inequality constraints by proficient NLP solvers. However, a drawback includes the computational effort involved, and the outcome represents an open-loop solution. Figure 10 summarizes the advantages and disadvantages of the indirect and direct methods.

Figure 10 – Classification of different transcription methods.

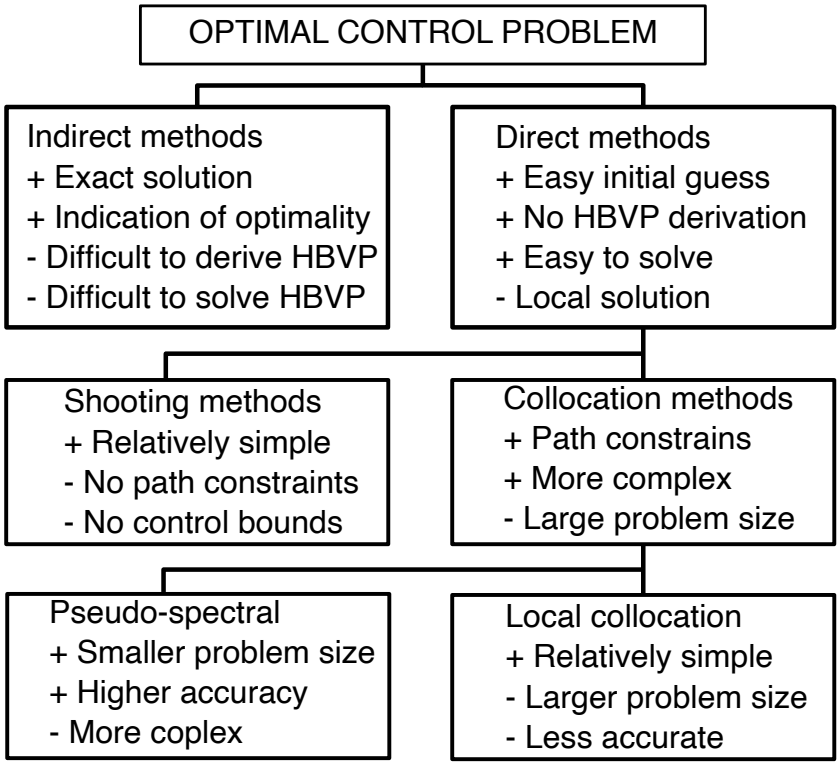

Source: Adapted from Swannet (2022).

2.3.4 Nonlinear program

The NLP problem involves finding a limited number of variables that can minimize an objective function or a performance index while abiding by a set of constraints. It is also referred to as parameter optimization. Linear programming, quadratic programming, and least square problems are all special instances of NLP (BETTS, 2010). Unlike in OCP, an NLP problem does not include any dynamics. The general NLP problem can be stated as:

$$\begin{aligned} &\text{minimize} && j(\boldsymbol{w}), \\ &\text{subject to} && \boldsymbol{g}^{min} \leq \boldsymbol{g}(\boldsymbol{w}) \leq \boldsymbol{g}^{max}, \\ & && \boldsymbol{w}^{min} \leq \boldsymbol{w} \leq \boldsymbol{w}^{max}, \end{aligned} \tag{21}$$

where $\boldsymbol{w}$ is the vector of variables with lower and upper bounds, $\boldsymbol{w}^{min}$ and $\boldsymbol{w}^{max}$, j is the cost function, and $\boldsymbol{g}$ is the vector with the nonlinear constraints. The constraint functions, $\boldsymbol{g}(\boldsymbol{w})$, have lower and upper bounds, $\boldsymbol{g}^{min}$ and $\boldsymbol{g}^{max}$. To impose equality constraints, set $g^{min} = g^{max}$.

2.3.5 Direct transcription methods

The central concept of direct methods involves the approximation of the continuous-time dynamics of the system by discretizing the trajectory into a sequence of discrete-time points. Figure 11 exemplifies this approximation process. Note that the continuous function is partitioned into distinct segments, with knot points as boundaries for each segment. Several direct transcription methods can be found in the literature, but they can all be divided into two classes: *shooting methods* and *simultaneous methods*. The difference is based on how each method enforces the constraint on the system dynamics. Shooting methods use a simulation to explicitly enforce the system dynamics. Simultaneous methods enforce the dynamics in a series of points along the trajectory. In this dissertation the Hermite-Simpson (HS) collocation method is used to solve the OCP since it provides solutions with high-order accuracy (BETTS, 2010).

Figure 11 – Function approximation using a quadratic spline.

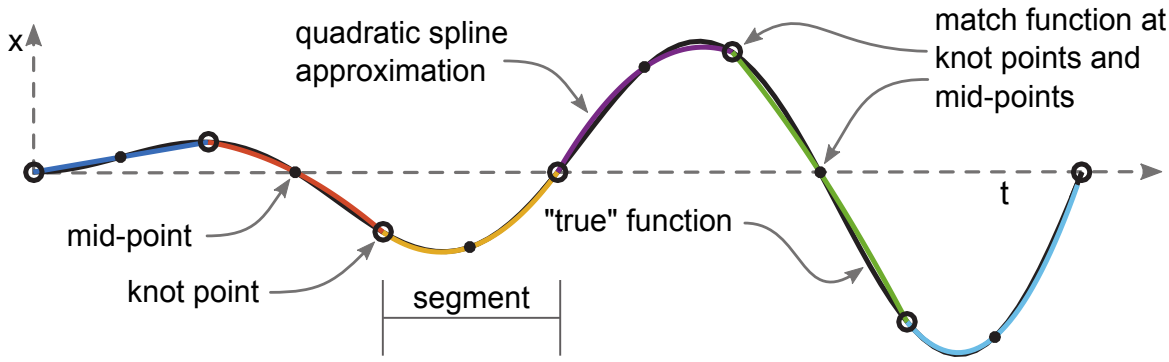

Source: Adapted from Kelly (2017a).

2.3.5.1 Hermite-Simpson Collocation

Hermite-Simpson collocation is a direct method, classified as simultaneous method, as shown in Figure 10. HS collocation employs the same discretization approach as other simpler methods, such as trapezoidal collocation, but leverages higher-order interpolation polynomials to achieve more precise numerical results.

The first step in the Hermite-Simpson collocation approach is to discretize the time into N segments, where $N \in \mathbb{N}$:

$$t_i = t_0 < t_1 < \cdots < t_N = t_f.$$

These segments have duration $h_k = t_k - t_{k-1}$ for $k \in \{1, \ldots, N\}$, that is,

$$\begin{aligned} t_0 &= t_i, \\ t_{k+1} &= t_k + h_k, \quad k \in \{0,1,\ldots,N-1\}. \end{aligned}$$

On each mesh point of the discretized time, the control and state trajectories are defined as

$$\mathbf{u}_k = \mathbf{u}(t_k), \qquad \mathbf{x}_k = \mathbf{x}(t_k), \qquad \text{for } k \in \{0, \ldots N\}.$$

The path constraints in (20d) are handle similarly:

$$\boldsymbol{g}_k(t_k,\boldsymbol{x}_k,\boldsymbol{u}_k) = g(t_k, \boldsymbol{x}(t_k), \boldsymbol{u}(t_k)) \leq 0, \qquad \text{for } k \in \{0, \ldots N\}. \tag{22}$$

The next step is to add the collocation points, which are the constraints used to construct the approximate system dynamics. They are defined as

$$\boldsymbol{x}_{k+1} - \boldsymbol{x}_k = \frac{1}{6} h_k \left(\boldsymbol{f}_k + 4\boldsymbol{f}_{k+\frac{1}{2}} + \boldsymbol{f}_{k+1} \right), \qquad \text{for } k \in \{0, \ldots N-1\} \tag{23}$$

where $\boldsymbol{f}_k = \boldsymbol{f}(t_k,\boldsymbol{x}(t_k),\mathbf{u}(t))$.

Note that (23) requires a second collocation equation since at the midpoint of the segment $\boldsymbol{f}_{k+\frac{1}{2}}$ is a function of the state $\boldsymbol{x}_{k+\frac{1}{2}}$, which is not known a prior. The value of the state at this midpoint can be computed by constructing an interpolant for the state trajectory and then evaluating it at the midpoint of the interval:

$$\boldsymbol{x}_{k+\frac{1}{2}} = \frac{1}{2} \left(\boldsymbol{x}_k + \boldsymbol{x}_{k+1} \right) + \frac{h_k}{8} \left(\boldsymbol{f}_k - \boldsymbol{f}_{k+1} \right), \qquad \text{for } k \in \{1, \ldots N-1\}. \tag{24}$$

Finally, the cost function (20a) is approximated using Simpson's quadrature rule for integrals. More precisely, the functional L is approximated as the following piecewise quadratic function:

$$\int_{t_0}^{t_F} L(t, \boldsymbol{x}(t), \boldsymbol{u}(t))\, dt \approx \sum_{k=0}^{N-1} \frac{h_k}{6} \left(L_k + 4L_{k+\frac{1}{2}} + L_{k+1} \right), \tag{25}$$

where $L_k = L(t_k,\boldsymbol{x}(t_k), \boldsymbol{u}(t_k))$.

Collecting all the discrete approximations of the OCP (20) developed in this section, the following NLP is obtained:

$$\underset{t_0,t_N,\boldsymbol{x}_k,\boldsymbol{u}_k}{\text{minimize}} \quad \sum_{k=0}^{N-1} \frac{h_k}{6} \left(L_k + 4L_{k+\frac{1}{2}} + L_{k+1} \right), \tag{26a}$$

$$\text{subject to} \quad \boldsymbol{x}_{k+1} - \boldsymbol{x}_k = \frac{1}{6} h_k \left(\boldsymbol{f}_k + 4\boldsymbol{f}_{k+\frac{1}{2}} + \boldsymbol{f}_{k+1} \right), \tag{26b}$$

$$\boldsymbol{x}_{k+\frac{1}{2}} = \frac{1}{2} \left(\boldsymbol{x}_k + \boldsymbol{x}_{k+1} \right) + \frac{h_k}{8} \left(\boldsymbol{f}_k - \boldsymbol{f}_{k+1} \right), \tag{26c}$$

$$\boldsymbol{g}_k(t_k,\boldsymbol{x}_k,\boldsymbol{u}_k) \leq \mathbf{0}, \tag{26d}$$

Once the NLP (26) is solved, the values of state and control trajectories are determined at each collocation point. The subsequent step is to construct a continuous trajectory that can connect the collocation points. The interpolation, illustrated in Figure 12, of the control variables is expressed as:

$$\boldsymbol{u}(t) = \frac{2}{h_k^2}\left(\tau - \frac{h_k}{2}\right)(\tau - h_k)\,\boldsymbol{u}_k - \frac{4}{h_k^2}(\tau)\,(\tau - h_k)\,\boldsymbol{u}_{k+\frac{1}{2}} + \frac{2}{h_k^2}(\tau)\left(\tau - \frac{h_k}{2}\right)\boldsymbol{u}_{k+1}, \tag{27}$$

where $t_{k+\frac{1}{2}} = \frac{1}{2}(t_k + t_{k+1})$. Similarly, the interpolation,illustrated in Figure 12 , of the states is given by:

$$\begin{aligned}\boldsymbol{x}(t) =& \boldsymbol{x}_k + \boldsymbol{f}_k(t - t_k) + \frac{1}{2h_k}\left(-3\boldsymbol{f}_k + 4\boldsymbol{f}_{k+\frac{1}{2}} - \boldsymbol{f}_{k+1}\right)(t - t_k)^2 \\ &+ \frac{1}{3h_k^2}\left(2\boldsymbol{f}_k - 4\boldsymbol{f}_{k+\frac{1}{2}} + 2\boldsymbol{f}_{k+1}\right)(t - t_k)^3.\end{aligned} \tag{28}$$

Figure 12 – Illustration of the quadratic and cubic interpolations used in Hermite–Simpson collocation.

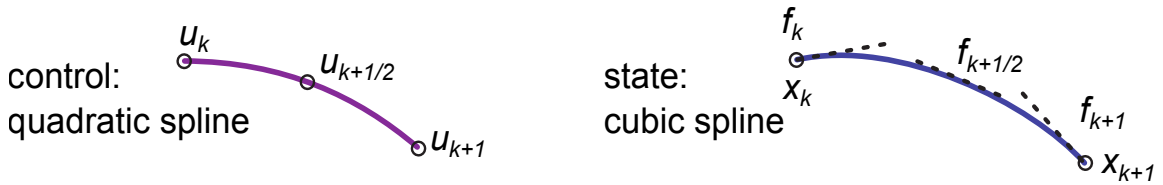

Source: Adapted from Kelly (2017a).

2.3.6 Multi-phase Optimal Control

Multi-phase optimal control strategies are suitable to solve OCP where the system dynamics can change since the evolution of the states can present discontinuities. Loosely speaking, these methodologies split the time domain associated with the OCP into small intervals, which are called *phases*, where the dynamic is the same or is continuous, and solve a single-phase OCP, such as the one presented in (20), individually. Note that this allows us to have different variable bounds, error tolerances, dynamic equations, cost functions, and even transcription methods. The phases are linked together by the phase boundary constraints, which ensure that the states, inputs, and time in the first point of a phase is equal to those in the last point of the previous phases.

Let the subscript p represents the phase index such that $p \in \{1, \ldots, N_p\}$, with $N_p \in \mathbb{N}$. Further, let $\mathbf{x}_p \in X_p \subset \mathbb{R}^{n_{x_p}}$ and $\mathbf{u}_p \in U_p \subset \mathbb{R}^{n_{x_p}}$ represent the state and the control vectors of the phase p, respectively. Define t_{i_p} and t_{f_p}, with $t_{i_p} < t_{f_p}$, as the initial and final time of the phase p, respectively. Additionally, let $t_p \in [t_{i_p}, t_{f_p}]$ represent the continuous time variable in phase p. Figure 13 exemplifies the above concepts in a

system with two phases. In this case, a time constraint at $t_{i_2} = t_{f_1}$ is set to ensure that phase 2 follows phase 1, and a state constraint $x_2(t_{i_2}) = x_1(t_{f_1})$ is imposed to maintain the continuity of the state. Notably, the control variable is not constrained, allowing for signal discontinuity.

Figure 13 – Example of a system with two phases, $N_p = 2$.

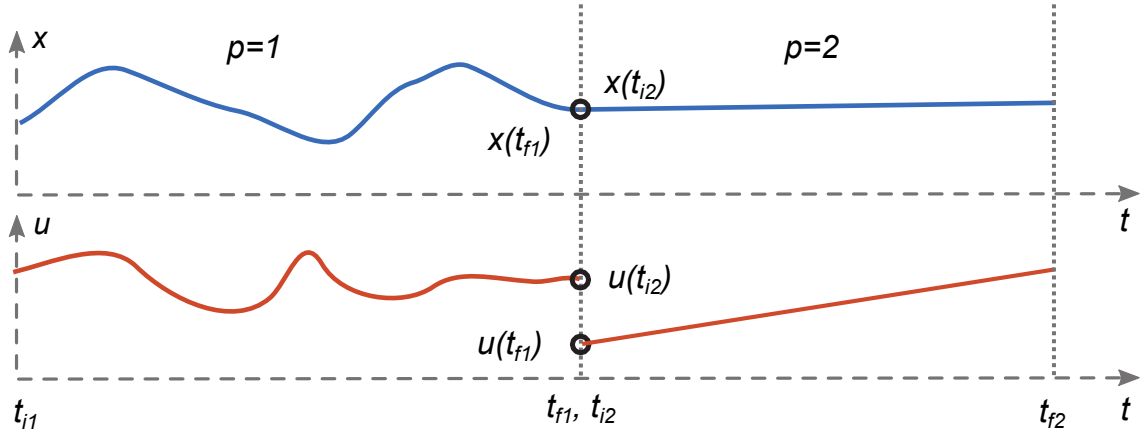

Source: Created by the author (2024).

The continuous-time multi-phase OCP in the Standard form is represented by the following equation, which is an extension of the problem (20):

$$
\begin{aligned}
\underset{t_{i,p},t_{f,p},\boldsymbol{u}_p(t_p)}{\text{minimize}} \quad & \sum_{p=1}^{N_p} \int_{t_{i_p}}^{t_{f_p}} L_p(t,\boldsymbol{x}_p(t),\boldsymbol{u}_p(t))\,dt \\
\text{subject to} \quad & \dot{\boldsymbol{x}}_p(t_p) = f_p(t_p,\boldsymbol{x}_p(t_p),\boldsymbol{u}_p(t_p)) \quad t_p \in [t_{i_p}, t_{f_p}], \\
& \boldsymbol{g}(t_p,\boldsymbol{x}_p(t_p),\boldsymbol{u}_p(t_p)) \leq \boldsymbol{0}, \\
& \boldsymbol{x}_{p+1}(t_{i_{p+1}}) = \boldsymbol{x}_p(t_{f_p}), \\
& \boldsymbol{x}_1(t_{i_1}) = \boldsymbol{x}_0,
\end{aligned}
\tag{29}
$$

where $f_p : [t_{i_p},t_{f_p}] \times \mathbb{R}^{n_{xp}} \times \mathbb{R}^{n_{up}} \to \mathbb{R}^{n_{xp}}$ is a given vector valued function and and $g : [t_{i_p},t_{f_p}] \times \mathbb{R}^{n_{xp}} \times \mathbb{R}^{n_{up}} \to \mathbb{R}^{n_{gp}}$ is the path inequality constraint. Finally, the running cost of the phase p, is given by $L_p : [t_{i_p},t_{f_p}] \times \mathbb{R}^{n_{xp}} \times \mathbb{R}^{n_{up}} \to \mathbb{R}$.

Note that the direct transcription of the problem (29) is similar to the single-phase OCP discussed in Section 2.3.5. Therefore this process is omitted here for the sake of brevity.

2.3.7 Hybrid Optimal Control

In the context of hybrid OCPs, or mixed-integer OCPs, the optimization problem has continuous and discrete decision variables. These problems commonly arise in various engineering applications, such as the hydrogen production systems studied in

this dissertation. A general formulation of an hybrid OPC can be given as

$$\begin{aligned} \underset{t_i,t_f,\boldsymbol{u}(t),\boldsymbol{z}(t)}{\text{minimize}} \quad & \int_{t_i}^{t_f} L(t,\boldsymbol{u}(t),\boldsymbol{x}(t),\boldsymbol{z}(t))\,dt \\ \text{subject to} \quad & \dot{\boldsymbol{x}}(t) = \boldsymbol{f}(t,\boldsymbol{x}(t),\boldsymbol{u}(t),\boldsymbol{z}(t)), \\ & \boldsymbol{g}(t,\boldsymbol{x}(t),\boldsymbol{u}(t),\boldsymbol{z}(t)) \leq \boldsymbol{0}, \\ & \boldsymbol{x}(t_i) = \boldsymbol{x}_0, \end{aligned} \tag{30}$$

where $\boldsymbol{x} \in X^z \subset \mathbb{R}^{n_{xz}}$ is the states vector, being X^z the set of allowable state values, $\boldsymbol{u} \in U^z \subset \mathbb{R}^{n_{uz}}$ is the vector of continuous control variables, being U^z the set of allowable control values, $\boldsymbol{z} \in \mathbb{R}^{n_z}$ is the vector of discrete control variables, $f : [t_i,t_f] \times \mathbb{R}^{n_x} \times \mathbb{R}^{n_u} \times \mathbb{R}^{n_z} \to \mathbb{R}^{n_{xz}}$ is a given vector valued function, and t_i and t_f, with $0 < t_i < t_f$, are the initial and the final time, respectively. The initial condition of the system is given by $\boldsymbol{x}_0 \in \mathbb{R}^{n_{xz}}$, and $g : [t_i,t_f] \times \mathbb{R}^{n_x} \times \mathbb{R}^{n_u} times \to \mathbb{R}^{n_{gz}}$ is the path inequality constraint. Finally, the running cost is given by $L : [t_i,t_f] \times \mathbb{R}^{n_x} \times \mathbb{R}^{n_u} \times \mathbb{R}^{n_z} \to \mathbb{R}$.

The direct transcription of a hybrid OCP results in a mixed-integer nonlinear program (MINLP) problem, which is generally NP-hard (ROBUSCHI et al., 2021). MINLP problems combine the modeling capabilities of Mixed-Integer Linear Programming (MILP) and Nonlinear Programming (NLP). Methods such as branch-and-bound (BB) and outer approximation (OA) are used to solve a MINLP problem (KRONQVIST et al., 2018). In this work, the integer variables z_k were held constant for the duration of a discretization segment $\{t_k, t_{k+\frac{1}{2}}, t_{k+1}\}$.

2.3.8 Software Solutions for Optimal Control Problems

Once an OCP has been transcribed, it then must be solved by a NLP solver. The following sections describe some details of available programs and packages that are helpful when working with each of them.

2.3.8.1 Turnkey Solvers

Multiple software programs have been developed that employ direct methods, which are extensively utilized in diverse areas of engineering. GPOPS II (PATTERSON; RAO, 2014) is a Matlab toolkit that uses pseudo-spectral methods to solve optimal control problems. It employs large-scale NLP solvers like SNOPT and IPOPT for the transcribed NLP problems. DIDO (ROSS, 2020) uses pseudo-spectral methods and sequential quadratic programming (SQP) to solve OCPs. SPARTAN (SAGLIANO; SEELBINDER; THEIL, 2021) is also a tool based on pseudo-spectral methods. IClocs2 (NIE; FAQIR; KERRIGAN, 2018) is another software suite for solving OCPs for Matlab and Simulink, which implements local and pseudo-spectral methods. PySCP (ZHANG, D.; ZHANG, Y., 2022) is a Python package to solve OCPs using sequential convex pro-

gramming methods. Focus on solver multi-phase OCPs, mpopt (THAMMISETTY, 2020) is another option of Python package.

2.3.8.2 Building Blocks for Solver Developent

CasADi is an open-source software framework designed to support algorithmic differentiation (AD), drawing its name and syntactical inspiration from the similarities it shares with computer algebra systems. This framework is primarily dedicated to the domain of numerical optimization, including the resolution of initial value problems in ordinary differential equations, quadratic programming, NLPs, and mixed-integer NLPs (ANDERSSON et al., 2019) . Developed in C++, CasADi is accessible through comprehensive interfaces in Python, MATLAB, or Octave, enhancing its utility and application across various computing environments.

Within the ecosystem of optimization tools, Ipopt appears as an open-source software package to solve NLP problems developed in C++. It is part of the Computational Infrastructure for Operations Research (COIN-OR) project. However, it needs a solver for linear equation systems, accommodating a variety of solvers such as HSL, Pardiso, SPRAL, MUMPS, or WSMP (WACHTER; BIEGLER, 2006).

In conjunction, Bonmin, which is another integral tool within the COIN-OR suite written in C++, specializes in tackling MINLP problems. This tool leverages the capabilities of Cbc, a solver dedicated to mixed-integer linear programming problems, and Ipopt, illustrating a synergistic approach within the optimization toolkit. It adeptly decomposes mixed-interger NLPs challenges into mixed-integer linear programming and NLP components, showcasing a strategic methodology for problem-solving in this complex domain (BONAMI et al., 2008).

The integration of CasADi with optimization solvers such as Ipopt and Bonmin facilitates the implementation of a broad spectrum of transcription methods to solve OCPs, from single-phase to multi-phase and hybrid optimal controllers.

2.4 RELATED WORKS

The operation time of an electric vertical takeoff and landing (eVTOL) aircraft is restricted by battery autonomy. Pradeep and Wei (2018) presents a formulation of a fixed final time multi-phase optimal control problem with energy consumption serving as the cost function for a eVTOL aircraft. The proposed multi-phase optimal control problem formulation and its numerical solution enable the eVTOL aircraft to reach the required time of arrival with an optimal speed profile for the most energy-efficient arrival. The problem comprises three distinct phases: cruise, transition, and descent (arrival). The solution was obtained using GPOPS-II, a commercial software for MATLAB.

In de Andrade et al. (2019), a study on the optimal control of a hydrogen production system powered by photovoltaic solar energy and assisted by the grid was presented. The system utilized an alkaline electrolyzer and a dynamic model was proposed to account for the system's main features, with the electrolyzer current serving as the control variable. The control law was determined to optimize grid energy consumption while accounting for the variability of solar energy. The solution was obtained through the application of Pontryagin's maximum principle to solve the Hamiltonian boundary-value problem (HBVP), resulting in an explicit piecewise continuous control law.

In de Andrade et al. (2020), the authors continue their work on the hydrogen production plant powered by photovoltaic solar energy and assisted by the electric grid by proposing a linear hybrid model predictive controller (HMPC). This control strategy is compared to the optimal control previously presented and the primary objective of the control system is to maintain the electrolyzer current at the desired operating point while optimizing grid energy consumption, even in the face of solar energy variability. The linear HMPC strategy consists of a mixed logical dynamical description of the linearized system equations to derive the control law by solving an optimization problem in the form of mixed-integer quadratic programming (MINLP). This control strategy utilizes three cost functions that relate grid energy consumption to the electrolyzer efficiency. The HMPC was implemented using the Yalmip toolbox for MATLAB.

A decomposition for MPC of linear dynamic systems with binary variables was presented by (VALDERRAMA et al., 2020). This decomposition transforms a centralized MPC into a decentralized MPC with a main controller and sub-controllers. The main controller deals with binary variables to enable or disable a subsystem with the respective subcontroller. Some benefits of this decentralization are scalability and flexibility (i.e., adding a new subsystem is easy) and reduction in computational complexity, and the resulting optimization problem is simpler and can be solved in parallel. An example of this application was presented by the authors, in which multiple battery-charging stations for electric vehicles were powered by a renewable energy source and the electric grid. The Julia Programming Language was employed to address the problem, and

the algorithm was implemented using JuMP, a modeling language for mathematical programming, along with the Gurobi solver.

In Robuschi et al. (2021), a multi-phase mixed-integer optimal control strategy is presented for a hybrid electric vehicle. The objective is to determine a minimum-fuel energy management strategy on a specific driving cycle through the optimization of gear choice, torque split, and engine on/off controls. To tackle this problem, the authors propose an algorithm tailored for this purpose by extending the combinatorial integral approximation technique. This technique involves breaking down the original mixed-integer nonlinear program (MINLP) into a sequence of nonlinear programs (NLP) and mixed-integer linear programs (MILP). The solution was developed using Python 2.7, and to address the NLPs, CasADi and IPOPT were employed. Additionally, to address the MILP, *pycombina* was utilized.

3 DEVELOPMENT OF OPTIMAL CONTROL STRATEGIES FOR HYDROGEN PRODUCTION IN PHOTOVOLTAIC-PEM ELECTROLYZERS

This chapter is concerned with the mathematical modeling and optimal control formulation of grid-assisted photovoltaic-hydrogen production systems based on a PEM electrolyzer. The main purpose of the control system is to maintain the electrolyzer current at the desired operating point and, at the same time, to optimize the grid energy consumption despite the solar energy variability. To tackle this problem, a simple dynamic model where the electrolyzer current is used as the control variable is proposed. The different operating modes of the plant are also studied since they are very important for the proper operation and control of the system. These results are based on very a well-established literature and brought together to describe the behavior of the whole process. Finally, three optimal control strategies, namely the single-phase, multi-phase, and hybrid optimal control, are formulated in continuous time.

3.1 SYSTEM DESCRIPTION

The plant studied in this chapter to test the optimal control strategies is depicted in Figure 14. This system is composed of a PEM electrolyzer linked with to two sources of electricity: the photovoltaic (PV) solar panels and the electric grid. The converters connected the DC bus to the power sources, and a storage tank is employed to store the hydrogen produced for the gas demand.

Figure 14 – Block diagram of a photovoltaic-hydrogen system assisted by grid.

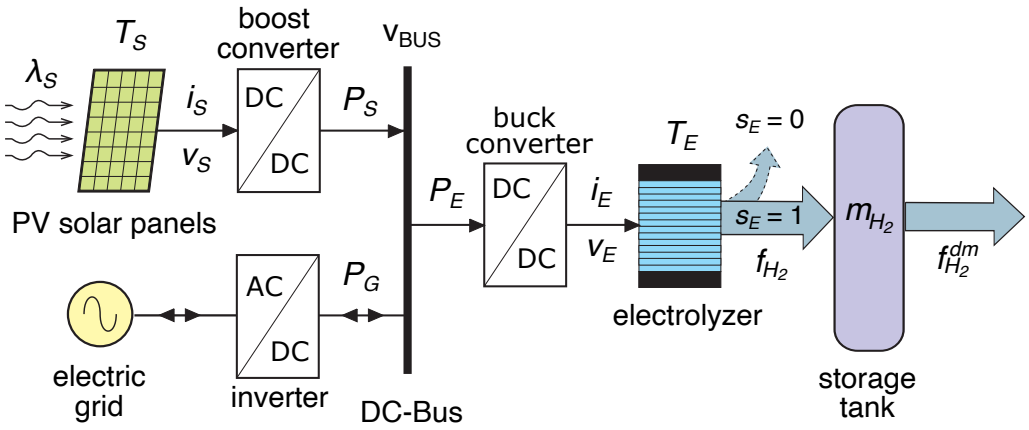

Source: Adapted from de Andrade et al. (2020).

3.2 MATHEMATICAL MODELING OF THE SYSTEM

3.2.1 Electrolyzer

The electrolyzer is the electrochemical device responsible for converting renewable electric energy into chemical energy stored in the form of hydrogen. As already

discussed in Chapter 2, its fundamental components are electrolysis cells connected in series according to the bipolar design, better known as filter-press (HOLLADAY et al., 2009). The direct current flow through each cell anode and cathode generates H_2 by water splitting in the electrolyte solution separating such electrodes. The electrolyzer model consist in the Equations (1-6).

Apart from the electrolysis stack, other equipment, e.g., refrigeration systems, pumps, compressors, control valves, manifolds, etc., are also used for the proper operation of the plant. However, they are not taken into account in the electrolyzer model of this work for practical purposes.

3.2.2 Photovoltaic Solar Panel

As presented in Chapter 2, the PV solar panels consist of a photovoltaic cell array exposed to solar radiation that generates electricity. A DC/DC converter will be considered at the output of the solar panel for connection to a DC microgrid. The photovoltaic solar panel model consist in the Equations (16-6).

3.2.2.1 Operating range

The operating range, illustrated in Figure 15, refers to the sub-interval between t_N^+ and t_D^- within the overall time range of $[t_N, t_D]$, where t_N^+ represents the earliest time when $P_S(t) \geq P_E^{min}$, where P_E^{min} is the minimum power required to produce H_2 in the electrolyzer, and t_D^- represents the latest time when $P_S(t) \geq P_E^{min}$. If solar radiation is ideal during this interval, the electrolyzer can operate solely on solar power. However, it is important to keep in mind that there is no guarantee that $P_S(t) \geq P_E^{min} \; \forall \, t \in [t_N^+, t_D^-]$, especially on days with low irradiation due to cloudy or rainy weather. The low irradiation ranges are defined as time intervals between t_N^+ and t_D^- where $\lambda_S(t) < \lambda_S^{min}$, indicating that $P_S(t) < P_E^{min}$.

Figure 15 – Operating range for the day.

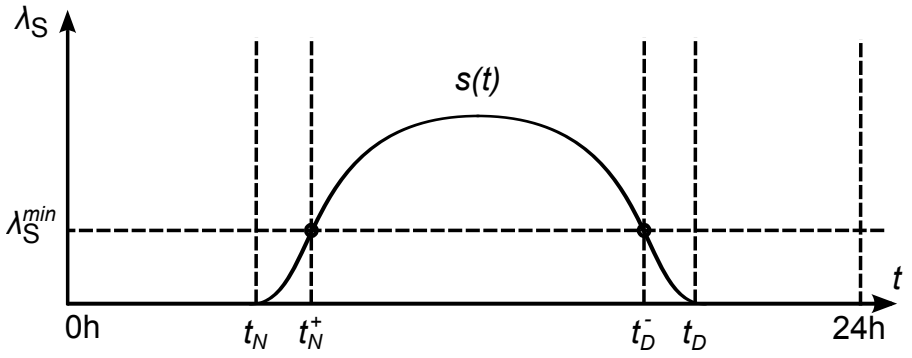

Source: Created by the author (2024).

3.2.3 Electric Grid

The inverter of Figure 4 adapts and controls the electrical assistance provided by the three-phase grid. Each phase is modeled as a sinusoidal voltage source of amplitude $\hat{V}_G$ and angular frequency ω_G in series with an inductance L_G. The three-phase power provided by such sources can be expressed as:

$$P_G = \frac{3}{2} i_G^d \hat{V}_G, \tag{31}$$

where i_G^d is the direct component of the grid current in the dq reference framework that regulates the active power P_G absorbed by the inverter when the quadrature component is zero. This must satisfy the following constraint to avoid control saturation:

$$\left| i_G^d \right| \leq \frac{1}{\omega_G L_G} \sqrt{\frac{V_{DC}^2}{3} - \hat{V}_G^2}. \tag{32}$$

The current assistance required by the electrolyzer to the DC-bus for a desired hydrogen production rate f_{H_2}, if losses in the inverter are neglected, is $i_G^{dc} = p_G / V_{DC}$. To regulate it, a feedback loop that commands the grid converter switching is applied. The following equation shows the grid assistance in terms of the imbalance between the current demanded by the electrolyzer and the current delivered by the solar panels:

$$i_G^{dc} = \frac{3}{2} i_G^d \hat{V}_G / V_{DC} = i_E^{dc} - i_S^{dc}. \tag{33}$$

The electrical grid is considered as an ideal energy source. It provides a continuous source of energy when photovoltaic panels cannot generate the required amount of power, and it can also absorb excess power generated by the panels during peak production. The energy exchanged with the grid E_G, whose derivative is the power P_G, is considered as a dynamic state. It defines the energy balance obtained by multiplying (33) by the DC-bus voltage:

$$\dot{E}_G(t) = P_E(t) - P_S(t) = v_E(t) i_E(t) - i_S(t) v_S^{\max}(\lambda(t)), \tag{34}$$

where i_S is computed using $v_S^{\max}$ in (16).

3.2.4 Storage Tank

The mass of hydrogen, m_{H_2}, in the tank can be expressed using the following mass balance equation:

$$\dot{m}_{H_2} = f_{H_2} - f_{H_2}^{dm}, \tag{35}$$

where the flow rate of hydrogen entering the tank f_{H_2} is in (6).

To guarantee a desired H_2 production, the buck reducer converter shown in Figure 14 must control the electrolyzer current around a value i_E^* according to (1) and

(6) by regulating the following duty cycle δ_E:

$$0 < \delta_E = \frac{v_E(i_E^*)}{V_{DC}} < 1. \tag{36}$$

Importantly, this model does not consider any losses or consumption of auxiliary equipment such as valves and compressors that may be associated with the process.

Assuming that the algorithm proposed in (GARCÍA-CLÚA; DE BATTISTA; MANTZ, 2010) is implemented to ensure such current i_E^* and neglecting converter power losses (that is, the input and output power is $P_E = v_E \cdot i_E$, the current demanded to the bus for the electrolysis can be approximated as follows:

$$i_E^{dc} = v_E(i_E^*) i_E^* / V_{DC}. \tag{37}$$

The dependency of (37) on the variable T_E is ignored assuming that it is fixed by the electrolyzer temperature controller.

3.2.5 Control objective and Operation Modes

The main control objective of the system is to continuously meet the hydrogen demand, which can be performed by regulating the electrolyzer current i_E (see Figure 14). This in turn can be regulated with the grid assistance according to the energy balance of the grid. Indeed, to regulate i_E according to the desired value i_E^*, the grid current i_G^{dc} required by the DC-bus can be obtained substituting (17) and (36) into (33):

$$i_G^{dc} = \delta_E \left(i_E^*\right) i_E^* - \left[1 - \delta_S \left(\lambda(t)\right)\right]^{-1} i_S \left(v_S^{\max} \left(\lambda(t)\right)\right). \tag{38}$$

The setpoint i_E^* is not a fixed value but may belong to a range that guarantees an adequate level of H_2 in the storage tank. This flexibility allows the formulation of an additional control objective. Here it is proposed to minimize the energy exchanged with the grid in a certain period. This ensures maximum renewable H_2 production. Such minimization must take into account certain operational restrictions of the electrolyzer. These are described below according to the operation mode of such a device.

1. **Minimum losses and maximum production rate**: The minimum energy required to generate 1 Nm^3 of H_2 is 3.54 kWh (LEEUWEN; MULDER, 2018). The energy efficiency, η_E, determines how much such consumption is exceeded due to losses in the electrolyzer. This parameter can be expressed as a function of the electrolyzer current as follows:

$$\eta_E \left(i_E\right) = \eta_F \left(i_E\right) \frac{N_{SE} V_{tn}}{v_E \left(i_E\right)}, \tag{39}$$

where V_{tn} is called the thermoneutral potential of the cell, which under normal conditions of pressure and temperature is 1.481 V (SMOLINKA; OJONG;

GARCHE, 2015). To optimize this expression, intermediate current values must be applied, since for lower values of i_E, η_F decreases because it is directly proportional to η_F, which in turn decreases according to (7). For higher current values, the same occurs because (39) is inversely proportional to v_E, which increases according to (1). Assuming that this operational condition was taken into account in the design stage, then the electrolyzer should be operated at its rated current I_E^N. In that case, the maximum flow $f_{H_2}^N$ will be generated, which is directly proportional to I_E^N according to (6).

2. **Minimum emissions**: It happens when the power supply comes exclusively from the PV panels, so the electrolyzer current can vary from zero to I_E^N. However, the H_2 production efficiency and purity of produced gases increase with current (KIRATI; HAMMOUDI; MOUSLI, 2018). Therefore, electrolyzers should operate above a minimum current $I_E^{\min}$, which is typically around 25% to 40% of I_E^N.
3. **Minimum assistance**: The application of minimum maintenance current I_E^m is critical for a good electrolyzer performance in order to protect its electrodes from corrosion due to continuous start-up and shut-down. By operating in this stand-by mode, the electrolyzer is able to maintain its internal working temperature and pressure for days and quickly restart the hydrogen production when renewable supply is restored. Gases produced by this maintenance current are ventilated because of the impurity level of H_2 in O_2, which usually exceeds the safety imposed limit of 2.0 vol. % (DUTTON et al., 2000).

From a control point of view, it is important to emphasize that the operation modes described above are computed by the control algorithm since the electrolyzer current, i_E, is the control variable. The operating modes are modeled by the binary variable s_E in (6). More precisely, the minimum losses, maximum production rate, and minimum emissions operation modes are combined as $s_E = 1$, and the minimum assistance is given by $s_E = 0$.

3.3 OPTIMAL CONTROL STRATEGIES

In this work, we propose three optimal control methodologies: a single-phase (SPS), a multi-phase (MPS), and a hybrid (HyS) optimal control strategy, to minimize energy consumption during operation and reduce the load of the electric grid.

To implement these optimal control strategies in practice, a hierarchical three-layer control system can be used, as shown in Figure 16. The supervisory control layer, is responsible for analyzing the solar radiation data, calculating the operating range for the day, and defining the sequence of phases in the case of the MPS controller. The optimal control layer is responsible for solving the OCP and defining the optimal

trajectories for i_E and s_E. The algorithm for supervisory and optimal control layers are presented in Figure 17. Finally, the field control layer ensures that the optimal trajectories will be tracked. This layer can be performed with simple PID controllers. This work focuses on the supervisory and optimal control layers.

Figure 16 – Proposed control system hierarchy.

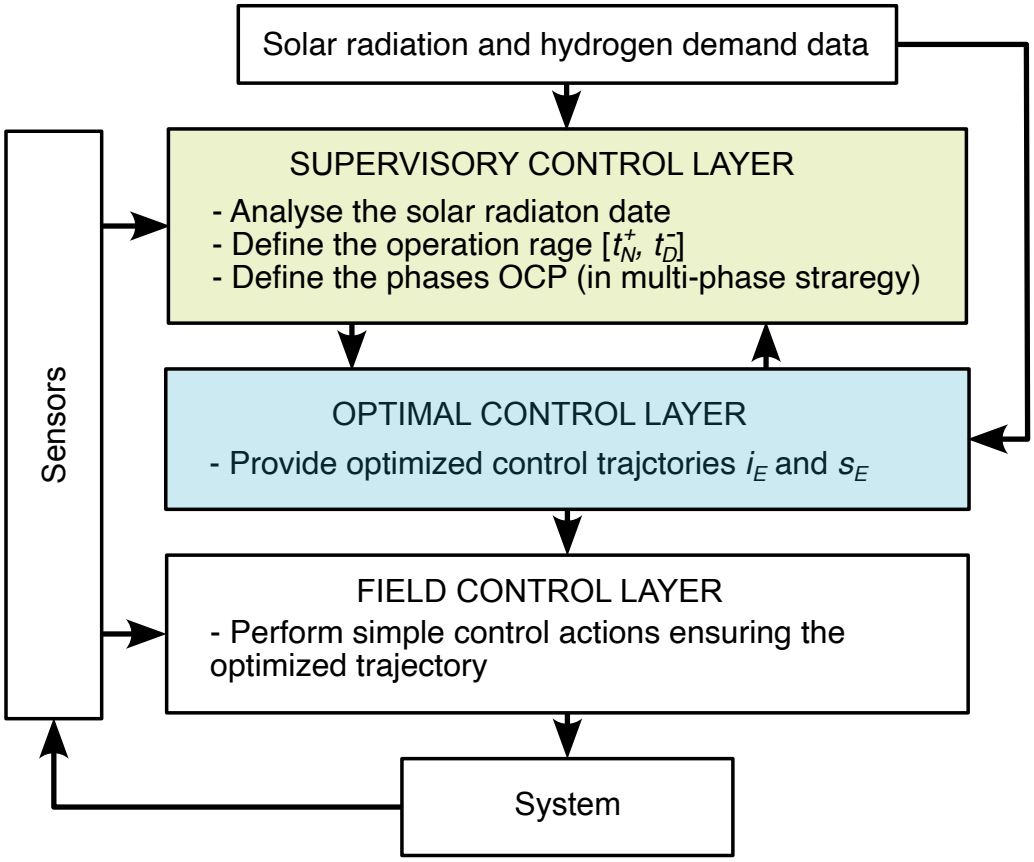

Source: Created by the author (2024).

3.3.1 Single-phase optimal control strategy

The single-phase strategy (SPS) consists of the electrolyzer being constantly active and generating hydrogen. The cost function is designed to reduce the difference between the power consumed by the electrolyzer P_E and the power generated by the solar panel P_S, as follows:

$$\begin{aligned} \underset{i_E(\cdot)}{\text{minimize}} \quad & \int_{t_N^+}^{t_D^-} \left[P_E(i_E) - P_S(t)\right]^2 \, dt, \\ \text{subject to} \quad & \dot{m}_{H_2} = f_{H_2} - f_{H_2}^{dm}, \\ & M_{H_2}^{min} \leq m_{H_2} \leq M_{H_2}^{max}, \\ & m_{H_2}(t_N^+) = M_0, \\ & I_E^{min} \leq i_E \leq I_E^{max}, \end{aligned} \tag{40}$$

Figure 17 – Algorithm for supervisory and optimal control layers.

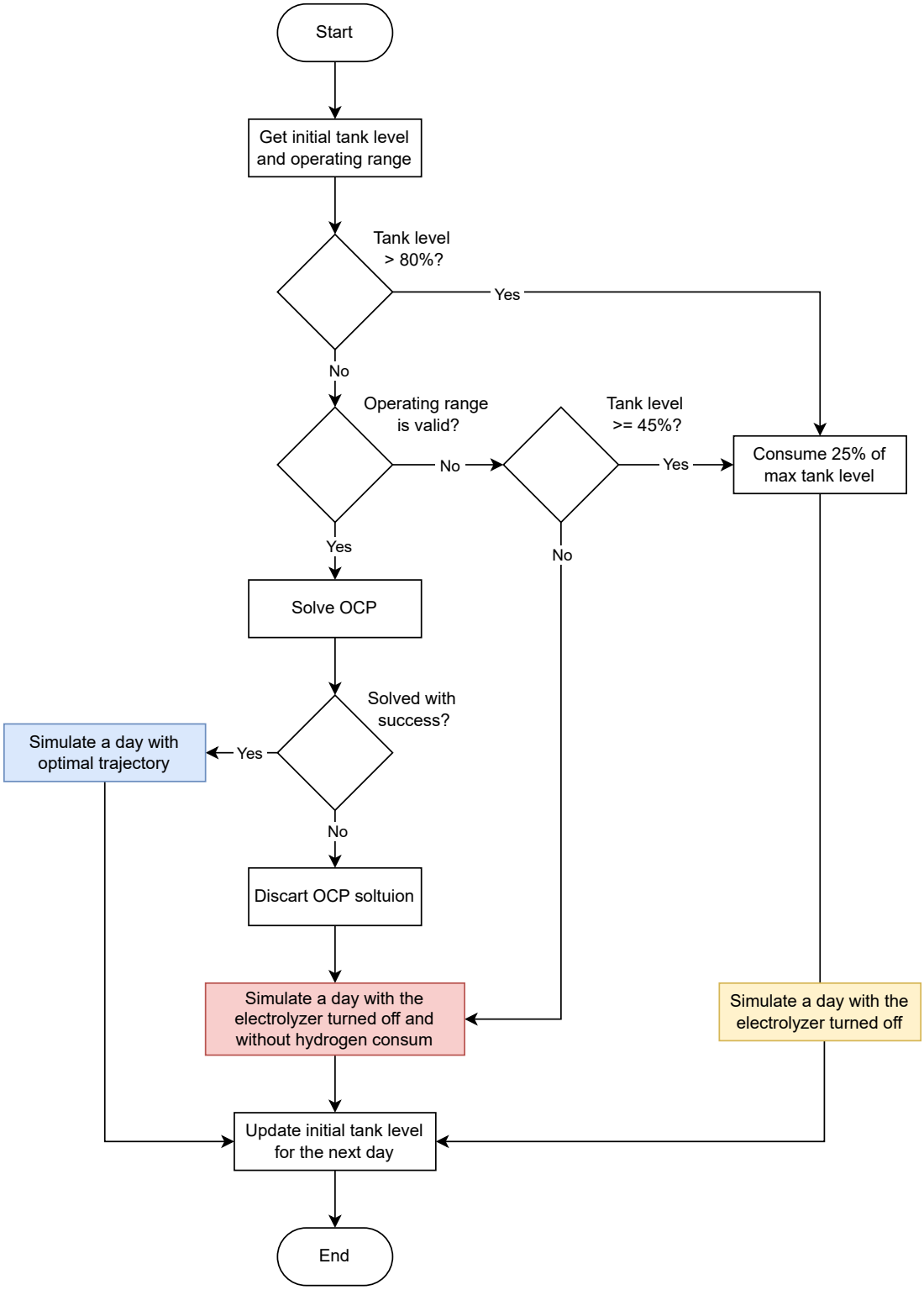

Source: Created by the author (2024).

where M_0 is the initial mass of hydrogen in the tank.

3.3.2 Multi-phase optimal control strategy

Unlike the SPS, the multi-phase strategy (MPS) involves the electrolyzer operating in two distinct modes: standby $s_E = 0$ and active $s_E = 1$. On standby, the electrolyzer requires fixed power $P_E(I_E^m)$ and does not generate useful hydrogen. In addition, the power consumption is less than that in the active mode.

The phases are sequential, and the state continues in the connections of phases. To solve a multi-phase OCP, it is necessary to include the number of phases and the duration of each phase. These definitions are made in the supervisory control layer. Two algorithms were made for it: a variable window (VW) and a fixed window (FW). Both algorithms receive the solar irradiation discretized with 1 min of the sampling period. In the VW algorithm, low irradiation ranges larger than 15 min are defined as a standby phase. In FW, the operating range is divided into segments with approximately 15 min, if the integral of $\lambda_S(t)$ in on interval was less than $\lambda_S^{min} \cdot 15\,\text{min}$, this interval was set as a standby phase.

This strategy is formulated as:

$$\begin{aligned}
\underset{i_E(\cdot)}{\text{minimize}} \quad & \sum_{p=\{1,3,...\}}^{N_p} \int_{t_{i_p}}^{t_{f_p}} \left[P_E(i_E) - P_S(t)\right]^2 \, dt + \\
& \sum_{p=\{2,4,...\}}^{N_p} \int_{t_{i_p}}^{t_{f_p}} \left[P_E(I_E^m)\right]^2 \, dt \\
\text{subject to} \quad & \\
& \dot{m}_{H_2} = f_{H_2} - f_{H_2}^{dm} && p \in \{1,3,...\}, \\
& \dot{m}_{H_2} = -f_{H_2}^{dm} && p \in \{2,4,...\}, \\
& M_{H_2}^{min} \leq m_{H_2} \leq M_{H_2}^{max}, \\
& m_{H_2}(t_{i_1}) = M_0, \\
& I_E^{min} \leq i_E \leq I_E^{max} && p \in \{1,3,...\}, \\
& i_E = I_E^m && p \in \{2,4,...\}, \\
& t_N^+ = t_{i_1} < t_{i_p} < t_{f_p} = t_{i_{(p+1)}} < t_{f_{(p+1)}} < t_{f_{N_p}} = t_D^-,
\end{aligned} \tag{41}$$

where N_p is the number of phases.

3.3.3 Hybrid optimal control strategy

The hybrid strategy (HyS), like the MPS, involves the electrolyzer operating in two distinct modes: standby $s_E = 0$ and active $s_E = 1$. However, to deal with this

switching behavior, a variable path constraint is added:

$$\left[s_E(I_E^{min} - I_E^m) + I_E^m\right] \leq i_E \leq \left[s_E(I_E^{max} - I_E^m) + I_E^m\right],$$

then the strategy is formulated as:

$$\begin{aligned}
\underset{i_E(\cdot), s_E(\cdot)}{\text{minimize}} \quad & \int_{t_N^+}^{t_D^-} \left[P_E(i_E) - P_S(t)\right]^2 \, dt, \\
\text{subject to} \quad & \dot{m}_{H_2} = s_E \cdot f_{H_2} - f_{H_2}^{dm}, \\
& M_{H_2}^{min} \leq m_{H_2} \leq M_{H_2}^{max}, \\
& m_{H_2}(t_N^+) = M_0, \\
& \left[s_E(I_E^{min} - I_E^m) + I_E^m\right] \leq i_E \leq \left[s_E(I_E^{max} - I_E^m) + I_E^m\right], \\
& s_E \in \{0, 1\}.
\end{aligned} \tag{42}$$

The transcription of this OCP results in a MINLP. The employed solver, Bonmin, makes some algorithm options available to transform the MINLP into a MILP and an NLP. This study tested two of these options: branch-and-bound (BB) and outer approximation (OA).

In the SPS and the MPS, the s_E is determined in the supervisory control layer. It is a constant equal to one in SPS, and it is equal to zero during the standby phases in MPS. However, in the HyS, s_E is an optimization variable and is defined in the optimal control layer.

3.4 RESULTS AND DISCUSSION

The research utilized a computational environment wherein all experiments took place. The system model was based on established models from academic literature. It is important to highlight that the power plant in question has not been constructed in reality, making experimental validation unfeasible.

The control systems were coded using MATLAB (MATHWORKS, 2023a) and MpOC Toolbox, presented in Appendix A. The simulations were performed on a Macbook Air M1 2020 with 8 GB of RAM and a GPU with eight cores (APPLE INC, 2020). To maintain consistent performance, all simulations were executed while the laptop was connected to a power source and situated within a temperature-controlled environment.

The OCPs were discretized into segments with 5 min. The initial mass of hydrogen in the tank, denoted by M_0, is 143.5 g (70 % of capacity). The initial guesses used to solve the NLP and MINLP problems are: for i_E and m_{H_2} the initial guess was the mean value of the constrained interval of these variables; for the control signal, for the binary variable s_E it was considered equal to one.

The performance of the control systems is analyzed by considering the solver numerical solution, and the H_2 production and electrical grid consumption. More precisely, the solver numerical solution performance indices encompass the number of

optimization variables, number of constraints, time spent in transcription, and time spent in the solution of NLP or MINLP problem. Each solution was executed three times consecutively to measure the time spent.

The performance indices were associated with the system response obtained in the simulation with the optimal control sequence. The performance indices include the energy consumed by the electrolyzer E_E, energy supplied E_G^- and absorbed E_G^+ by the electric grid, the participation of the delivered grid energy in the energy consumed in the electrolyzer E_G^-/E_E, hydrogen produced M_{H_2}, and the production per kilowatt-hour η_E.

3.4.1 Numerical Value of the Parameters of the Plant

The parameters and constants used in the electrolyzer model described in Section 2.1.4 were extracted from Valverde et al. (2013b) and Valverde (2013) and are listed in Table 8 of Appendix B. The limits of current are I_E^m = 10 A, I_E^{min} = 50 A, and I_E^{max} = 100 A. These values were estimated by the author based on presented experiments in Valverde (2013) and common values for electrolyzer. The maximum power consumption P_E^{max} is attained at I_E^{max}, resulting in a power output of 1000 W. Conversely, the minimum power consumption P_E^{min} is computed using I_E^{min}, producing a power output of 524 W. The power consumed in standby mode P_E^m is 100 W and was computed using the value of I_E^m.

Regarding the PV solar panel, the parameters presented in Table 7 of Appendix B were considered with the panel temperature T_S constant at 25 °C and with maximum solar radiation λ_S = 1, which results in the maximum power P_S equal to 3.5 kW.

Finally, the maximum hydrogen capacity in the tank $M_{H_2}^{max}$ is 205 g, which is equivalent to 2.5 Nm^3. The minimum desired $M_{H_2}^{min}$ is 20 % of the maximum capacity, which is 41 g.

3.4.2 Input Data

To solve the formulated OCPs, previous knowledge of hydrogen demand $f_{H_2}^{dm}$ and solar irradiation λ_S data is required. The simulations considered one year of real solar radiation data collected in Cachoeira Paulista, São Paulo, Brazil, located at $22°41'22.65''S$, $45°0'22.28''W$. This location was chosen because it has high-quality data for the analyzed year, which was obtained from the SONDA Project (BRASIL, 2018). Regarding the hydrogen demand profile, the data was borrowed from de Andrade et al. (2020).

3.4.3 Analysis of the Optimal Control Operation During One Day

The result of the SPS controller operating during one day is presented in Figure 18, whereas the results of the MPS controller with the VW and FW algorithms and the HyS controller with the BB and OA algorithms are presented in Figure 19 and Figure 20, respectively. In these figures, the top graphic shows the PV panel power and the electrolyzer power; the second graphic shows the hydrogen demand and production, respectively; the third graphic shows the H_2 stored in the tank and the operating mode of the plant; and the bottom graphic shows the electrolyzer current (control variable).

In periods with high-solar radiation, i.e., between $t \approx 8\,\text{h}$ and $t \approx 15.7\,\text{h}$, all the control systems behaved similarly by tracking the power generated by the PV panel as can be seen in the top graphics of Figures 18-20. Importantly, the maximum power consumed by the electrolyzer is 1 kW while P_S^{max} is 3.5 kW resulting in the saturation of the hydrogen production and the injection of the exceeding electricity generated in the PV panels to the electric grid.

Figure 18 – Results with SPS control system operating during one day.

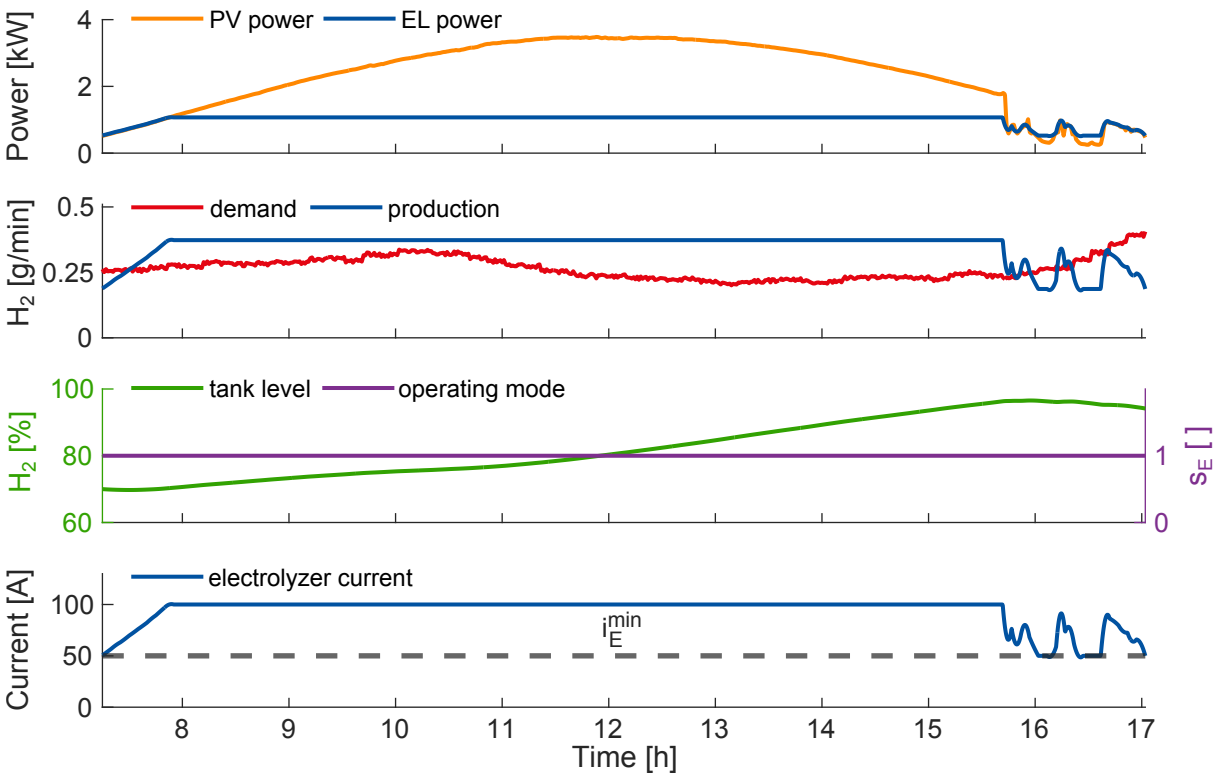

Source: Created by the author (2024).

The differences between the control strategies can be seen in periods with low radiation, i.e., between $t \approx 16\,\text{h}$ and $t \approx 17\,\text{h}$, which are detailed in Figure 21. In the cases of the MPS-VW, MPS-FW, and HyS-BB, the electrolyzer operated in the standby mode, as can be seen in the third graphic of columns 2 to 4 in Figure 21. Furthermore, the time interval in standby mode is similar in the MPS-VW and the HyS-BB strategies

(see the third graphic of columns 2 and 3 in Figure 21). Nevertheless, the HyS-OA method showed a behavior similar to that of SPS, the third graphic of columns 1 and 5 in Figure 21, setting the electrolyzer on standby mode only in the last minutes of the day.

Figure 19 – Results with MPS control system operating during one day.

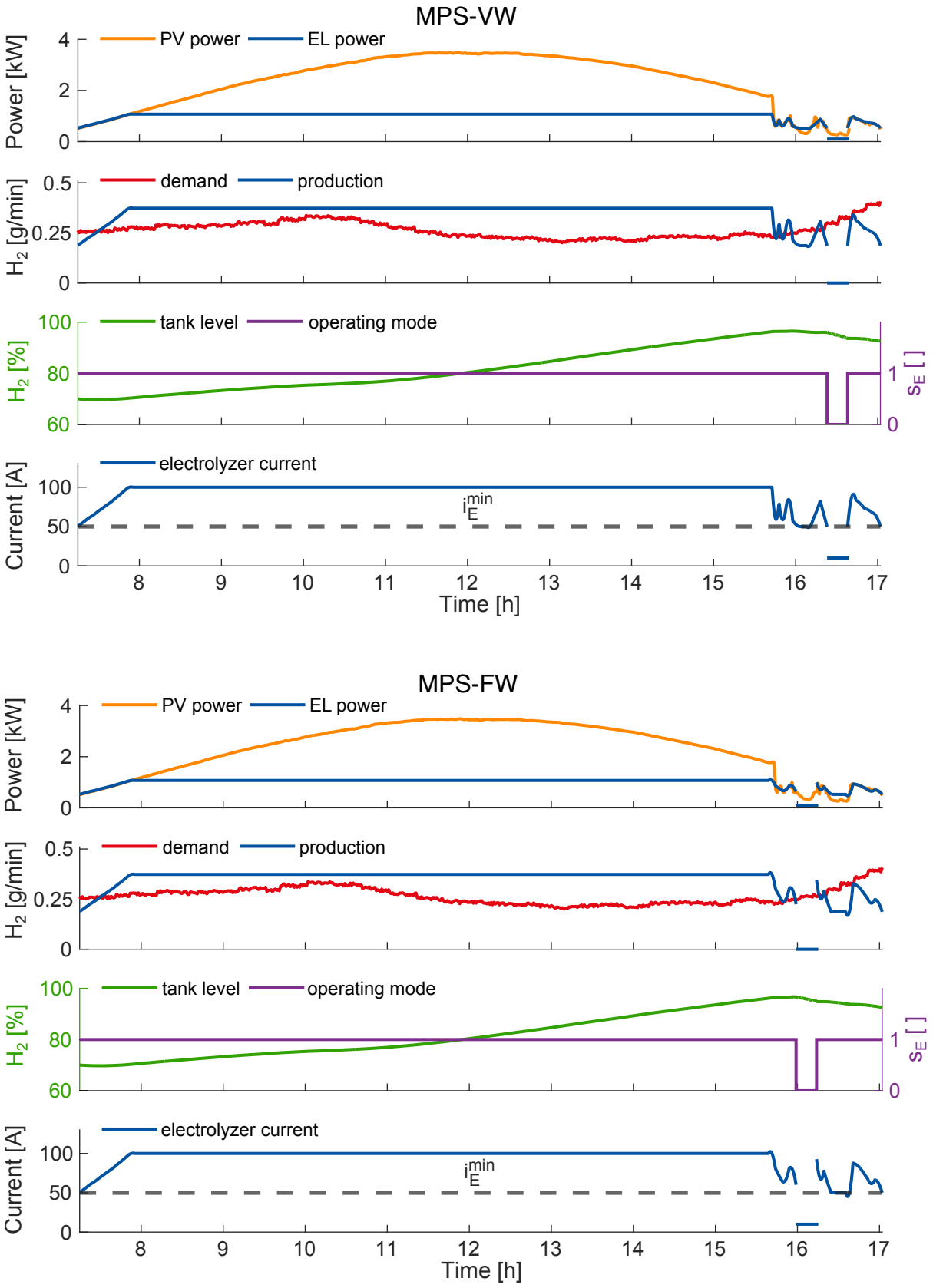

Source: Created by the author (2024).

Figure 20 – Results with HyS control system during one day.

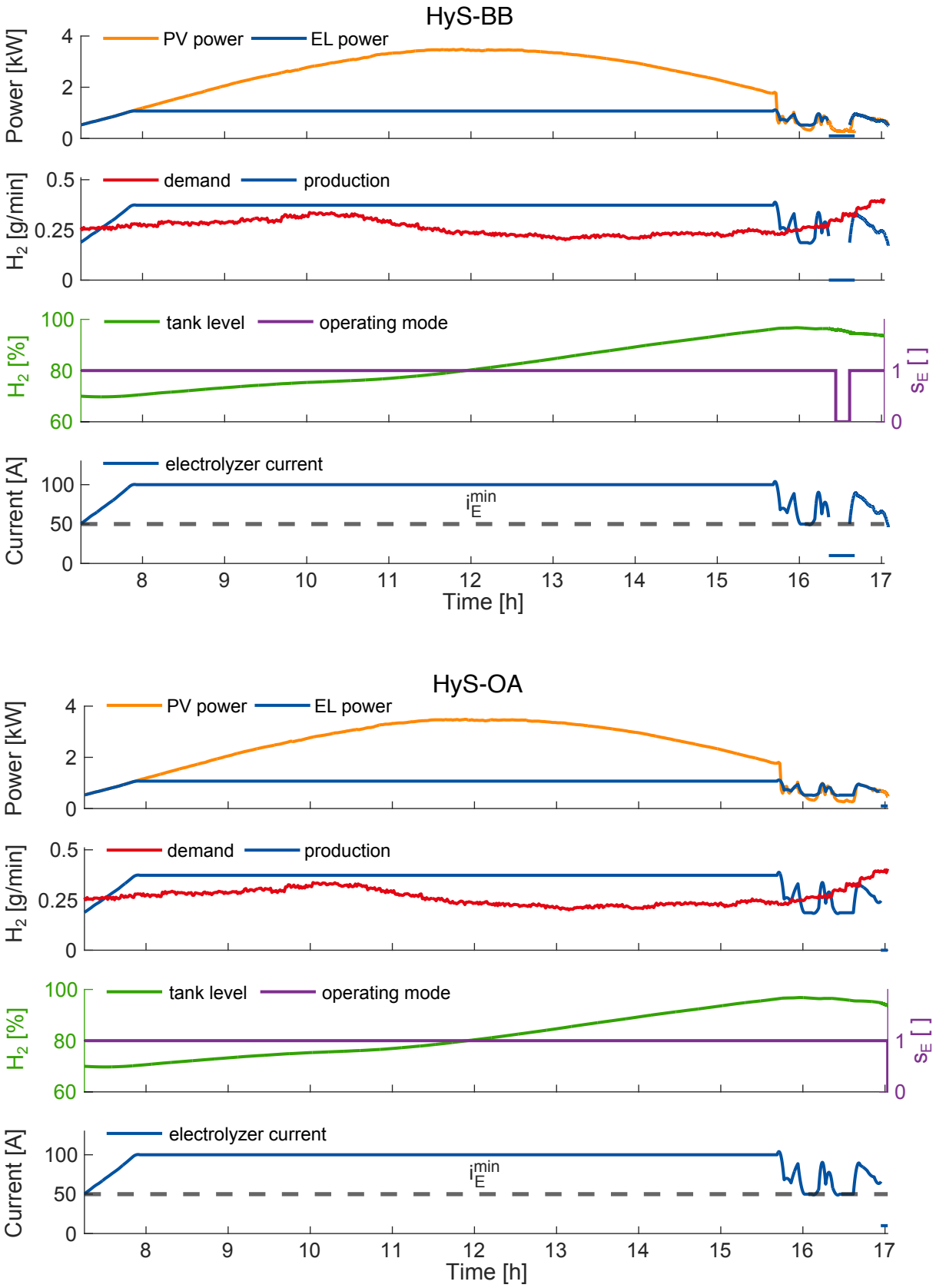

Source: Created by the author (2024).

The performance of all controllers is summarized in Table 4. As expected all

Figure 21 – Comparison of the results for one day of operation during low radiation periods.

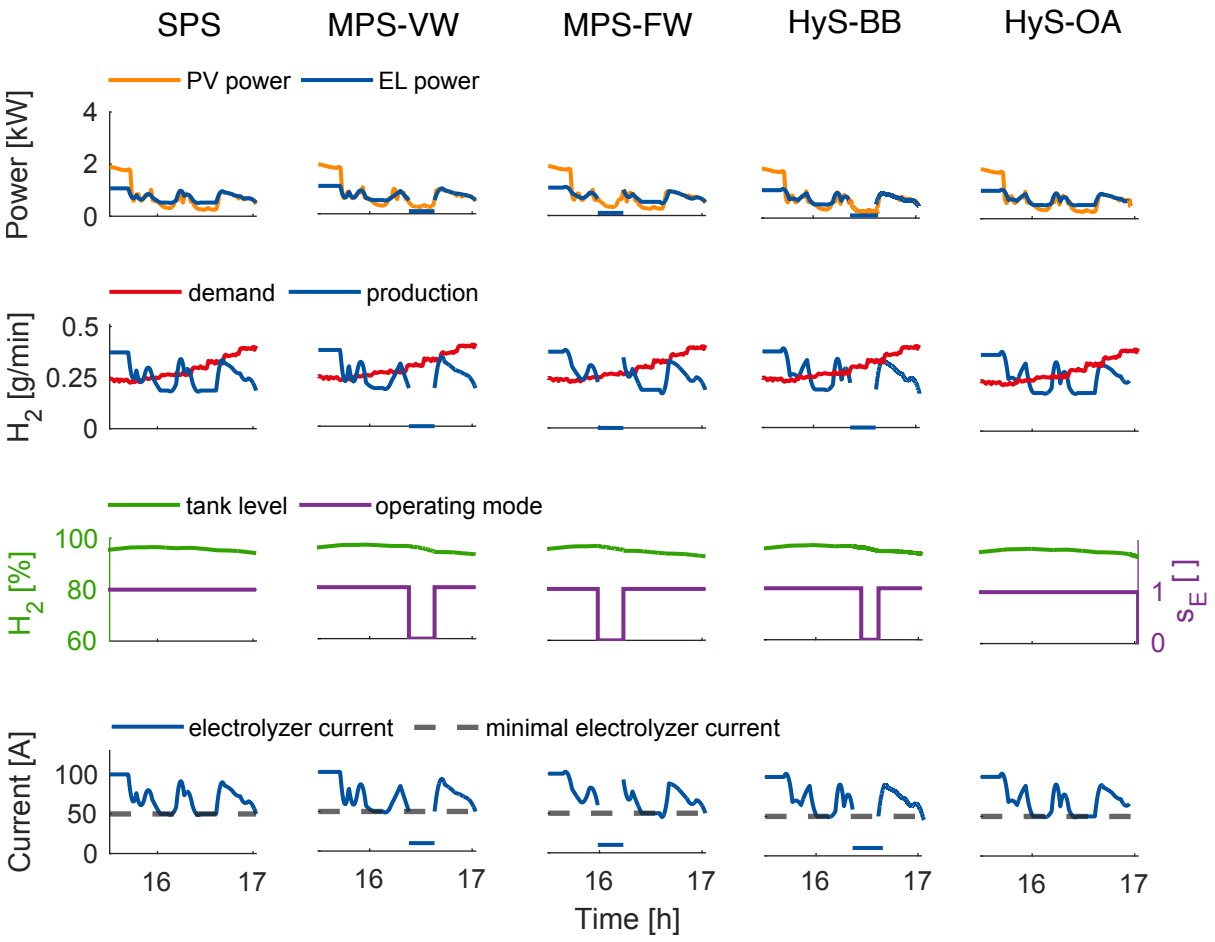

Source: Created by the author (2024).

the indices are very similar since the plant operated similarly for most of the time in all cases. Despite this, a difference exists caused by the low radiation ranges. Note that the SPS optimal controller presents the highest values of energy consumed by the electrolyzer E_E, assistance of the grid energy E_G^-/E_E, total hydrogen production M_{H_2} and efficiency η_E because the electrolyzer remains active even in periods when the solar panel does not generate sufficient power for the production of H_2. On the other hand, the MPSs and HySs controllers have less assistance from the grid because the system switched to standby mode during low radiation ranges.

The solver solution indices are displayed in Table 5. The HyS method requires more optimization variables and constraints to represent s_E in the MINLP, whereas the SPS and MPS methods use fewer variables and constraints. The difference in the number of optimization variables and constraints between SPS and MPS strategies is due to the additional constraints required to connect the phases.

All strategies, except for the HyS-BB methodology, took less than 1 s to transcribe and solve the formulated OCPs. The HyS-BB methodology took at least 20 times more

Table 4 – Control performance indices for one day of operation.

Index	**Unity**	**SPS**	**MPS-VW**	**MPS-FW**	**HyS-BB**	**HyS-OA**
E_E	kWh	9.80	9.58	9.57	9.70	9.77
E_G^-	kWh	0.13	0.02	0.05	0.06	0.11
E_G^+	kWh	12.96	13.06	13.03	13.09	13.02
E_G^-/E_E	%	1.32	0.20	0.52	0.67	1.17
M_{H_2}	g	205.16	199.79	199.48	202.64	204.37
η_E	g/(kW h)	20.94	20.85	20.84	20.88	20.92

Source: Created by the author (2024).

time than the other strategies. Even with an additional step to calculate the low radiation periods and define standby phases, the MPSs required less time than HyS. The primary reason for this is that MPSs controller resulted in an NLP, while the HyS controller resulted in a combined mixed-integer linear program and an NLP.

Table 5 – Solution Indices in during one day.

Index	**Unity**	**SPS**	**MPS-VW**	**MPS-FW**	**HyS-BB**	**HyS-OA**
Opt. variables		470	474	474	583	583
Constraints		234	236	236	696	696
Pre-calc. time	ms		0.5 ± 0.1	3 ± 1		
Transc. time	ms	270 ± 3	291 ± 14	318 ± 24	399 ± 4	405 ± 11
Sol. time	ms	244 ± 2	243 ± 3	244 ± 3	$21\,362 \pm 136$	515 ± 4

Source: Created by the author (2024).

3.4.4 Analysis of the Optimal Control Operating During One Year

The solar radiation used in this analysis is shown in Figure 22, and the profile of hydrogen demand was assumed to be the same as the one presented in the previous section. Importantly, the HyS-BB was not evaluated in this scenario because simulation attempts took over 4 hours (without conclusion), while the other strategies required less than 5 minutes.

Figure 22 – Solar radiation during one year.

Normalized at 1 kW/m^2.

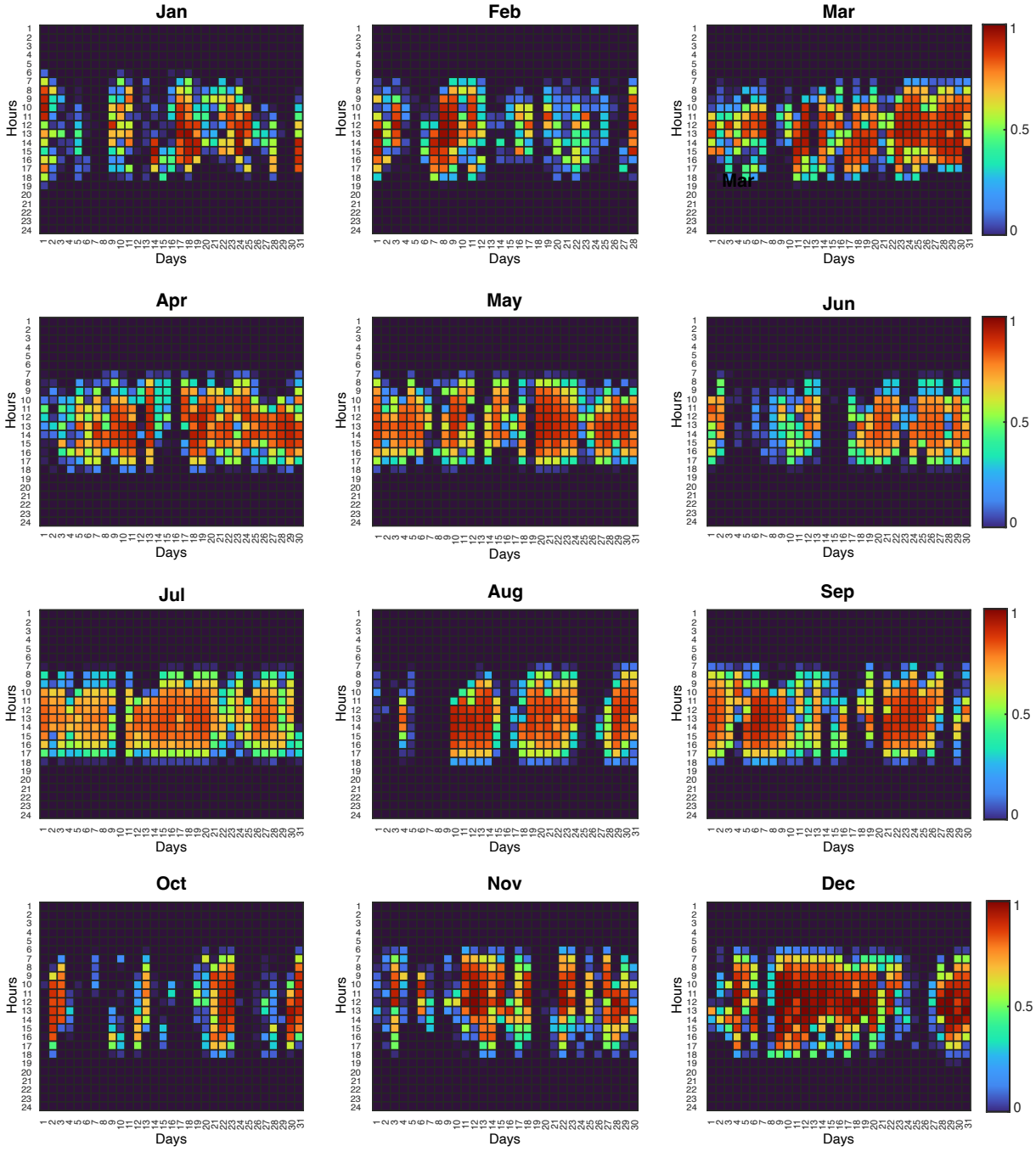

Source: Adapted from Brasil (2018).

The role of the supervisory system is pronounced in this scenario because this layer needs to decide the operating range and the standby phases (in MPSs) and which electrolyzer will be kept off. To facilitate a comprehensive evaluation of these strategies, three indices have been introduced: D_{off}, representing the number of days the electrolyzer remains inactive without hydrogen consumption; D_{off}^{dm}, indicating the days the electrolyzer is inactive but with a hydrogen consumption at 25 % of M_{H_2}; and

Table 6 – Controller Performance Indices in during one year.

Index	Unity	SPS	MPS-VW	MPS-FW	HyS-OA
E_E	MW h	1.79	1.63	1.40	1.79
E_G^-	MW h	0.26	0.09	0.05	0.26
E_G^+	MW h	315.92	423.15	538.64	318.40
E_G^-/E_E	%	14.67	5.68	3.57	14.72
M_{H_2}	kg	37.60	32.45	28.26	32.83
η_E	g/(kW h)	20.99	19.90	20.23	18.33
D_{off}		14	63	104	13
D_{off}^{dm}		118	90	86	119
D_{off}^{Total}		132	153	190	132

Source: Created by the author (2024).

D_{off}^{Total}, which is the aggregate of inactive days, calculated as $D_{off} + D_{off}^{dm}$.

The hydrogen production is present for SPS and MPS-VW in Figure 23 and Figure 24 in this chapter, for the other strategies is presented in Figure 27 and Figure 28 in Appendix C. The tank level throughout the year is also presented in the Appendix C. For all the approaches, the EL was inactive at least for a third of the year due to the weather conditions. The MPS presents the biggest D_{off}^{Total}. The difference in D_{off}^{Total} between SPS and MPS-VW can be seen by comparing Figure 23 and Figure 24.

In HyS-OA, the E_E was equal to in SPS, however, with less M_{H_2} due to the standby periods. This leads to the recommendation not to use this HyS-OA. The strategy that produced the most hydrogen was the SPS, as expected. Nevertheless, present a high use of the electric grid with approximately 15 % applied in EL originating from the electrical grid. In this aspect, the MPS are better alternatives because they use up to four times less grid energy. Considering the objective of reducing the electricity consumption from grid, MPS are the best choices.

Figure 23 – Hydrogen production f_{H_2} with SPS during one year.

Normalized at 373 mg/min.

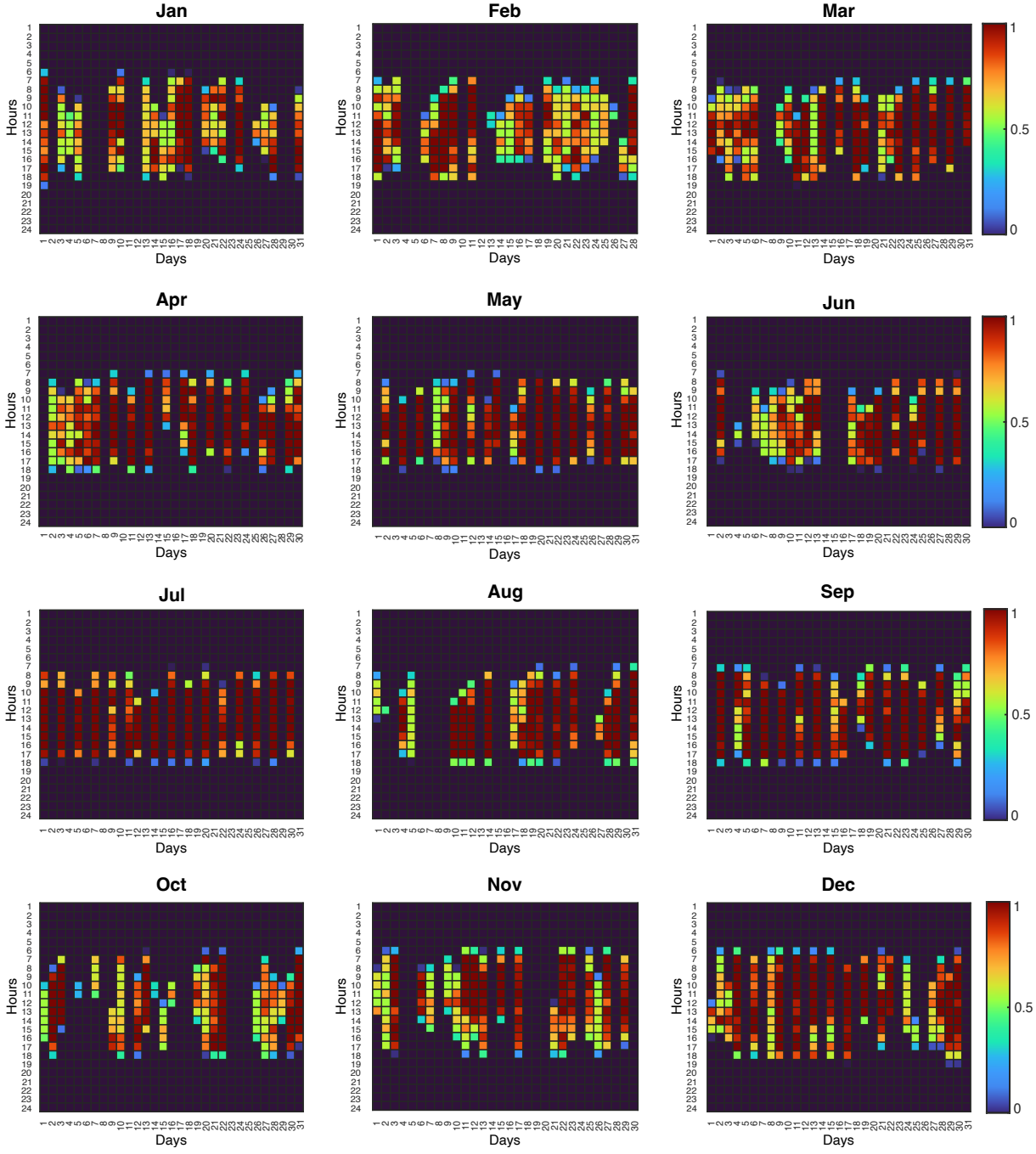

Source: Created by the author (2024).

Figure 24 – Hydrogen production f_{H_2} with MPS-VW in during one year.

Normalized at 373 mg/min.

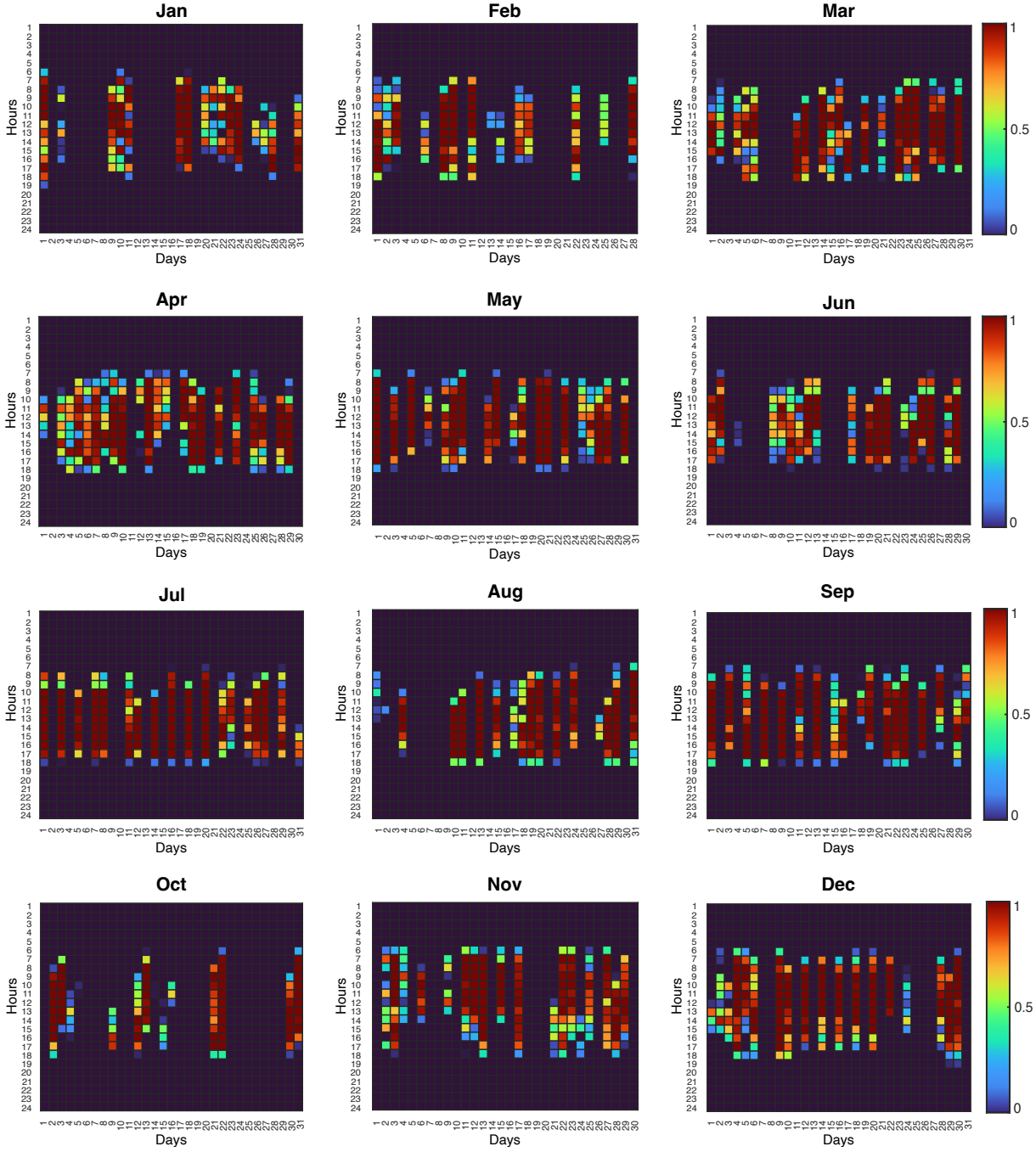

Source: Created by the author (2024).

4 DEVELOPMENT OF A MULTI-PHASE OPTIMAL CONTROL STRATEGY FOR ENERGY STORAGE IN PHOTOVOLTAIC-PEM UNITIZED REVERSIBLE FUEL CELL

This chapter focuses on the mathematical modeling and optimal control formulation of a grid-assisted photovoltaic-hydrogen energy storage system based on a PEM unitized regenerative fuel cell (URFC). The main objective of the control system is to maintain the URFC current at the desired operating point and optimize the grid energy consumption despite the variability of solar energy. To address this, a simple dynamic model is proposed where the URFC current is used as the control variable. These results are based on well-established literature and are combined to describe the behavior of the entire process. Finally, a multi-phase optimal control strategy is formulated in continuous time and simulation results are discussed. The results of this chapter were motivated by the Sustainability and Renewable Energy Challenge organized by MathWorks (see Figure 33 in the Annex A).

4.1 SYSTEM MODELING

The microgrid considered in this chapter is shown in Figure 25. This domestic system is primarily powered by a PV solar panel. To avoid power interruptions caused by the intermittency of the solar energy, the system is assisted by the electric grid. In case of power excess from the PV panels, the electricity is used to produce H_2 in the PEM-URFC and storing the gas in the tank. The stored H_2 can be used to attend a given demand or to feed the URFC to produce electricity to maintain a fixed voltage on the line. These equipment are interconnected by a DC bus using converters and inverters. Note that most of the topology of this microgrid is similar to the one presented in Chapter 3, except for the domestic consumer and the URFC.

4.1.1 Fuel cell

A URFC is a device that operates both as a fuel cell and as an electrolyzer, capable of converting chemical energy into electrical energy and vice versa. In FC mode, the URFC generates electricity by combining hydrogen and oxygen, producing water and heat as byproducts. In EL mode, it consumes electrical energy to split water into hydrogen and oxygen. This dual functionality allows the system to store energy during periods of excess power generation and to generate power during periods of high demand.

The equations utilized in the model of URFC are Equation 8-Equation 15, as presented in Chapter 2. The parameters was extracted from Ogbonnaya et al. (2021) and are presented in Table 9 in Appendix B. The maximum current I_F^{max} was set, by the author, as 200 A and the minimal current I_F^{min} was set as 50 A With this parameters

Figure 25 – Block diagram of a microgrid with hydrogen energy storage.

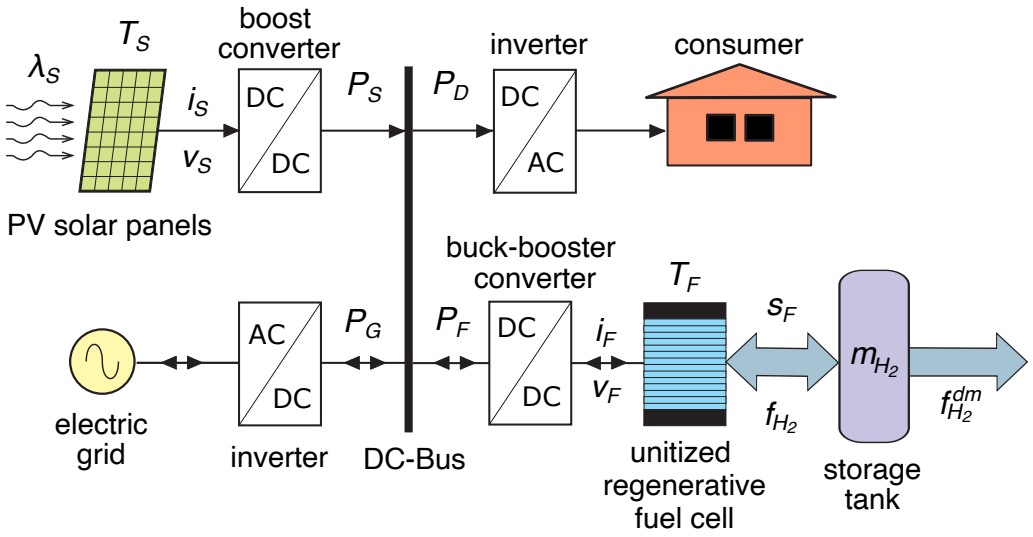

Source: Created by the author (2024).

the maximum power generated in FC mode $P_{F,FC}^{max}$ is 3.7 kW and the maximum power consumed in EL mode $P_{F,EL}^{max}$ is 1.2 kW.

4.1.2 Storage tank

The mass of hydrogen m_{H_2} in the tank can be expressed using the following mass balance equation:

$$\dot{m}_{H_2} = f_{H_2} - f_{H_2}^{dm}, \tag{43}$$

where f_F is the rate of hydrogen produced or consumed by the URFC. This model does not consider any losses or consumption of auxiliary equipment such as valves and compressors that may be associated with the process.

4.1.3 Eletric grid

The inverter shown in Figure 25 adapts and regulates the electrical assistance provided by the three-phase grid. Each phase is modeled as a sinusoidal voltage source with an amplitude of $\hat{V}_G$ and an angular frequency of ω_G, in series with an inductance L_G. The three-phase power provided by these sources is expressed as:

$$P_G = \frac{3}{2} i_G^d \hat{V}_G, \tag{44}$$

where i_G^d is the direct component of the grid current in the dq reference frame, which regulates the active power P_G absorbed by the inverter when the quadrature component is zero. This must meet the following constraint to avoid control saturation:

$$\left| i_G^d \right| \leq \frac{1}{\omega_G L_G} \sqrt{\frac{V_{DC}^2}{3} - \hat{V}_G^2}. \tag{45}$$

The current assistance required by the electrolyzer from the DC-bus for a desired hydrogen flow rate f_{H_2}, neglecting losses in the inverter, is $i_G^{dc} = P_G/V_{DC}$. To regulate this, a feedback loop that controls the grid converter switching is applied. The following equation shows the grid assistance in terms of the imbalance between the current demanded by the electrolyzer and the current delivered by the solar panels:

$$i_G^{dc} = \frac{3}{2} i_G^d \hat{V}_G / V_{DC} = i_F^{dc} - i_S^{dc}. \tag{46}$$

The electrical grid is considered an ideal energy source. It provides a continuous energy supply when photovoltaic panels cannot generate the required amount of power and can also absorb excess power generated by the panels during peak production. The energy exchanged with the grid E_G, whose derivative is the power P_G, is considered a dynamic state. It defines the energy balance obtained by multiplying (46) by the DC-bus voltage:

$$\dot{E}_G(t) = P_F(t) - P_S(t) - P_D(t), \tag{47}$$

where i_S is computed using $v_S^{\max}$ in (16).

4.2 OPTIMAL CONTROL FORMULATION

The proposed optimal control approach has a fixed number of phases which is three. In the first and last phases, the URFC operates in FC mode, producing electric energy to the microgrid and consuming stored hydrogen. In the second phase, delimited by t_N^+ and t_D^-, the URFC operates in EL mode, converting solar energy from the PV panel to hydrogen that will be stored in the tank. The approach is presented below:

$$\begin{aligned}
\underset{i_F(\cdot)}{\text{minimize}} \quad & \int_{0\,\text{h}}^{t_N^+} [P_F(i_F) - P_D(t)]^2 \, dt + \\
& \int_{t_N^+}^{t_D^-} \left[P_S(t) - P_F(i_F) - P_D(t)\right]^2 \, dt + \\
& \int_{t_D^-}^{24\,\text{h}} [P_F(i_F) - P_D(t)]^2 \, dt, \\
\text{subject to} \quad & \dot{m}_{H_2} = f_{H_2} - f_{H_2}^{dm}, \\
& M_{H_2}^{min} \leq m_{H_2} \leq M_{H_2}^{max}, \\
& m_{H_2}(0\,\text{h}) = M_0, \\
& I_F^{min} \leq i_F \leq I_F^{max}.
\end{aligned} \tag{48}$$

4.3 RESULTS AND DISCUSSION

The research was carried out in a computational environment where all the experiments were conducted. The system model was developed based on established

models from academic literature. It is essential to note that the microgrid being studied has not been built in reality, so experimental validation was not realized. The simulations were carried out using MATLAB (MATHWORKS, 2023a), Simscape (MATHWORKS, 2023b), and MpOC Toolbox, presented in Appendix A.

The OCP (48) was discretized into segments with 5 min. The initial mass of hydrogen in the tank, denoted by M_0, is 700 g (70 % of capacity). The maximum hydrogen capacity in the tank $M_{H_2}^{max}$ is 1000 g, which is equivalent to 11.126 Nm^3. The minimum desired $M_{H_2}^{min}$ is 20 % of the maximum capacity, which is 200 g. The calculated values for t_N^+ and t_D^- are 7.5 h and 16.8 h, respectively. The guesses utilized to solve NLP are: for the control, i_F, and the state, m_{H_2}, the guess was the mean between the maximum and minimum values for these variables. The solar radiation and hydrogen demand data were extracted from de Andrade et al. (2020). The power demand was acquired from the supplementary material of Bordons, Garcia-Torres, and Ridao (2020). The sample applied time is 1 min. Linear interpolation was employed to integrate these data into the optimization framework seamlessly.

Figure 26 – Results of the multi-phase optimal control approach applied to the hydrogen energy storage system.

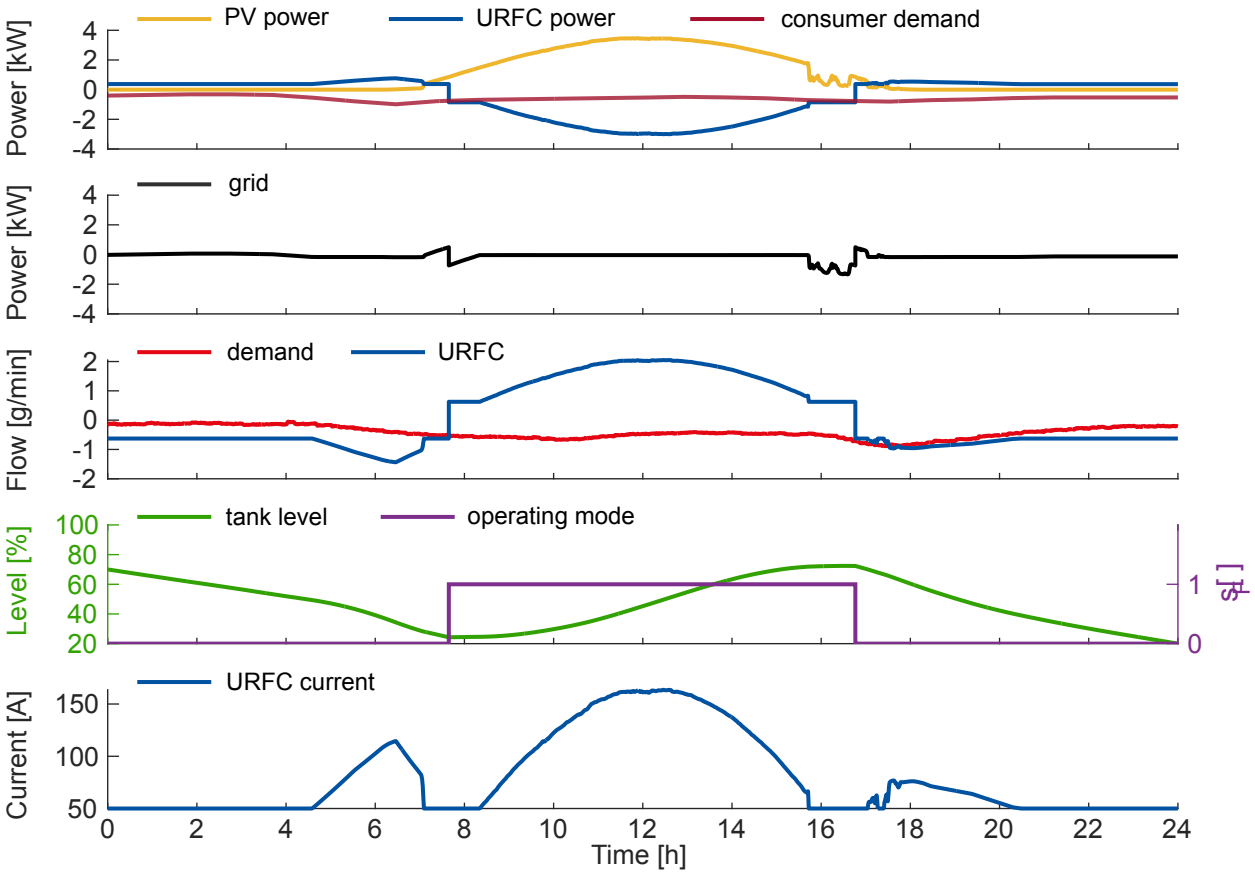

Source: Created by the author (2024).

The results of the multi-phase optimal control approach applied to the hydrogen energy storage system are shown in Figure 26. During the time intervals [0 h, t_N^+] and

$[t_D^-, 24\,\text{h}]$, the URFC was able to meet all of the electricity demand of the consumer with low grid energy consume. For $[t_N^+, t_D^-]$, the system could convert solar energy to hydrogen and meet the consumers' electricity demand without using grid energy.

The energy demand was $E_D = 14.3\,\text{kWh}$; however, the consumed grid energy was $E_G^- = 2.4\,\text{kWh}$. Furthermore, it was sold to the grid $E_G^+ = 0.5\,\text{kWh}$ and delivered 600 g of hydrogen without considering what was consumed when operating in FC mode. These results show that the proposed control system is a valuable option for dealing with systems with multiple operating modes because the solar radiation follows a pattern (19), which makes it possible to define a satisfactory sequence of phases without the need to resolve a more complex optimization like a MINLP problem.

5 CONCLUSIONS

5.1 SUMMARY OF KEY FINDINGS

Hydrogen presents a promising sustainable energy storage and generation opportunity, particularly when paired with renewable energy sources, such as solar energy. However, the intermittent nature of renewable energy poses a significant challenge for control systems that manage it and minimize the cost.

The objective of this study was to delve into and apply a multi-phase optimal control method for RHGS and renewable hydrogen generation and utilization systems RHGUS. The approach was tailored to accommodate various system operation modes. Specifically, the focus was on two photovoltaic energy-based systems: an RHGS equipped with a PEM electrolyzer, and an RHGUS equipped with a PEM unitized reversible fuel cell.

The simulation results allowed us to assess the potential of the proposals to reduce electric energy from the grid utilized on the plants. Notably, for the studied RHGS, in one year of evaluating the proposal with the Brazilian scenario, the reduction was up to four times when comparing multi-phase with a single-phase strategy. For the analyzed RHGUS, in one day, the energy consumed from the grid was reduced from 14.3 kWh to 2.4 kWh when compared to a system without energy storage and photovoltaic power generation.

The multi-phase optimal control strategy is a useful method for managing systems that have multiple operating modes, particularly when it is easy to identify the sequence and duration of each phase using a simple algorithm. In the systems under study, this determination was possible due to the pattern of solar radiation. As a result, the multi-phase strategy was faster to solve than the hybrid approach.

It is crucial to highlight that the analysis was conducted under an ideal scenario for the control problem. It incorporates the assumption of precise future data on solar radiation, hydrogen demand, and power demand, along with an exact match between the model and the dynamics of the plant. Consequently, the performance achieved serves as a theoretical benchmark for system operation, which, under real-world conditions, will encounter challenges such as modeling inaccuracies, disturbances that were not accounted for in the model, and uncertainties in weather predictions.

5.2 PUBLICATIONS

Parts of this document were published in the following conference paper:
Barbosa, M. F. da S, Garcia-Clúa, J. G., de Andrade, G. A. e Normey-Rico, J. E. Control óptimo multifase de sistema fotovoltaico-hidrógeno asistido por red. In: Actas de la XX Reuniõn de Trabajo en Procesamiento de la Información y Control, p. 860-865, 2023.

5.3 FUTURE RESEARCH DIRECTIONS

Possible future works are listed below:

- To apply multi-phase optimal control in systems based on multiple renewable energy sources. Increasing the number of components in the system will require new algorithms to determine the sequence of phases.
- To implement multi-phase optimal control in low-cost embedded hardware (like Beaglebone and Raspberry Pi) and compare with other optimal control strategies. These hardware have limited storage and processing capabilities, leading to difficulties installing necessary software and slower control system processing.
- To extend the proposed control methodology to a model predictive control, a closed-loop control system, and evaluate the controller performance due to disturbance in the input data (solar radiation, hydrogen, and power demand data).
- To collaborate with the Green Hydrogen Laboratory at UFSC, inaugurated in August 2023, to test optimal control strategies in hydrogen production. This state-of-the-art facility, supported by Brazil-Germany cooperation, boasts a maximum generation potential of 4.1 Nm^3/h of green hydrogen (BRASIL, 2023a). The collaboration would provide a practical setting to evaluate the effectiveness of the control strategies under varying solar radiation and photovoltaic generation conditions.

REFERENCES

AJANOVIC, A.; SAYER, M.; HAAS, R. The economics and the environmental benignity of different colors of hydrogen. **International Journal of Hydrogen Energy**, v. 2022, p. 24136–24154, 2022.

AMIR, Mohammad et al. Energy storage technologies: An integrated survey of developments, global economical/environmental effects, optimal scheduling model, and sustainable adaption policies. **Journal of Energy Storage**, v. 72, p. 108694, 2023.

ANDERSSON, J. A. E.; GILLIS, J.; HORN, G.; RAWLINGS, J. B.; DIEHL, M. CasADi – A software framework for nonlinear optimization and optimal control. **Mathematical Programming Computation**, Springer, v. 11, n. 1, p. 1–36, 2019.

ANDRÉS-MARTÍNEZ, O.; PALMA-FLORES, O.; RICARDEZ-SANDOVAL, L. A. Optimal control and the Pontryagin's principle in chemical engineering: History, theory, and challenges. **AIChE journal**, v. 68, n. 8, p. 1–22, 2022.

APPLE INC. **MacBook Air (M1, 2020) - Technical Specifications**. [S.l.: s.n.], 2020. Available from: `https://support.apple.com/kb/SP825?viewlocale=en_US`.

BATZELIS, E. I.; ANAGNOSTOU, G.; CHAKRABORTY, C.; PAL, B. C. Computation of the Lambert W Function in Photovoltaic Modeling. In: ELECTRIMACS 2019. [S.l.]: Springer International Publishing, 2020. P. 583–595.

BETTS, J. T. **Practical Methods for Optimal Control and Estimation Using Nonlinear Programming**. [S.l.]: Society for Industrial and Applied Mathematics, 2010.

BLAY-ROGER, Rubén; BACH, Wolfgang; BOBADILLA, Luis F.; REINA, Tomas Ramirez; ODRIOZOLA, José A.; AMILS, Ricardo; BLAY, Vincent. Natural hydrogen in the energy transition: Fundamentals, promise, and enigmas. **Renewable and Sustainable Energy Reviews**, v. 189, p. 113888, 2024.

BOCKRIS, J. **Energy: The solar-hydrogen alternative**. [S.l.]: John Wiley and Sons, 1975.

BOLLIPO, R. B.; MIKKILI, S.; BONTHAGORLA, P. K. Hybrid, optimal, intelligent and classical PV MPPT techniques: A review. **CSEE Journal of Power and Energy Systems**, v. 7, n. 1, p. 9–33, 2020.

BONAMI, P. et al. An algorithmic framework for convex mixed integer nonlinear programs. **Discrete optimization**, AMSTERDAM, v. 5, n. 2, p. 186–204, 2008.

BORDONS, C.; GARCIA-TORRES, F.; RIDAO, M. A. **Model Predictive Control of Microgrids**. [S.l.]: Springer International Publishing, 2020.

BRASIL. Ministério da Ciência, Tecnologia e Inovação. Instituto Nacional de Pesquisas Espaciais. **Sistema de Organização Nacional de Dados Ambientais**. [S.l.: s.n.], 2018. Available from: `http://sonda.ccst.inpe.br/basedados/cachoeira.html`.

BRASIL. Ministério de Minas e Energia. **MME participa da inauguração do laboratório de Hidrogênio Verde da UFSC**. [S.l.: s.n.], 2023. Visited on: 1 Dez. 2023. Available from: `https://www.gov.br/mme/pt-br/assuntos/noticias/mme-participa-da-inauguracao-do-laboratorio-de-hidrogenio-verde-da-ufsc`.

BRASIL. Ministério de Minas e Energia. **Programa Nacional de Hidrogênio: Plano de Trabalho Trienal 2023-2025**. Brasilia, DF, 2023. P. 79.

BRASIL. Ministério de Minas e Energia. Empresa de Pesquisa Energética. **Balanço Energético Nacional 2023: Ano base 2022**. Rio de Janeiro, RJ, 2023. P. 292.

BRASIL. Ministério de Minas e Energia. Empresa de Pesquisa Energética. **Balanço Energético Nacional Interativo**. [S.l.: s.n.], 2023. Visited on: 1 Dez. 2023. Available from: `https://dashboard.epe.gov.br/apps/ben/`.

BRASIL. Ministério de Minas e Energia. Empresa de Pesquisa Energética. **Plano decenal de expansão de energia 2030**. Brasília, DF, 2020. P. 445.

BRYSON, A. E. Optimal control - 1950 to 1985. **IEEE Control Systems Magazine**, v. 16, p. 26–33, 1996.

CRUTZEN, P. Geology of mankind. **Nature**, v. 415, p. 23–23, 2002.

DAWOOD, F.; ANDA, M.; SHAFIULLAH, G. M. Hydrogen production for energy: An overview. **International journal of hydrogen energy**, v. 45, n. 7, p. 3847–3869, 2020.

DE ANDRADE, G. A.; GARCÍA-CLÚA, J. G.; MENDES, P. R.C.; NORMEY-RICO, J. E. Optimal Control of a Grid Assisted Photovoltaic-Hydrogen Production System. In:

PROCEEDINGS of the 12th IFAC Symposium on Dynamics and Control of Process Systems, including Biosystems. [S.l.: s.n.], 2019. v. 52, p. 1012–1017.

DE ANDRADE, G. A.; MENDES, P. R. C.; GARCÍA-CLÚA, J. G.; NORMEY-RICO, J. E. Control of a grid assisted PV-H2 production system: A comparative study between optimal control and hybrid MPC. **Journal of Process Control**, v. 92, p. 220–233, 2020.

DESHMUKH, S. S.; BOEHM, R. F. Review of modeling details related to renewably powered hydrogen systems. **Renewable & Sustainable Energy Reviews**, v. 12, p. 2301–2330, 2008.

DUTTON, A. G.; BLEIJS, J. A. M.; DIENHART, H.; FALCHETTA, M.; HUG, W.; PRISCHICH, D.; RUDDELL, A. J. Experience in the design, sizing, economics, and implementation of autonomous wind-powered hydrogen production systems. **International Journal of Hydrogen Energy**, v. 25, n. 8, p. 705–722, 2000.

FALCÃO, D. S.; PINTO, A. M. F. R. A review on PEM electrolyzer modelling: Guidelines for beginners. **Journal of cleaner production**, v. 261, p. 121184, 2020.

FAWZY, S.; OSMAN, A.; DORAN, J.; ROONEY, D. Strategies for mitigation of climate change: a review. **Environmental Chemistry Letters**, v. 18, p. 2069–2094, 2020.

GARCÍA-CLÚA, J. G. **Sistemas de control híbrido: Aplicación a sistemas de generación de hidrógeno a partir de recursos energéticos renovables**. 2013. Ph.D. thesis – Universidad Nacional de La Plata.

GARCÍA-CLÚA, J. G.; DE BATTISTA, H.; MANTZ, R. J. Control of a grid-assisted wind-powered hydrogen production system. **International Journal of Hydrogen Energy**, v. 35, n. 11, p. 5786–5792, 2010.

GENOVESE, Matteo; SCHLÜTER, Alexander; SCIONTI, Eugenio; PIRAINO, Francesco; CORIGLIANO, Orlando; FRAGIACOMO, Petronilla. Power-to-hydrogen and hydrogen-to-X energy systems for the industry of the future in Europe. **International Journal of Hydrogen Energy**, v. 48, n. 44, p. 16545–16568, 2023.

GOLTSOV, V.; VEZIROGLU, T.; GOLTSOVA, L. Hydrogen civilization of the future - a new conception of the iahe. **International Journal of Hydrogen Energy**, v. 31, p. 153–159, 2006.

GOLTSOV, V. A. **Sustainable human future, Hydrogen Civilization**. [S.l.]: Donetsk: “Knowledge”, 2010.

GREEN, M. A. Solar cells: operating principles, technology, and system applications. **Englewood Cliffs, NJ, Prentice-Hall, Inc.**, 1982.

HERNÁNDEZ-GÓMEZ, A.; RAMIREZ, V.; GUILDBERT, D. Investigation of PEM electrolyzer modeling: Electrical domain, efficiency, and specific energy consumption. **International Journal of Hydrogen Energy**, v. 45, p. 14625–14639, 2020.

HOLLADAY, J. D.; HU, J.; KING, D. L.; WANG, Y. An overview of hydrogen production technologies. **Catalysis Today**, v. 139, n. 4, p. 244–260, 2009.

HOTZA, D.; DINIZ DA COSTA, J.C. Fuel cells development and hydrogen production from renewable resources in Brazil. **International Journal of Hydrogen Energy**, v. 33, n. 19, p. 4915–4935, 2008. 2nd Asian Bio Hydrogen Symposium.

HOWLETT, P. G.; PUDNEY P. J.AND VU, X. Local energy minimization in optimal train control. **Automatica**, v. 45, n. 11, p. 2692–2698, 2009.

HYDROGEN COUNCIL. **Hydrogen for Net-Zero: A Critical Cost-Competitive Energy Vector**. [S.l.], 2021. Available from: `https://hydrogencouncil.com/wp-content/uploads/2021/11/Hydrogen-for-Net-Zero.pdf`.

IEA. International Energy Agency. **Global Hydrogen Review 2022**. [S.l.], 2022. Available from: `https://www.iea.org/reports/global-hydrogen-review-2022`.

IEA. International Energy Agency. **Key World Energy Statistics 2020**. [S.l.], 2020. P. 81.

IEA. International Energy Agency. **World Energy Balances 2020**. [S.l.], 2020. (Statistics).

ISHAQ, H.; DINCER, I.; CRAWFORD, C. A review on hydrogen production and utilization: Challenges and opportunities. Elsevier Ltd, v. 47, n. 62, p. 26238–26264, 2022.

KELLY, M. P. An Introduction to Trajectory Optimization: How to Do Your Own Direct Collocation. **SIAM Review**, v. 59, p. 849–904, 2017.

KELLY, M. P. **Transcription Methods for Trajectory Optimization: a beginners tutorial**. [S.l.: s.n.], 2017. arXiv: 1707.00284 [math.OC].

KIRATI, S. K.; HAMMOUDI, M.; MOUSLI, I. M. A. Hybrid energy system for hydrogen production in the Adrar region (Algeria): Production rate and purity level. **International Journal of Hydrogen Energy**, v. 43, p. 3378–3393, 2018.

KIRK, D. E. **Optimal control theory: an introduction**. [S.l.]: Courier Corporation, 2004.

KRONQVIST, J.; BERNAL, D. E.; LUNDELL, A.; GROSSMANN, I. E. A review and comparison of solvers for convex MINLP. **Optimization and Engineering**, Springer Science and Business Media LLC, v. 20, n. 2, p. 397–455, 2018.

KROPOSKI, B.; LEVENE, J.; HARRISON, K.; SEN, P.K.; NOVACHEK, F. **Electrolysis: Information and Opportunities for Electric Power Utilities**. [S.l.], 2006.

KUMAR, S. S.; LIM, H. An overview of water electrolysis technologies for green hydrogen production. **Energy Reports**, v. 8, p. 13793–13813, 2022.

LEEK, V. **An Optimal Control Toolbox for MATLAB Based on CasADi**. 2016. S. 56. MA thesis – Linköping University, Vehicular Systems.

LEEUWEN, C. Van; MULDER, M. Power-to-gas in electricity markets dominated by renewables. **Applied Energy**, v. 232, p. 258–272, 2018.

LIN, W. S.; ZHENG, C. H. Energy management of a fuel cell/ultracapacitor hybrid power system using an adaptive optimal-control method. **Journal of Power Sources**, v. 196, n. 6, p. 3280–3289, 2011.

LIU, Y.; HENG, S.; ZANG, X.; LIN, Z.; ZHAO, J. Multiphase trajectory generation for planar biped robot using direct collocation method. **Mathematical Problems in Engineering**, Hindawi Limited, v. 2021, p. 1–14, 2021.

LOTKER, M. Hydrogen for the electric utilities - Long range possibilities. In: 9TH Intersociety Energy Conversion Engineering Conference. [S.l.: s.n.], 1974. P. 423–427.

MATHWORKS. **MATLAB version: 23.2.0.2485118 (R2023b) Update 6**. [S.l.: s.n.], 2023. Available from: https://www.mathworks.com.

MATHWORKS. **Simscape version: 23.2**. [S.l.: s.n.], 2023. Available from: https://www.mathworks.com/products/simscape.html.

MATHWORKS. **Sustainability and Renewable Energy Challenge**. [S.l.: s.n.], 2023. Visited on: 1 Dez. 2023. Available from: https://www.mathworks.com/academia/student-challenge/sustainability-and-renewable-energy-challenge-2023.html.

NEWBOROUGH, M.; COOLEY, G. Developments in the global hydrogen market: The spectrum of hydrogen colours. **Fuel Cells Bulletin**, v. 2020, n. 11, p. 16–22, 2020.

NIE, Y.; FAQIR, O. J.; KERRIGAN, E. C. ICLOCS2: Solve your optimal control problems with less pain. In: PROCEEDINGS of the 6th IFAC Conference on Nonlinear Model Predictive Control. [S.l.: s.n.], 2018.

OGBONNAYA, C.; ABEYKOON, C.; NASSER, A.; TURAN, A. Unitized regenerative proton exchange membrane fuel cell system for renewable power and hydrogen generation: Modelling, simulation, and a case study. **Cleaner Engineering and Technology**, v. 4, p. 100241, 2021.

PATTERSON, M. A.; RAO, A. V. GPOPS-II: A MATLAB Software for Solving Multiple-Phase Optimal Control Problems Using hp-Adaptive Gaussian Quadrature Collocation Methods and Sparse Nonlinear Programming. **ACM Transactions on Mathematical Software**, Association for Computing Machinery (ACM), v. 41, n. 1, p. 1–37, 2014.

PRADEEP, P.; WEI, P. Energy Optimal Speed Profile for Arrival of Tandem Tilt-Wing eVTOL Aircraft with RTA Constraint. In: PROCEEDINGS of the 2018 IEEE CSAA Guidance, Navigation and Control Conference. [S.l.: s.n.], 2018.

ROBUSCHI, N.; ZEILE, C.; SAGER, S.; BRAGHIN, F. Multiphase mixed-integer nonlinear optimal control of hybrid electric vehicles. **Automatica**, v. 123, p. 109325, 2021.

ROSS, I. M. **Enhancements to the DIDO Optimal Control Toolbox**. [S.l.]: arXiv, 2020.

SAGLIANO, M.; SEELBINDER, D.; THEIL, S. SPARTAN: Rapid Trajectory Analysis via Pseudospectral Methods. In: 8TH International Conference on Astrodynamics Tools and Techniques (ICATT). [S.l.: s.n.], 2021.

SCIARRETTA, A.; BACK, M.; GUZZELLA, L. Optimal control of parallel hybrid electric vehicles. **IEEE Transactions on Control Systems Technology**, v. 12, n. 3, p. 352–363, 2004.

SMOLINKA, T.; OJONG, E. T.; GARCHE, J. Chapter 8 - Hydrogen Production from Renewable Energies - Electrolyzer Technologies. In: MOSELEY, Patrick T.; GARCHE, Jürgen (Eds.). **Electrochemical Energy Storage for Renewable Sources and Grid Balancing**. Amsterdam: [s.n.], 2015. P. 103–128.

SOOD, S.; PRAKASH, O.; BOUKERDJA, M.; DIEULOT, J.-Y.; OULD-BOUAMAMA, B.; BRESSEL, M.; GEHIN, A.-L. Generic Dynamical Model of PEM Electrolyser under Intermittent Sources. **Energies**, v. 13, n. 24, 2020.

SWANNET, K. **Optimal Control And Energy Management For Hybrid Aircraft**. 2022. Dissertation – Delft University of Technology.

THAMMISETTY, D. **Development of a multi-phase optimal control software for aerospace applications (mpopt)**. 2020. MA thesis – Master's thesis, Lausanne, EPFL.

TIBA, C. **Atlas solamerico do Brasil**. [S.l.]: Editora Universitária da Universidade Federal do Pernambuco, 2000.

TOPPUTO, F.; ZHANG, C. Survey of Direct Transcription for Low-Thrust Space Trajectory Optimization with Applications. **Abstract and Applied Analysis**, v. 2014, p. 1–15, 2014.

UNFCCC. **The Paris Agreement**. [S.l.]: United Nations Climate Change, 2020. Available from: `https://unfccc.int/process-and-meetings/the-paris-agreement/the-paris-agreement`.

USA. Department of Energy. **U.S. National Clean Hydrogen Strategy and Roadmap**. [S.l.], 2023. P. 97.

VALDERRAMA, P. H. B. da S.; CAMPONOGARA, E.; SEMAN, L. O.; GONZÁLEZ, G. V.; LEITHARDT, V. R. Q. Decompositions for MPC of Linear Dynamic Systems with Activation Constraints. **Energies**, v. 13, n. 21, 2020.

VALVERDE, L. **Gestión de energía en sistemas con fuentes renovables y almacenamiento de energía basado en hidrógeno mediante control predictivo**. 2013. Ph.D. thesis – Universidad de Sevilla, Sevilla.

VALVERDE, L.; ABDEL-WAHAB, M.; GUERRA, J.; HOGG, D. F. A technical evaluation of Wind-Hydrogen (WH) demonstration projects in Europe. In: PROCEEDINGS of the 4th International Conference on Power Engineering, Energy and Electrical Drives. [S.l.: s.n.], 2013. P. 1098–1104.

VALVERDE, L.; ROSA, F.; DEL REAL, A.J.; ARCE, A.; BORDONS, C. Modeling, simulation and experimental set-up of a renewable hydrogen-based domestic microgrid. **International Journal of Hydrogen Energy**, v. 38, n. 27, p. 11672–11684, 2013.

VAN, L. P.; CHI, K. D.; DUC, T. N. Review of hydrogen technologies based microgrid: Energy management systems, challenges and future recommendations. **International Journal of Hydrogen Energy**, v. 48, p. 13793–13813, 2023.

VERNE, Jules. **The mysterious island**. New York: Airmont publishing, 1965.

VEZIROGLU, T. N. Quarter century of hydrogen movement 1974-2000. **International Journal of Hydrogen Energy**, v. 25, p. 1143–1150, 2000.

WACHTER, A.; BIEGLER, L. T. On the implementation of an interior-point filter line-search algorithm for large-scale nonlinear programming. **Mathematical programming**, Springer Nature, v. 106, n. 1, p. 25–57, 2006.

WILLEMS, J. C. 1696: The birth of optimal control. In: PROCEEDINGS of 35th IEEE Conference on Decision and Control. [S.l.: s.n.], 1996. P. 1586–1587.

WITKOWSKI, A.; RUSIN, A.; MAJKUT, M.; STOLECKA, K. Comprehensive analysis of hydrogen compression and pipeline transportation from thermodynamics and safety aspects. **Energy**, v. 141, p. 2508–2518, 2017.

WU, S.; DING, K.; CHENG, P.; SHI, L. Optimal scheduling of multiple sensors over lossy and bandwidth limited channels. **IEEE Transactions on Control of Network Systems**, v. 7, n. 3, p. 1188–1200, 2020.

WULF, Christina; ZAPP, Petra; SCHREIBER, Andrea. Review of Power-to-X Demonstration Projects in Europe. **Frontiers in Energy Research**, v. 8, 2020.

XIAOFENG, T. Ecological driving on multiphase trajectories and multiobjective optimization for autonomous electric vehicle platoon. **Scientific Reports**, Springer Science and Business Media LLC, v. 12, n. 1, 2022.

YAN, J. Energy systems in transition: Challenges and opportunities. **Advances in Applied Energy**, v. 1, p. 7100005, 2020.

YAN, J.; YANG, Y.; CAMPANA, E. P.; HE, J. City-level analysis of subsidy-free solar photovoltaic electricity price, profits and grid parity in China. **Nat Energy**, v. 8, p. 709–717, 2020.

YANG, L.; LI, H.; ZHANG, J.; LUO, Y. Multiphase trajectory optimization of a lunar return mission to an LEO space station. **International Journal of Aerospace Engineering**, Hindawi Limited, v. 2021, p. 1–15, 2021.

YU, M.; WANG, K.; VREDENBURG, H. Insights into low-carbon hydrogen production methods: Green, blue and aqua hydrogen. **International Journal of Hydrogen Energy**, v. 46, n. 41, p. 21261–21273, 2021.

ZHANG, D.; ZHANG, Y. PySCP: A Multiple-Phase Optimal Control Software Using Sequential Convex Programming. **International Journal of Aerospace Engineering**, Hindawi Limited, v. 2022, p. 1–18, 2022.

ZHANG, F.; ZHAO, P.; NIU, M.; MADDY, J. The survey of key technologies in hydrogen energy storage. **International Journal of Hydrogen Energy**, v. 41, p. 14535–14552, 2016.

ZHAO, N.; YOU, F. New York state's 100% renewable electricity transition planning under uncertainty using a data-driven multistage adaptive robust optimization approach with machine-learning. **Advances in Applied Energy**, p. 100019, 2021.

ZWEIBEL, K. **Harnessing solar power: The photovoltaics challenge**. [S.l.]: Springer, 2013.

APPENDIX A – MULTI-PHASE OPTIMAL CONTROL TOOLBOX

The Multi-phase Optimal Control Toolbox (MpOC), developed in this study, uses object-oriented programming within MATLAB to address multi-phase optimal control problems. Utilizing the features provided by CasADi, MpOC integrates a suite of NLP solver plugins, including the renowned Ipopt, SNOPT, WORHP, and Knitro, thus offering a versatile solution for both single and multi-phase OCPs without necessitating manual implementation of transcription methods.

The the implementation of the Hermite-Simpson collocation method in its separate form, introduced into subsection 2.3.5.1, is key functionality of the MpOC. The object-oriented design provides scalability and flexibility, facilitating the incorporation of additional transcription methods, such as Trapezoidal collocation and Pseudo-spectral methods, in future versions.

Comprehensive documentation, installation guides, and illustrative examples are made available through a public GitHub repository. The repository can be accessed at `https://github.com/michaelfsb/mpoc-toolbox`.

However, MpOC's current version presents certain limitations, including: (*i*) the absence of support for hybrid OCPs, (*ii*) lack of automatic refinement for discretization points, (*iii*) adoption of equidistant discretization intervals, and (*iv*) support restricted to single state and control variables. Addressing these limitations remains a priority for future development, aiming to enhance its applicability.

APPENDIX B – MODEL PARAMETERS

This appendix details the parameters used in the photovoltaic solar panel model, the electrolyzer model, and the URFC system model.

Table 7 – Parameters of photovoltaic solar panel model.

Description	Symbol	Value
Boltzmann constant	K	1.38×10^{-23} J/K
Cell deviation factor	A_S	1.6
Elementary charge	Q	1.6×10^{-19} C
Number of panels in parallel	N_{PS}	8
Number of panels in series	N_{SS}	300
I_{rs} at T_{RS}	I_{or}	2.0793 µA
Reference temperature	T_{SR}	298 K
Semiconductor band gap	E_g	1.1 V
Short circuit current at T_{SR}	I_{sc}	3.27 A
Short circuit current by temp.	K_L	0.0017 A/K

Source: Adapted from (DE ANDRADE et al., 2020).

Table 8 – Parameters of the electrolyzer model.

Description	Symbol	Value
Anode current density	I_a	1.0631 µA/cm
Cathode current density	I_c	1 mA/cm
Faraday constant	F	96 485.332 89 C/mol
Gas constant	R	8.314 J/(mol K)
Hydrogen partial pressure	p_{H_2}	6.9 bar
Membrane thickness	δ_B	178 µm
Membrane water content	λ_E	21 $\text{mol}_{H_2}/\text{mol}_{SO_3}$
Number of cells	N_{SE}	6
Oxygen partial pressure	p_{O_2}	1.3 bar
Stack area	A_E	212.5 cm^2
Electrolyzer temperature	T_E	298 K

Source: Adapted from (VALVERDE et al., 2013b).

Table 9 – Parameters of the URFC system.

Parameter	**Symbol**	**Value**
Active cell area	A_F	100 cm^2
Faraday's constant	F	96485 C/mol
Lost internal current density	i_{loss}	0.008 A/cm^2
Anode exchange current density	$i_{0_{anode}}$	0.15 A/cm^2
Cathode exchange current density	$i_{0_{cathode}}$	0.15 A/cm^2
Anode limiting current density	$i_{l_{anode}}$	15 A/cm^2
Cathode limiting current density	$i_{l_{cathode}}$	2.5 A/cm^2
Number of electrons	n	2
Number of cells in of URFC	N_S	10
Hydrogen partial pressure	p_{H_2}	1 atm
Water partial pressure	p_{H_2O}	1 atm
Oxygen partial pressure	p_{O_2}	0.21 atm
Gas constant	R	8.3145 J/(mol K)
Area specific resistance	R_{elec}	0 Ω/m^2
Area specific ion resistance	R_{ion}	0.01 Ω/m^2
Area specific contact resistance	R_{cr}	0.03 Ω/m^2
Temperature of of URFC	T_F	353.15 K
Reversible potential of URFC	v_{rev}	1.23 V

Source: Adapted from Ogbonnaya et al. (2021).

APPENDIX C – COMPLEMENTARY RESULTS

This appendix presents additional results from the hydrogen production and storage simulations conducted over a one-year period. Figures 27 and 28 show the hydrogen production f_{H_2} using the MPS-FW and HyS-OA methods, respectively.

Figure 27 – Hydrogen production f_{H_2} with MPS-FW during one year.
Normalized at 373 mg/min.

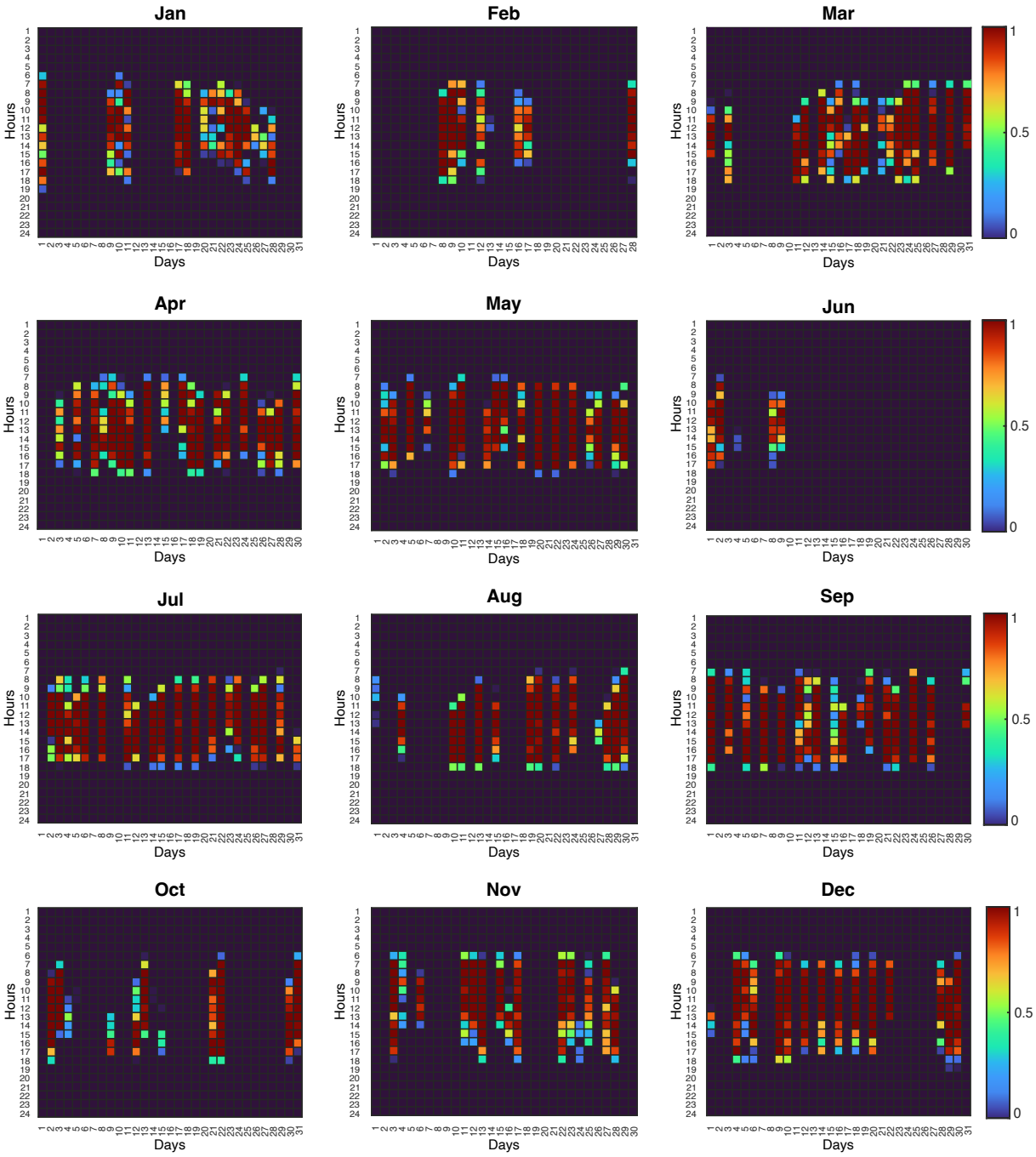

Source: Created by the author (2024).

Figure 28 – Hydrogen production f_{H_2} with HyS-OA during one year.

Normalized at 373 mg/min.

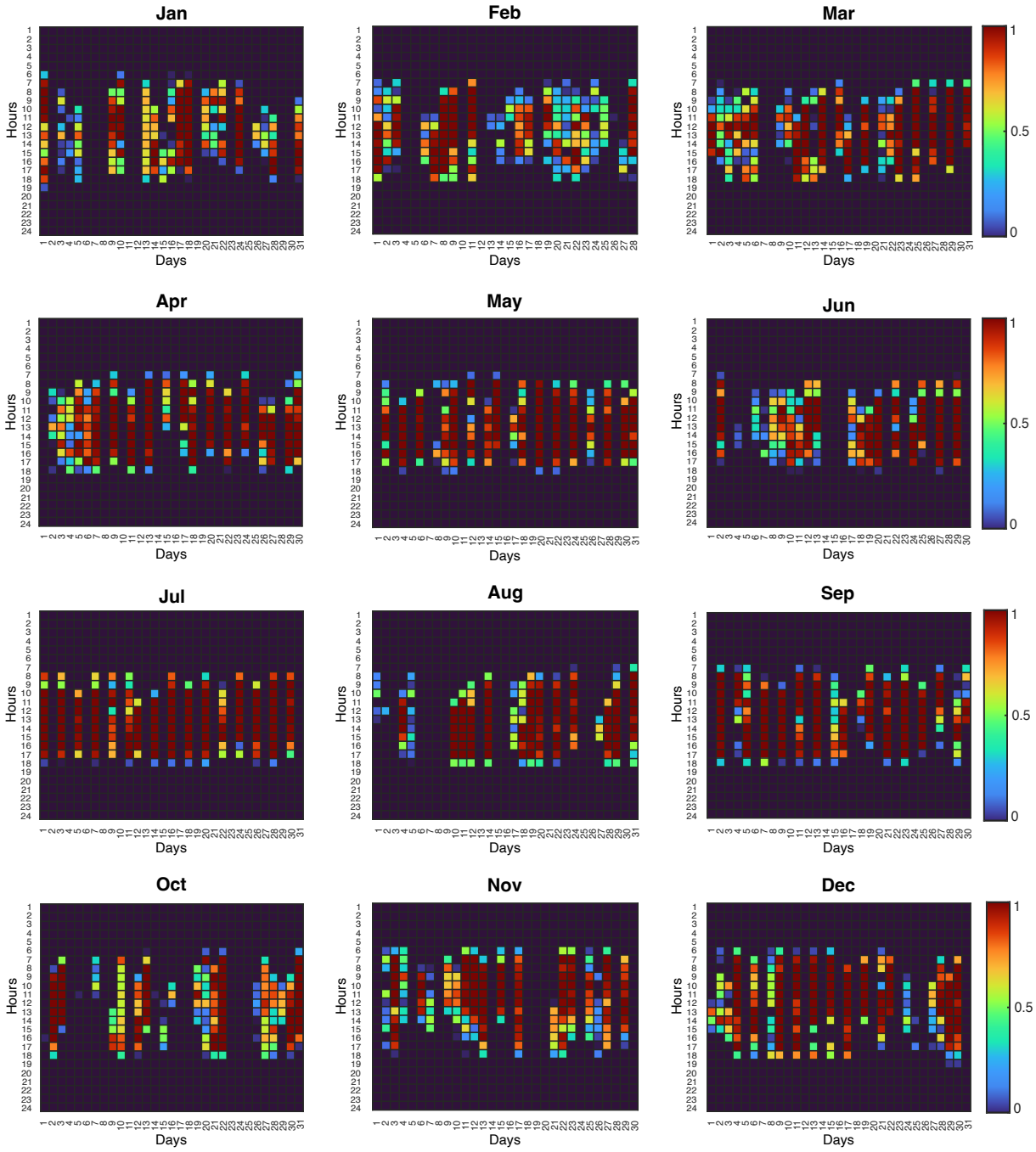

Source: Created by the author (2024).

Figures 29, 30, 31, and 32 illustrate the tank levels m_{H_2} with SPS, MPS-VW, MPS-FW, and HyS-OA methods over a one-year period. The days marked with a blue line indicate when the system produced and supplied hydrogen. On the yellow-marked days, D_{off}, the system only supplied hydrogen, meaning the electrolyzer was off, and hydrogen consumption occurred. The days with a red line, D_{off}^{dm}, signify that the electrolyzer was off, and no hydrogen was consumed. The decision to turn the electrolyzer on or off and whether hydrogen can be consumed is made by the control system proposed in Figure 16 of section 3.3. On all days, the excess solar energy is sold to the power grid.

Figure 29 – Tank level m_{H_2} with SPS during one year.

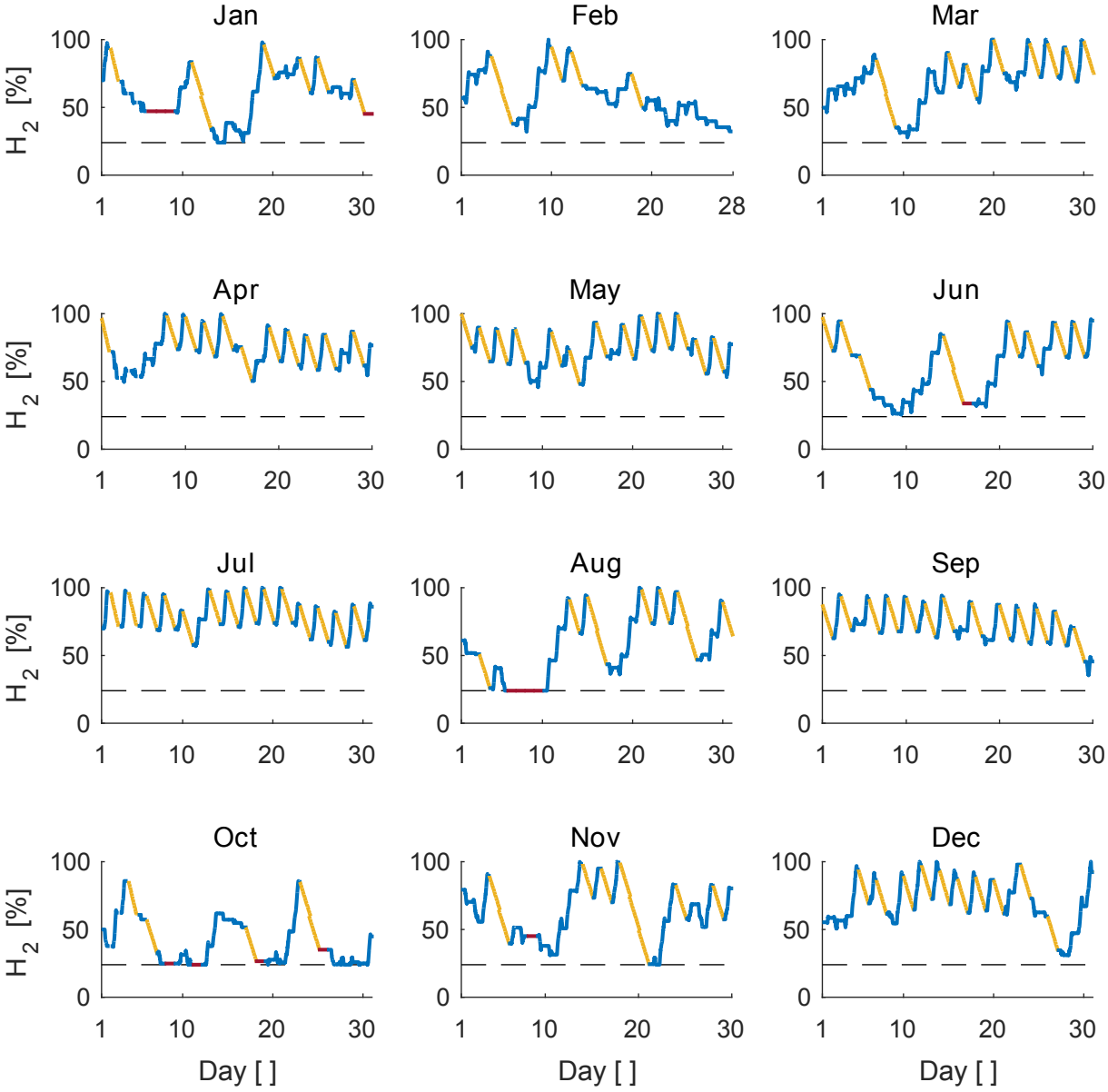

Source: Created by the author (2024).

Figure 30 – Tank level m_{H_2} with MPS-VW during one year.

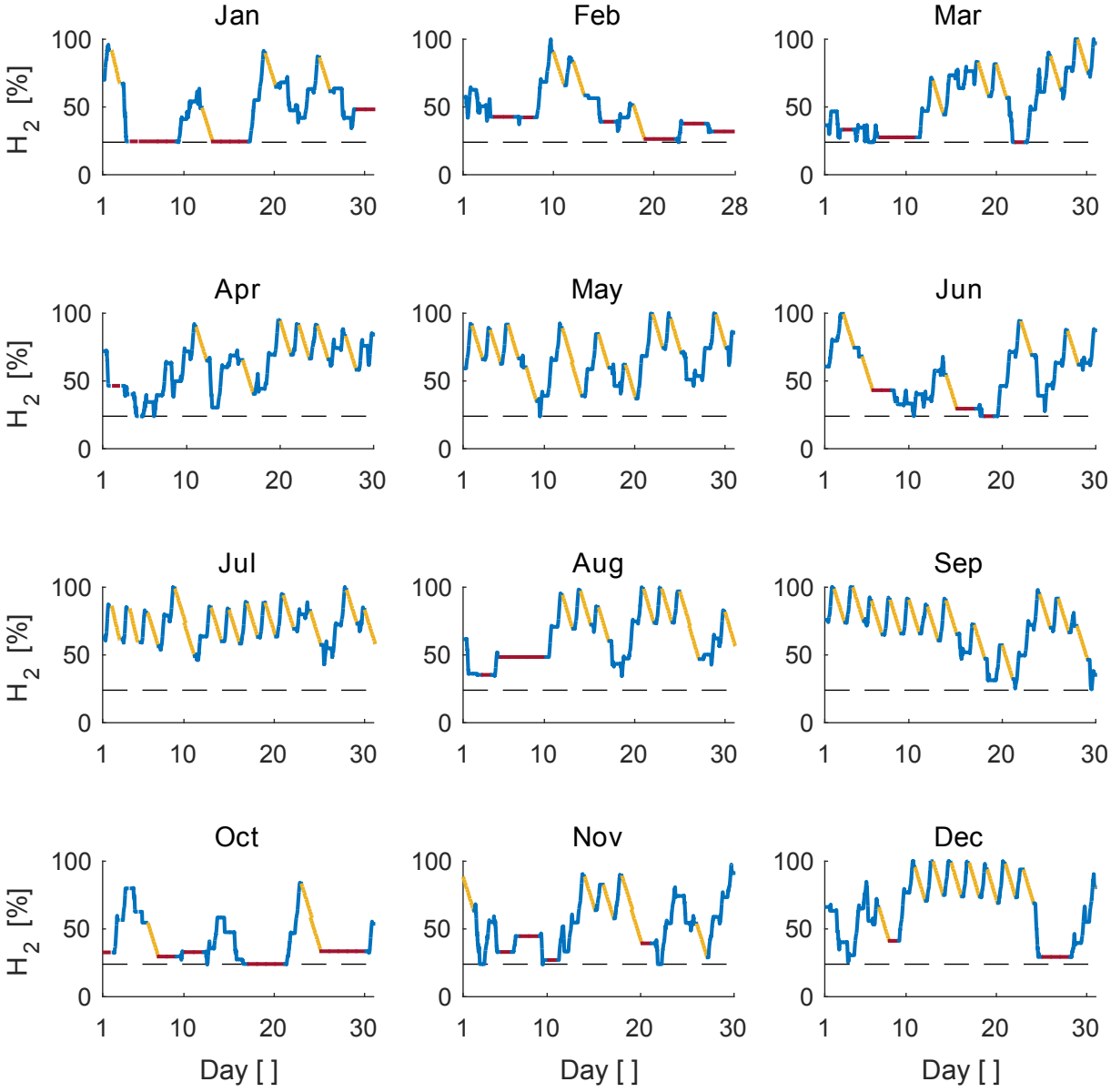

Source: Created by the author (2024).

Figure 31 – Tank level m_{H_2} with MPS-FW during one year.

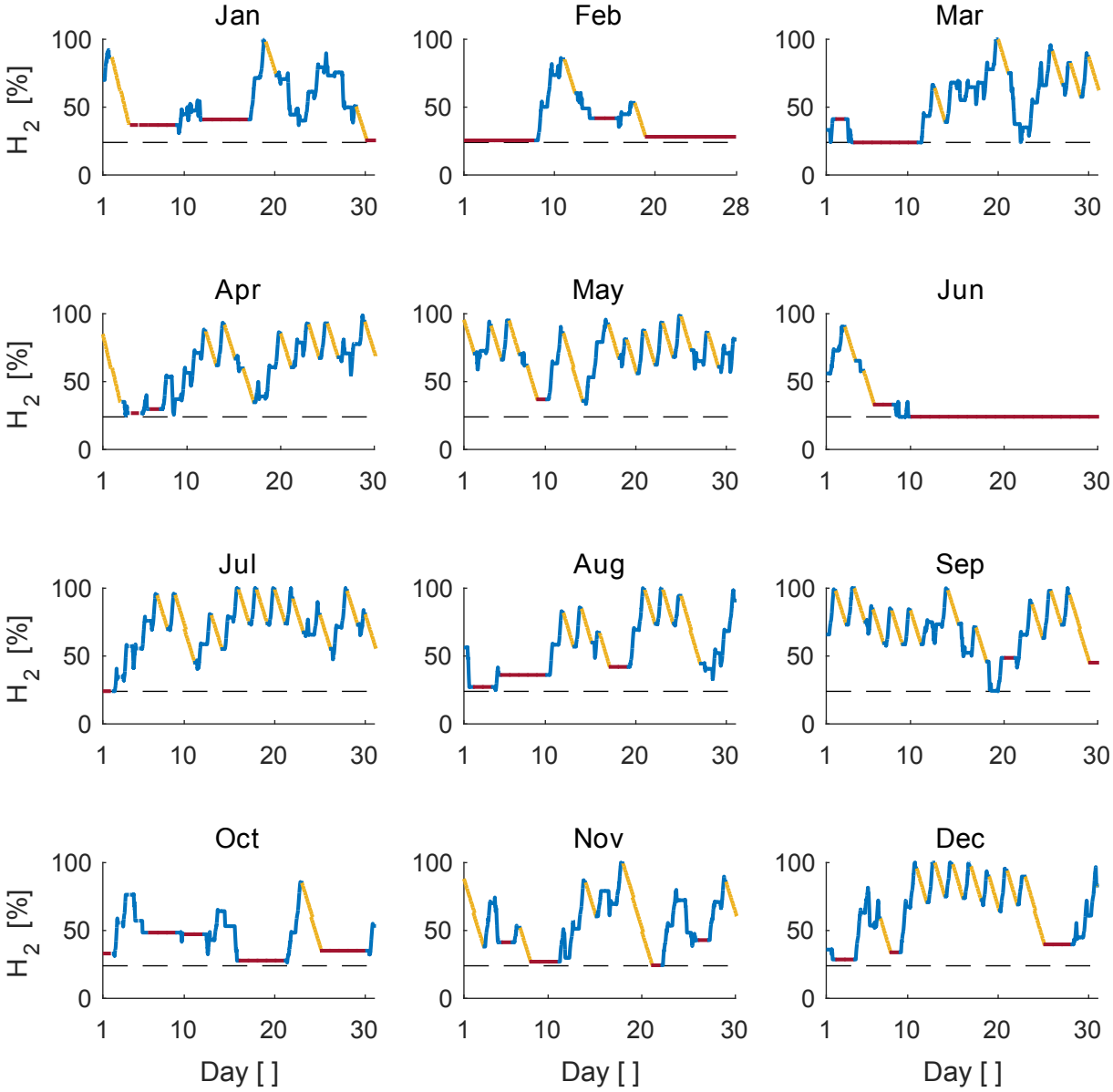

Source: Created by the author (2024).

Figure 32 – Tank level m_{H_2} with HyS-OA during one year.

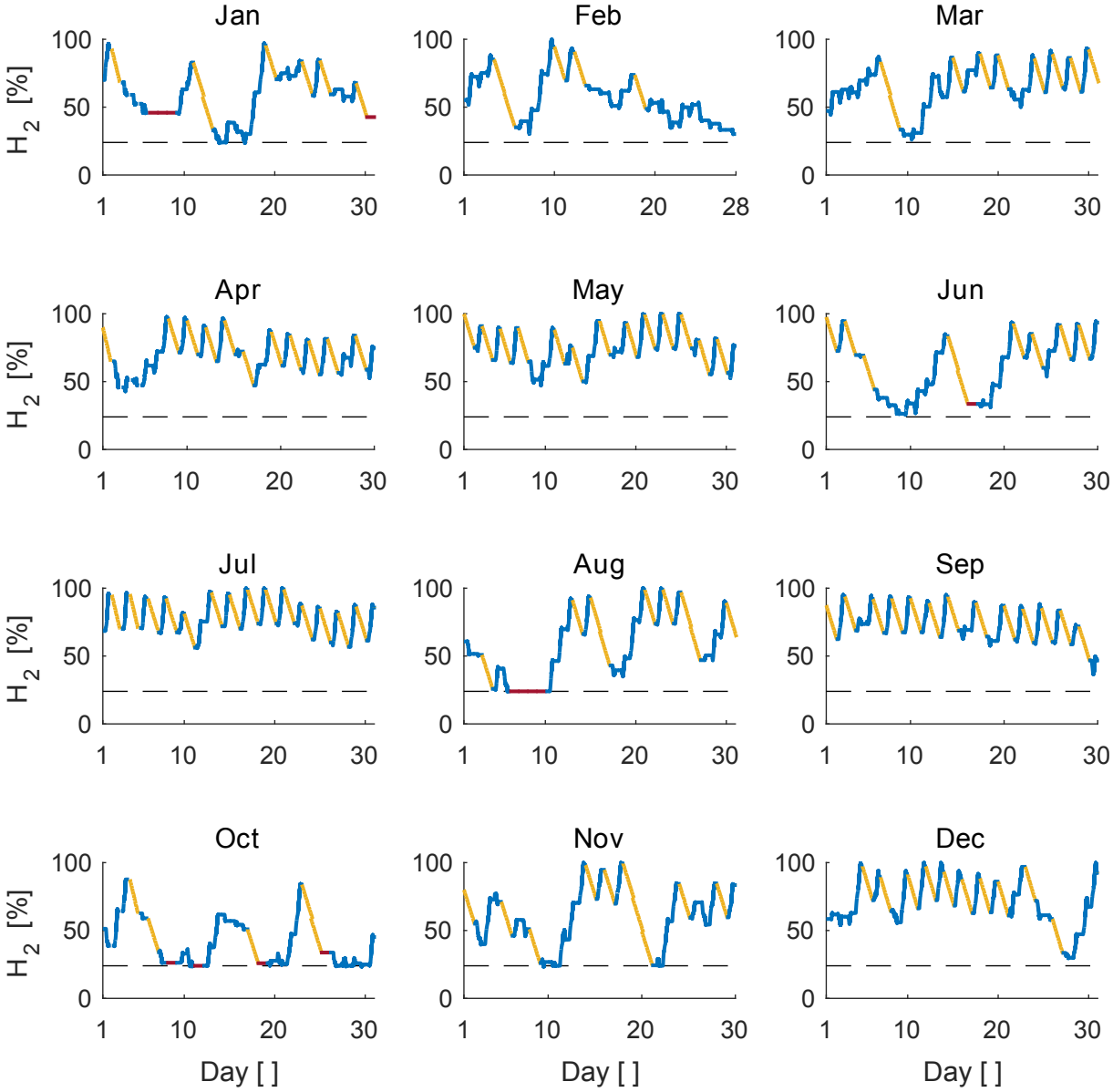

Source: Created by the author (2024).

ANNEX A – SUSTAINABILITY AND RENEWABLE ENERGY CHALLENGE

Figure 33 below presents the certificate of successful completion for the project "Green Hydrogen Production", issued by MathWorks. Detailed specifications of the project can be found in the GitHub repository mathworks/MATLAB-Simulink-Challenge-Project-Hub. Additionally, the model I developed for this project is available in the GitHub repository michaelfsb/hydrogen-energy-storage.

Figure 33 – Certificate of completion of the project Green Hydrogen Production.